공학박사학위논문

외부 구조물을 장착한 저 세장비 발사체의 공력 특성 연구

Investigation of the Aerodynamic Characteristics for the Low Aspect Ratio Launch Vehicle with the External Structure

2020년 8월

서울대학교 대학원

기계항공공학부

김 영 훈

외부 구조물을 장착한 저 세장비 발사체의 공력 특성 연구

Investigation of the Aerodynamic Characteristics for the Low Aspect Ratio Launch Vehicle with the External Structure

지도교수 김 규 홍

이 논문을 공학박사 학위논문으로 제출함

2020년 5월

서울대학교 대학원

기계항공공학부

김 영 훈

김영훈의 공학박사 학위논문을 인준함

2020년 6월

위 원 장 : _____

부위원장 : _____

위 원 : _____

위 원 : _____

위 원 : _____

Abstract

Investigation of the Aerodynamic Characteristics for the Low Aspect Ratio Launch Vehicle with the External Structure

Younghoon Kim
School of Mechanical and Aerospace Engineering
The Graduate School
Seoul National University

The Korea Aerospace Research Institute(KARI) has developed the Test Launch Vehicle(TLV) to confirm the performance of a 75 tonf engine in the Korea Space Launch Vehicle(KSLV)-II. And the TLV flight test was successful on November 28, 2018. In this paper, the solutions using CFD of the problem related to the longitudinal control of the launch vehicle due to the flow around the umbilical plate during the development process of the TLV, which intends to use the second and third stages of the KSLV-II with slight changes in configuration has been summarized. Owing to the influence of the flow around the umbilical plate, the normal force changed with the change in roll angle, and the center of pressure shifted accordingly. The controllability of the "Resemblant TLV" was verified by obtaining the Control Ratio(CR, the ratio of control torque to aerodynamic torque), which is the control requirement of the launch vehicle. Meanwhile, the height of the umbilical plate is lowered and the aerodynamic characteristics are predicted to confirm that the controllability increases compared to the

original umbilical plate. In addition, the section shape of the umbilical plate is changed from one ellipse to two small circles to confirm that the CR increases. Finally, the position of the umbilical plate moves forward to Payload Fairing.

There are various possible approaches to increase the CR of the "Resemblant TLV", such as increasing the deviation angle of the nozzle and increasing the thrust of the engine. However, the simplest way to improve the controllability by increasing the CR is to reduce the height of the protuberance such as the umbilical plate and minimize the influence of the flow around the protuberance. And the section of this plate is smaller circular shape rather than an elliptical shape to increase the controllability.

When developing the low aspect ratio launch vehicle using some stages and parts of the mother launch vehicle for the specific purpose such as the engine performance testing during the development of the mother launch vehicle, careful attention should be paid to the design of the protuberance such as the umbilical plate owing to control problems. This study confirmed that controllability can be a problem when the umbilical plate is mounted in the aft body of the low aspect ratio launch vehicle. It is expected that this paper could be used as a reference material in the design of low aspect ratio launch vehicles by providing an intuitive input for the design of the protuberance and control device of this type of launch vehicle.

---

keywords : Korea Space Launch Vehicle, Test Launch Vehicle, Aerodynamic Characteristics, Controllability, Low Aspect Ratio, Protuberance, CFD

Student Number : 2013 - 30946

Table of Contents

List of Figures

1. Introduction

The Korea Aerospace Research Institute (KARI) is developing the Korea space launch vehicle (KSLV)-II with the goal of launching in 2021 after the success of the KSLV-I launch in 2013. And the KSLV-II is being developed considering the long term plan of Korean government to possess the ability to launch the space vehicle without any help of other countries. Korean government will build a base to entry into the global launch service market by retaining reliability and competitiveness for the KSLV-II launch service by 2025. Korean government will also increase the reliability more by launching KSLV-II to the moon for the exploration and transfer technologies about the KSLV-II launch service such as the manufacture of sub-parts, the system integration and the launch operation to the Korean industries to achieve this plan.

The KSLV-II is a three-stage launch vehicle, approximately 47.2 m in length, 3.5 m in diameter, and a weight of about 200 tonf. A 1500 kg payload will be placed on a low earth orbit of 600 to 800 km using the KSLV-II. In order to verify the performance of the turbo-pump type 75 tonf liquid engine developed by an independent technology prior to the KSLV-II flight test in 2021, the test launch vehicle(TLV), with a total length of 25.8m, a diameter of 2.6m, and at total weight of 52.1 tonf, was developed. As the only objective of the TLV is to verify the performance of the 75 tonf liquid engine, it will not place a payload on the specified orbit; it will reach an altitude of 177 km and then freely fall to terminate the mission [1-4].

In order to reduce the development cost and to minimize the development period in the TLV were directly used the second and third stage of the KSLV-II, without changing its configuration as much as

possible, except for the first stage of KSLV-II, and utilizing the technology and parts applied to the development of the KSLV-II. However, the shape was changed for some parts since the modification was inevitable (Fig. 1). First, the payload and 7 tonf engine system of the KSLV-II 3rd stage were deleted, and the aftbody of the KSLV-II 2nd stage was changed from the cone shape to the cylinder shape owing to an interference problem with the launch pad. In the meantime, as the development purpose of TLV is the performance test of the 75 tonf liquid engine, only the nozzle length is adjusted in order to have the ground launch available.

For the charge and discharge of the propellant, the TLV uses the umbilical plate mounted on this launch vehicle and the retraction device on the launch pad that connects to the umbilical plate. This propellant supply system is composed of the umbilical plate and retraction device, and it is the same system used in the KSLV-II at the beginning of the TLV development (Fig. 2). As the KSLV-II propellant supply system is used, the umbilical plate protrudes significantly out the aft body of the TLV.

Fig. 3 (A) shows the schematics of the connection between the umbilical plate and the retraction device before launch. When the second stage of the KSLV-II is connected to the launching pad, the umbilical plate slightly from the aft body is “AA” in Fig. 3 because the aft body has a frustum shape rather than a cylindrical shape. However, the umbilical plate of the TLV on the cylindrical aft body increases in thickness by the additional amount “BB” in Fig. 3 if the same retraction device is used. Fig. 3 (B) shows the shape of the umbilical plate on the aft body of the TLV after launch.

The umbilical plate is an essential component for the launch vehicle using the liquid engine. The flow around the umbilical plate

has normally adverse effects on the aerodynamic characteristics in case of the launch vehicle using the small aspect ratio and the large umbilical plate like the TLV. Therefore, it is necessary to predict clearly the aerodynamic characteristics around the large umbilical plate since the aerodynamic characteristics affect the controllability of this launch vehicle.

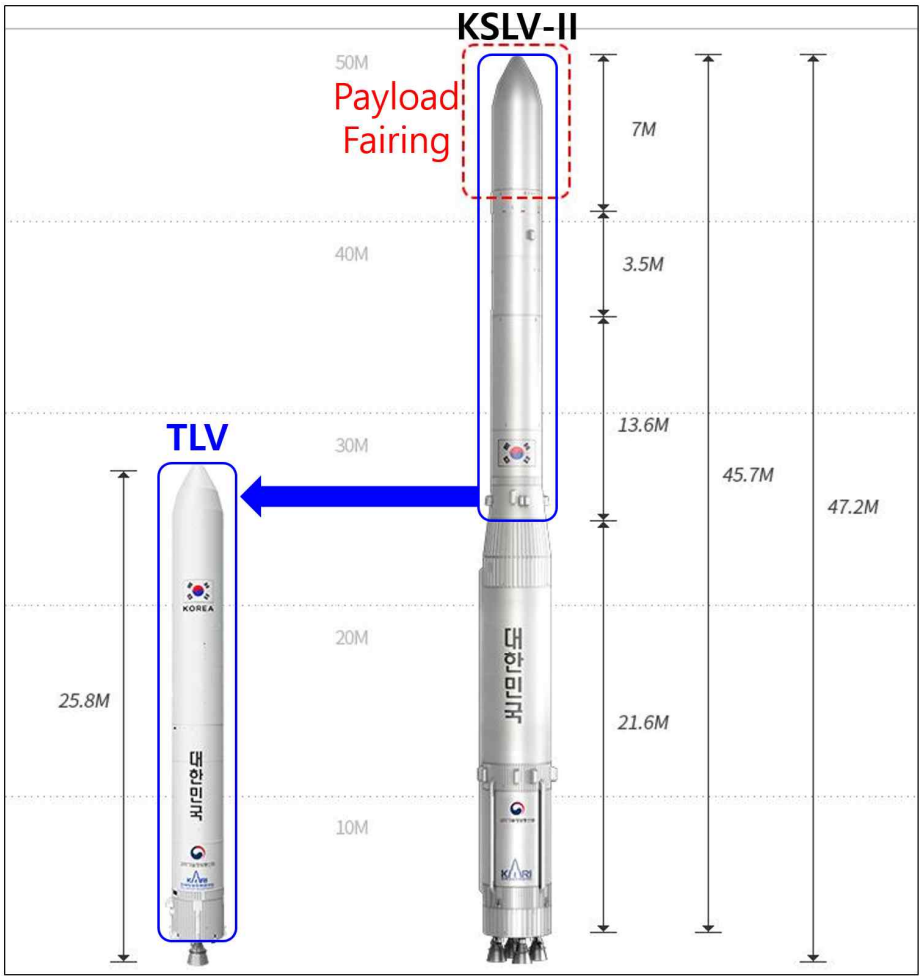

Fig. 1. Configuration of KSLV-II and TLV

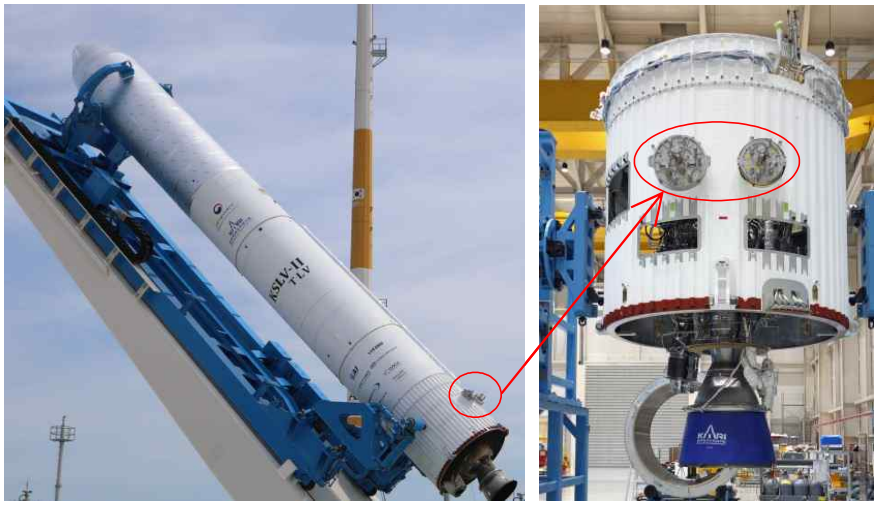

Fig. 2. Configuration of TLV umbilical plate

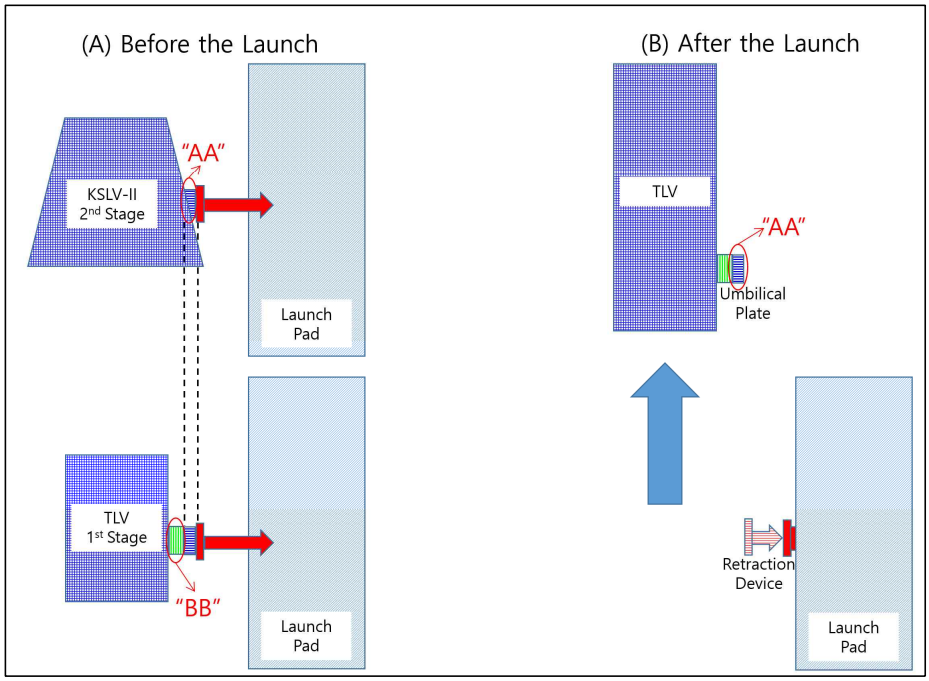

Fig. 3. Configuration of umbilical plate and retraction device

2. Research objectives

The wind tunnel test, the empirical data base and the CFD analysis are generally applied to predict the aerodynamic characteristics of the launch vehicle.

An approach using the empirical data base can produce the aerodynamic data base quickly, but this approach is less accurate while the wind tunnel test can produce more accurate data, but cost and time are increased. Therefore, CFD analysis is mainly used to predict the aerodynamic characteristics of the launch vehicle.

The CFD analysis for the launch vehicle with the external and complex protuberances is so much time consuming process because of the increase of the number of the mesh around the launch vehicle. Therefore, at the beginning of the development process for the launch vehicle, the configuration of all external protuberances were ignored since the configuration of the protuberances was not determined precisely and the simple shape of the launch vehicle as the body of revolution shape was considered to predict the aerodynamic characteristics quickly. The CFD analysis for this simple body of revolution was firstly performed to make the aerodynamic data. The influence of the external protuberances was added using the correction factors from the wind tunnel test after the CFD analysis. This approach has the simplicity of analysis, but the accuracy is poor and the influence of each protuberance cannot be accurately reflected. As the method of constructing the unstructured grid system in the boundary layer develops, it is possible to quickly construct the unstructured grid system around a small and complex protuberance. And due to the growth of the parallel computation technique and the improvement of

the performance of the computing power, the CFD approach can be applied to the aerodynamic analysis for the launch vehicle considering all external structures while it is difficult to realistically model the shape of all protuberances due to the difficulty of manufacturing the wind tunnel model in case of the wind tunnel test [5-15].

For the calculation of the aerodynamic characteristics of the TLV, the structured grid system was applied to the body of revolution at the beginning of the TLV development and the effect of the external protuberances from the wind tunnel test was corrected after the CFD analysis. The direct CFD analysis for the TLV considering all external protuberances is applied without compensating the effect of the external structures from the wind tunnel test as the improvement of the CFD analysis skill which can predict the aerodynamic characteristics around the complex geometry in the late of the TLV development. At the beginning of the TLV development, as it was not possible to predict the exact effect of the external structures, the effect of the roll angle was also not be ignored. If the external structures are properly positioned in the circumferential direction of the launch vehicle, the effect of the roll angle may be negligible. However, if a large structure such as an umbilical plate is attached asymmetrically in the circumferential direction, the effect of the roll angle can not be ignored. In particular, in case of the launch vehicle with the low aspect ratio, the influence of the flow around the large structure on the overall aerodynamic characteristics is greater than that of the launch vehicle with the large aspect ratio.

Even during the TLV development, the aerodynamic data with the initial TLV body of revolution shape and the correction of the external protuberance effect were applied by the late of the TLV development. But the aerodynamic prediction for the final configuration of the TLV

must be performed before the TLV flight test to confirm finally the flight performance of the flight model. And the CFD prediction was conducted considering the configuration of the TLV with all external protuberances for the first time for the TLV development. For the analysis of the aerodynamic characteristics of the final TLV configuration, it was confirmed that the change in the normal force was very large according to the variation of the roll angle under the maximum dynamic pressure condition. As the normal force changes, the center of pressure changes accordingly, which affects the flight stability of the TLV. As a result of performing the aerodynamic characteristics analysis on the final configuration and analyzing the flight stability, it was confirmed that the flight test for the designated trajectory can be fail due to insufficient flight control power. While analyzing the cause of the normal force change, it was discovered that the flow around the umbilical plate on the rear part of the TLV caused a change in the normal force at the rear part of the TLV to affect flight stability. Afterwards, the umbilical plate shape of the TLV was changed rapidly, and the aerodynamic characteristics analysis was performed on the new shape of the umbilical plate to confirm flight stability again. On November 28, 2018, The TLV flight test with the modified umbilical plate was performed and the flight test was successfully completed without any flight stability problem. When using existing systems such as the launch vehicle such as the TLV for a simple flight test, the unusual external structure can be attached to the launch vehicle. In particular, the smaller the aspect ratio, the greater the impact of these protuberances on the overall aerodynamic properties of the launch vehicle. The effect of the protuberance on the overall aerodynamic characteristics decreases as the aspect ratio increases for the launch vehicle which has the same diameter and protuberance. In addition, the

overall weight of the launch vehicle increases as the aspect ratio increases for the same diameter. Therefore the engine thrust should also grows to launch the heavier vehicle. The control torque by the engine thrust to make the reverse moment to remove the aerodynamic torque fully increases as the engine thrust increases. And the possibility to yield the lack of the controllability of the launch vehicle decreases during the flight.

The specification of the launch vehicles in the world can be obtained in Reference [11]. In this book, the minimum aspect ratio of the launch vehicles is about 5.5 and the maximum aspect ratio of the launch vehicles is approximately 20. And the averaged aspect ratio is about 14. The aspect ratio for 90% of the launch vehicles is more than 10. Therefore, the low aspect ratio launch vehicle mentioned in this paper can be the launch vehicle which has the aspect ratio of approximately 10 or less than 10 including KSLV-II TLV.

The studies related to the TLV predicted the heat flux of its engine plume and analyzed the performance of the heat shield by conducting a CFD analysis and a thermal analysis [16, 17]. The vent valve was designed by analyzing the external aerodynamic characteristics of the TLV during the flight using a CFD analysis and the vent characteristics of the internal compartment inside the TLV [18, 19]. Previous studies on the TLV did not include the prediction of aerodynamic characteristics for the full configuration of the TLV during the flight.

In a previous study on the aerodynamic characteristics of the low aspect ratio launch vehicle, the aerodynamic characteristics of Epsilon at max Mach 1.5 near the maximum dynamic pressure are predicted by CFD analysis and wind tunnel test [20]. The flow characteristics around the protrusions of the low aspect ratio launch vehicle were analyzed

according to the change in Reynolds number. In a prior study [21], it was investigated how the aerodynamic coefficient changes owing to the change in flow characteristics around the fin by using the flow around the small attitude control device of a low-aspect ratio missile, not of the launch vehicle. Previous researchers on aerodynamic characteristics of the low aspect ratio launch vehicle presented only the effects of small protuberances such as stringers, flanges, cable ducts and the attitude control device on the aerodynamic characteristics of the launch vehicle. And the prior researches for the single external structure on the plate were conducted [22-24]. Although many researchers have studied aerodynamic characteristics for the low aspect ratio launch vehicle with these protuberances, these researches have not been conducted on how the control ability of this launch vehicle changes due to the aerodynamic characteristics around the large protrusion such as umbilical plates.

In fact, the single umbilical plate of an elliptical shape of which the height was relatively high in the initial development stage of the TLV was applied. After the calculation of the control ratio, the height of an elliptical umbilical plate was reduced in the middle of the development stage because of the problem of the controllability. But a lower elliptical umbilical plate was changed to two round-type umbilical plates in the final development stage because of the manufacturing difficulty without the change of the height.

In this study, using a CFD analysis, we investigate the effect of the umbilical plate on the aerodynamic characteristics when the umbilical plate is exposed outside of the low aspect ratio launch vehicle as the TLV aft body. Furthermore, when the existing mechanical design of the KSLV-II is used, as in the case of the TLV umbilical plate, the influence of the flow characteristics around the

existing umbilical plate on the controllability of the launch vehicle is analyzed, enabling its consideration when designing the low aspect ratio launch vehicle based on the same concept, such as the TLV.

3. Method and Validation

3.1. Simulation methods

The wind tunnel test and CFD analysis are normally applied to predict the aerodynamic characteristics of the launch vehicle [25-27]. CFD analysis is mostly used to get the aerodynamic data because this approach can obtain the reliable aerodynamic data of the launch vehicle relatively easily compared with the wind tunnel test.

In this study, A CFD analysis was applied to predict the aerodynamic characteristics of the low aspect ratio launch vehicle. The CFD analysis was performed using the commercial software STAR-CCM+. The governing equations satisfying the mass, momentum and energy conservation to analysis the aerodynamic characteristics of the launch vehicle in this study are as follows [28-31].

- Conservation of Mass

$$\frac{\partial \rho}{\partial t} + \nabla \cdot (\rho \mathbf{v}) = 0 \tag{1}$$

$\mathbf{v}$: the continuum velocity

- Conservation of Linear Momentum

$$\frac{\partial \rho \mathbf{v}}{\partial t} + \nabla \cdot (\rho \mathbf{v} \otimes \mathbf{v}) = \nabla \cdot \sigma + \mathbf{f_b} \tag{2}$$

$\mathbf{f}_b$: the resultant of the body forces per unit volume

σ : the stress tensor, $\sigma = -p\mathbf{I} + \mathbf{T}$

$\mathbf{T}$: the viscous stress tensor

- Conservation of Energy

$$\frac{\partial \rho \mathbf{E}}{\partial t} + \nabla \cdot (\rho \mathbf{E} \mathbf{v}) = \mathbf{f}_b \cdot \mathbf{v} + \nabla \cdot (\mathbf{v} \cdot \sigma) - \nabla \cdot \mathbf{q} + S_E \quad (3)$$

$\mathbf{E}$: the total energy per unit mass

$\mathbf{q}$: the heat flux

S_E : an energy source per unit volume

Compressible Reynolds-averaged Navier-Stokes equations are solved numerically in a finite volume framework with the second order Advection Upstream Splitting Method(AUSM)+ flux-vector splitting scheme and the k-ω Shear Stress Transport(SST) turbulence model for steady state [32-34].

3.2. Validation case

Numerical approach above mentioned is validated for the TLV with various cowls, cable ducts and stringers for structural reinforcement. Fig. 4 shows the scaled wind tunnel model with external attachments around the initial configuration of the TLV. The wind tunnel test was carried out in the transonic region and the CFD analysis was performed using STAR-CCM+ for the same wind tunnel test model and flow conditions (Fig. 5). Fig. 6 to Fig. 9 show the comparison of the axial force coefficient (CA), the normal force coefficient (CN), the pitching moment coefficient (CM) from the base of the TLV and the non-dimensional center of pressure (XCP/D) as Eq. (4) between the wind tunnel test results and the numerical analysis results. The maximum error of the aerodynamic coefficients is approximately 5% and the discrepancy of the center of pressure is less than 0.5 caliber. Therefore, the two results are empirically in good agreement [20, 35-39].

$$XCP/D = \frac{CM}{CN} \tag{4}$$

Based on the results of the wind-tunnel test model, aimed at verifying the TLV configuration considering both the protrusions and stringers, this study confirms that the CFD analysis using STAR-CCM+ is able to analyze the aerodynamic characteristics of the shape that considers only one umbilical plate on the low aspect ratio launch vehicle.

Fig. 4. TLV wind tunnel test model

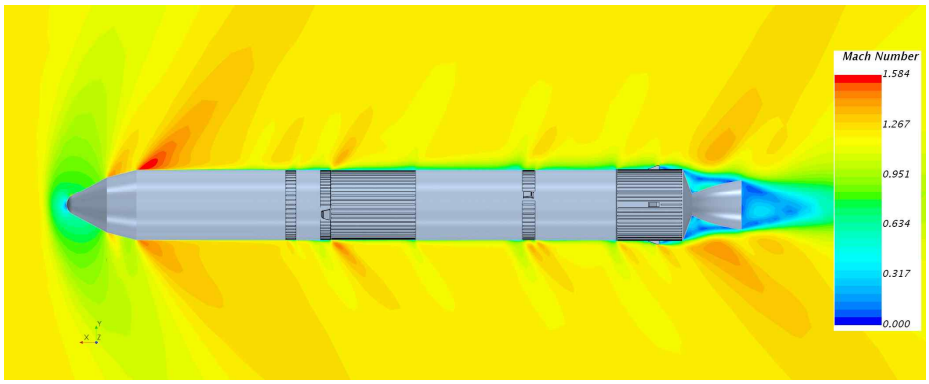

Fig. 5. Mach number contour of TLV wind tunnel test model (M_{∞}=1.2, α=5°)

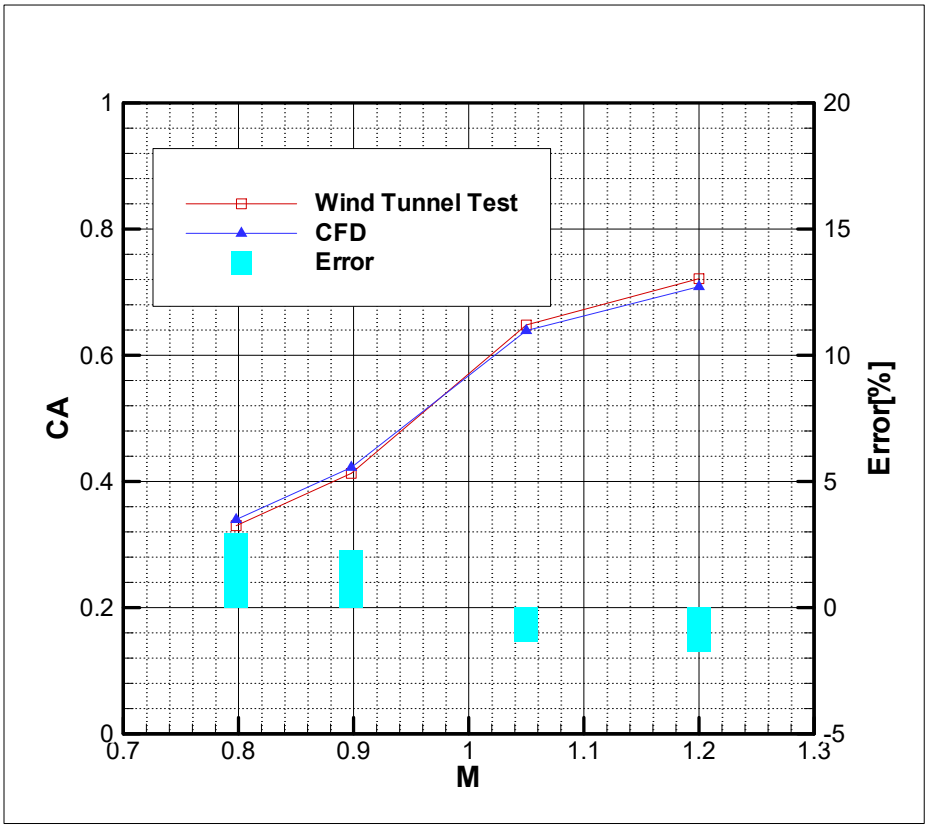

Fig. 6. Comparison between wind tunnel test and numerical simulation (CA, $0.8 \leq M_{\infty} \leq 1.2$, $\alpha=5°$)

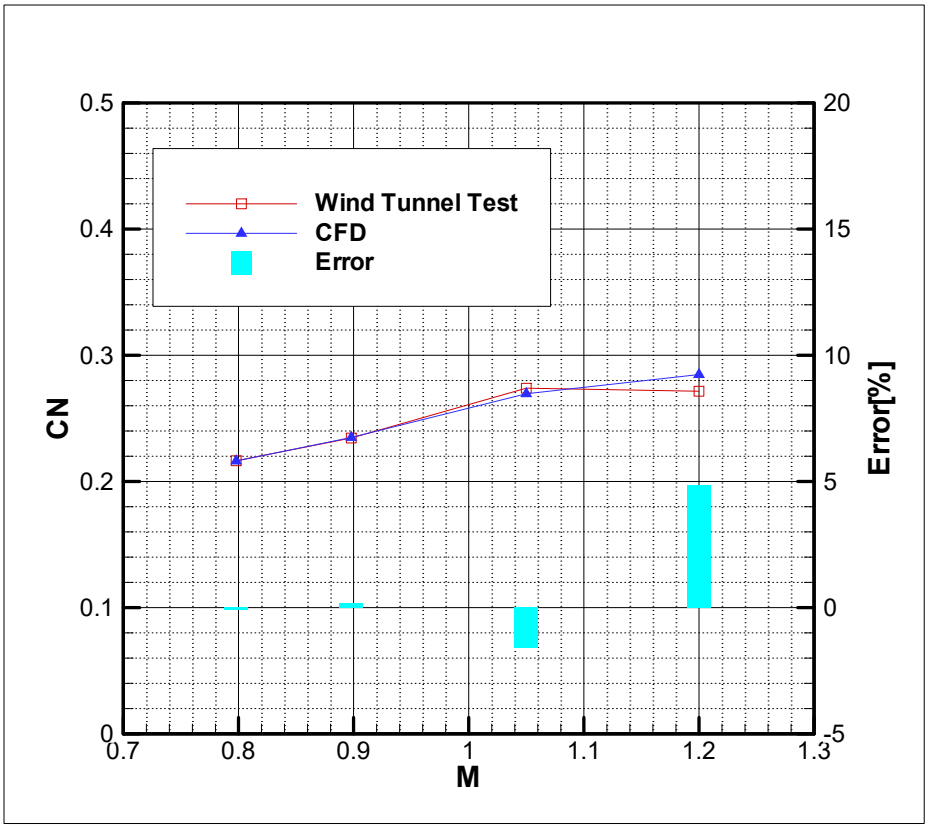

Fig. 7. Comparison between wind tunnel test and numerical simulation (CN, $0.8 \leq M_{\infty} \leq 1.2$, $\alpha=5°$)

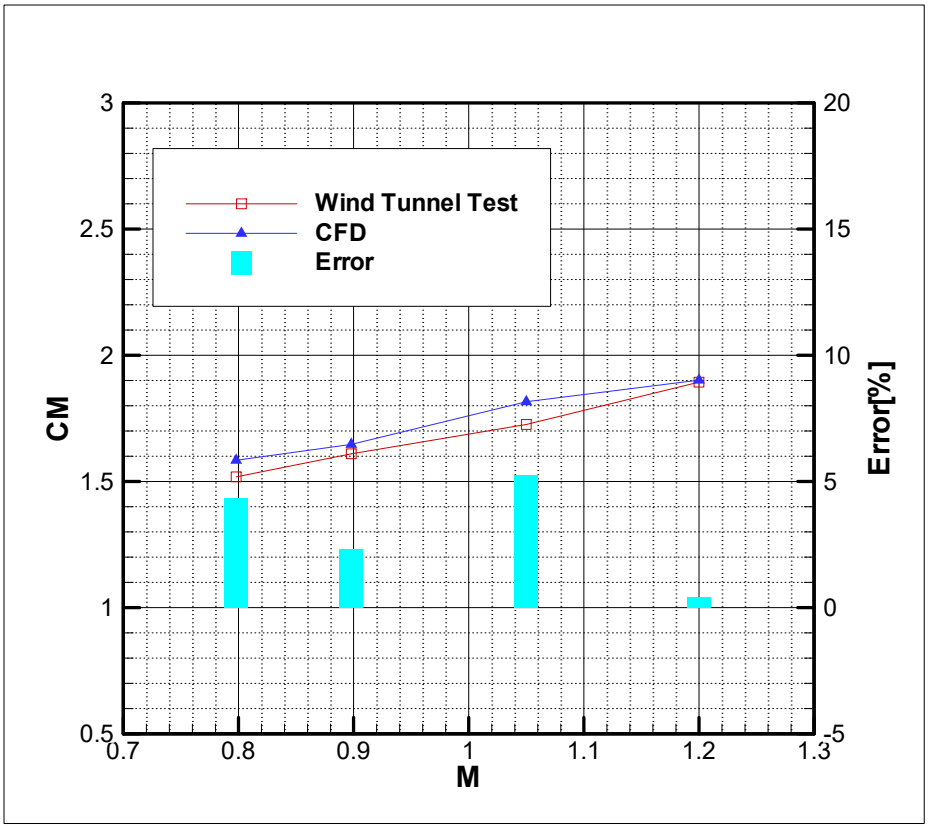

Fig. 8. Comparison between wind tunnel test and numerical simulation (CM, $0.8 \leq M_{\infty} \leq 1.2$, $\alpha=5°$)

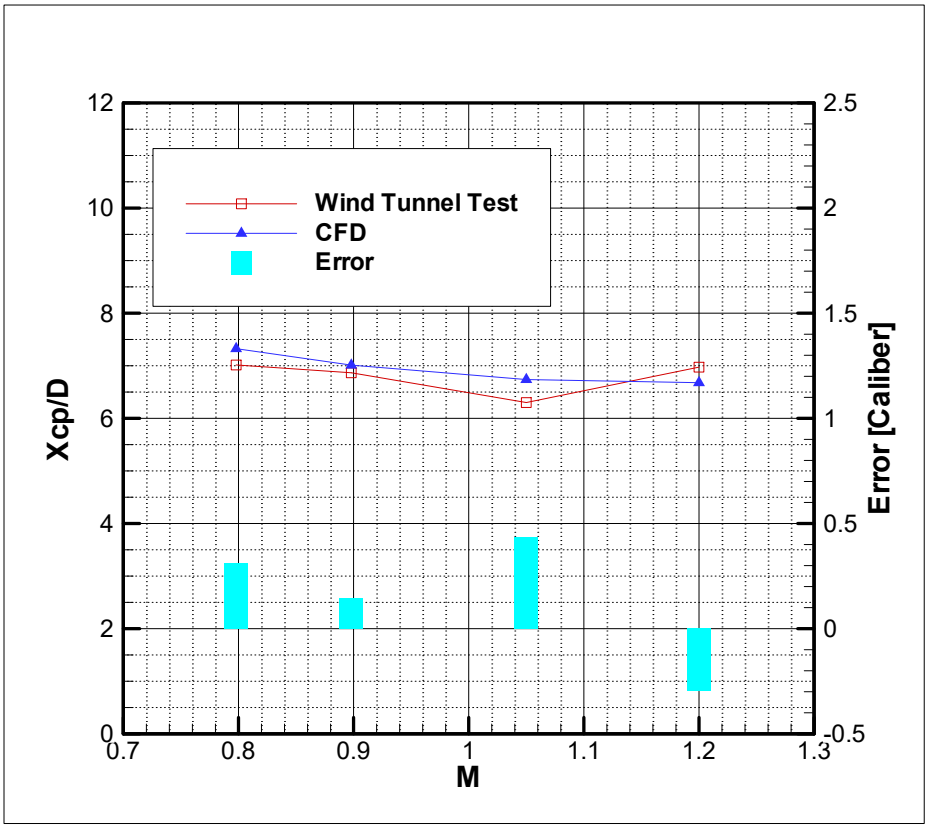

Fig. 9. Comparison between wind tunnel test and numerical simulation (XCP/D, $0.8 \leq M_{\infty} \leq 1.2$, $\alpha=5°$)

4. Simulation results and analysis

4.1. Effects of flight trajectories regard to aerodynamic characteristics

4.1.1 Aerodynamic characteristics for flight trajectory using constant Reynolds number and temperature

The exact shape of the KSLV-II TLV was not disclosed owing to a confidentiality problem, and thus, the analysis was performed for the "Resemblant TLV," which has a similar configuration to that of the TLV (Fig. 10). The radius of the "Resemblant TLV" is 2.5 m and its aspect ratio is 10. The shape of the umbilical plate was simply modeled as shown in Fig. 10. The initial shape of the umbilical plate for the TLV was elliptical at the beginning of development, but it changed into two small round-type plates of which the height is lower than that of the elliptical umbilical plate in the final flight model of the TLV during the system integration (Fig. 2). In this work, the elliptical-type umbilical plate is modeled and analyzed since the effect of the aerodynamic characteristics around the elliptical-type umbilical plate is larger than that around two round-type umbilical plates.

The polyhedral type grid system, including the "Resemblant TLV" umbilical plate, is composed of 30 prism layers inside the boundary layer. The first-normal grid point in the wall unit, y + is under 1.0 and the spherical far field with the diameter of 100 Resemblant TLV lengths is applied in this study. The total number of grids in the system is 5,880,000.

It is known that complex vortex structure around a large protrusion

may never give grid convergence [20]. However, the grid convergence study around the umbilical plate was performed as shown in Fig. 11, and the optimal grid was applied in this study.

And the efficiency of computation is increased by using the parallel processing method because the number of grids increases excessively when considering the protrusion outside the “Resemblant TLV”. It took approximately 1.45 second per iteration in case of using 200 cores for each case. And the aerodynamic force and moment coefficients are considered to be converged if there is no change in three decimal place (Fig. 12).

It is expected that the flow conditions of the launch vehicle range from the Mach number of 0.2 to 3.0. As the exact flight path of the TLV cannot be disclosed, the Reynolds numbers is estimated to be 10,000,000. The angle of attack is 5 degrees. The pitching moment was calculated from the base of the “Resemblant TLV.”

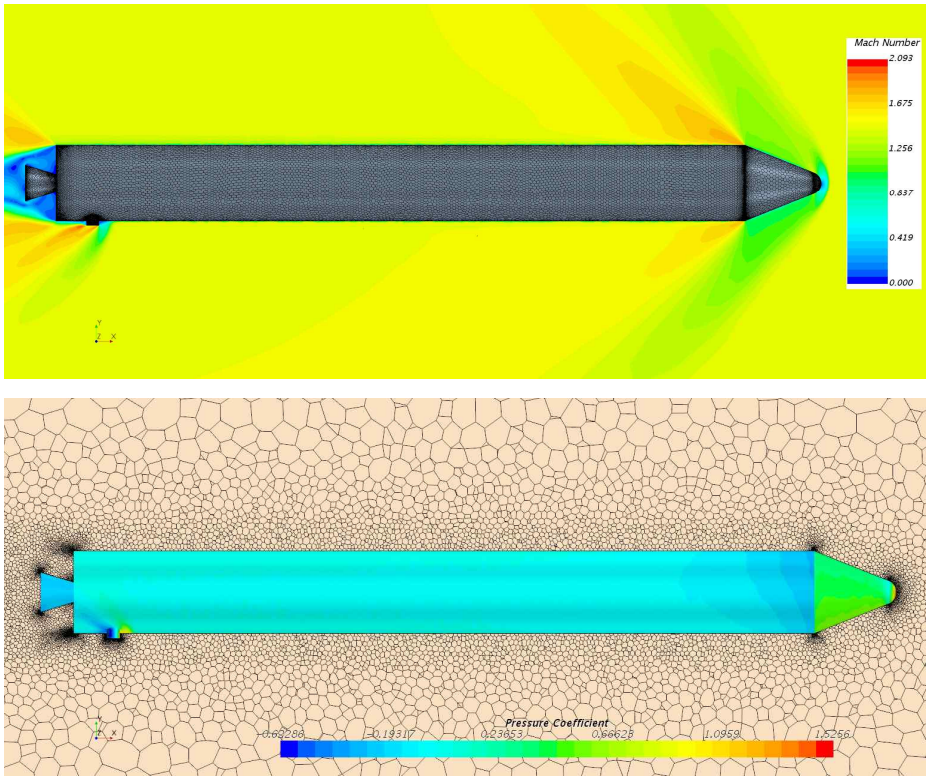

Fig. 10. Configuration of "Resemblant TLV" and numerical simulation result (M_∞=1.5, α=5°, ϕ=0°)

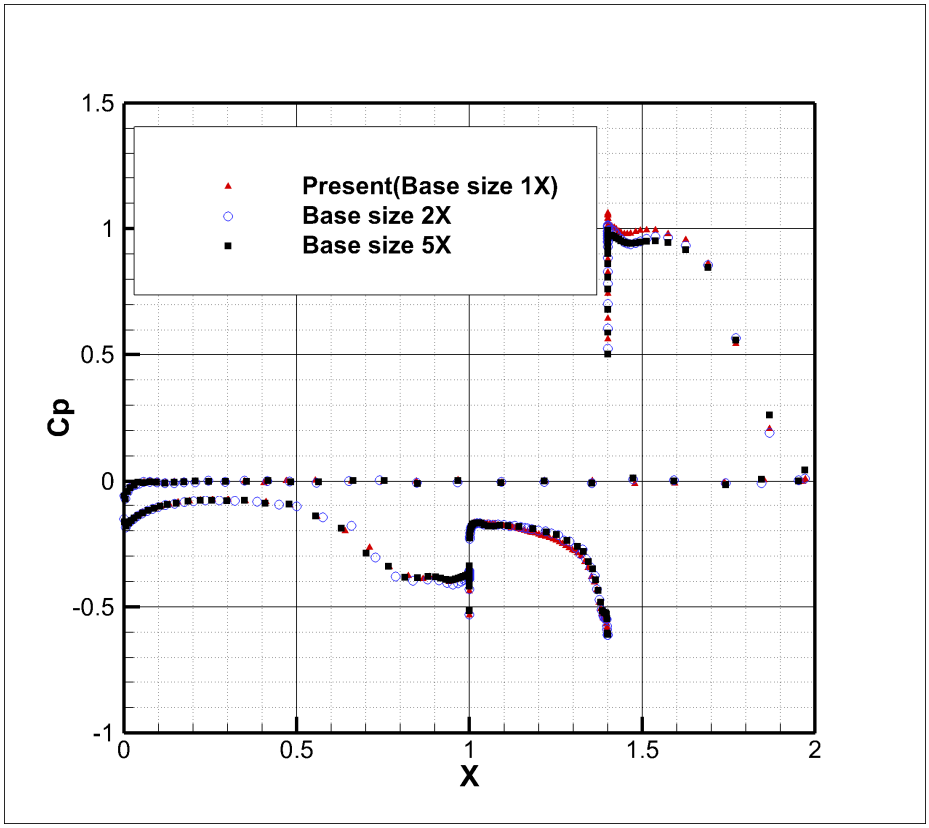

Fig. 11. Cp around for the umbilical plate for the grid test (M_∞=1.5, α=5°, ϕ=0°)

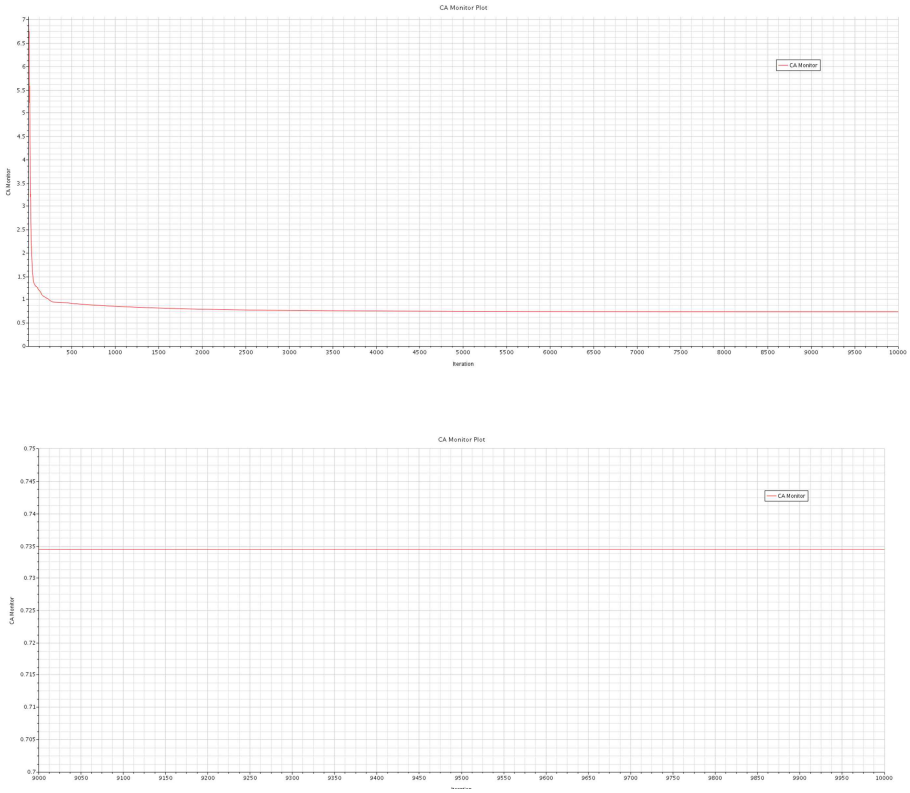

Fig. 12. Convergence test of the aerodynamic coefficient (M_{∞}=1.5, α=5°, ϕ=0°)

Fig. 13 to Fig. 16 show the aerodynamic coefficients predicted for a deviation of 30° in roll angle according to the Mach number. The axial force coefficient (CA) does not change significantly with changes in roll angle. However, it can be seen that the normal force coefficient (CN) greatly changes with the variation in roll angle. The difference between the maximum and minimum CN with changes in roll angle is large in the subsonic region and increases up to Mach number 1. However, this difference suddenly decreases beyond Mach 1 to a minimum at Mach 1.5; from Mach 1.5, this difference increases and remains almost constant above Mach 2.

Fig. 17 shows that in the case of Mach 0.8 and roll angle 0° there is a pressure drop zone in the large area behind the umbilical plate on the windward side. As a result, a negative normal force is generated in this region and the overall normal force is decreased. On the contrary, when Mach number is 0.8 and roll angle is 180°, the umbilical plate is on the leeward side and a positive normal force is generated owing to the influence of the low pressure area around the rear region of the umbilical plate (Fig. 18). However, when the umbilical plate is on the leeward side, the influence of the wind is reduced compared to the situation when the umbilical plate is on the windward side, and the low-pressure area of the umbilical plate is reduced. As a result, the amount of added vertical force is not particularly large. Fig. 19 shows the result of comparing the normal forces of divided component of the "Resemblant TLV," except for the payload fairing and nozzle, in half (dividing it into the front and rear of the cylindrical body). It can be seen that a negative normal force acts on the rear part of the cylindrical body at the roll angle of 0° and a positive normal force acts at the roll angle of 180°. Fig. 20 shows that, as the roll angle increases, the negative normal force at roll angle 0° changes gradually

to a positive normal force.

The supersonic region shows a positive normal force owing to the increase in pressure as a result of the effect of shock waves in front of the umbilical plate on the windward side at Mach 1.5 and roll of 0°. Of course, there is a region where the pressure drops owing to the expansion wave behind the umbilical plate, but this pressure decrease is smaller than the pressure increase at the rear end of the shock wave, and thus, the overall normal force increases. However, if there is an umbilical plate in the leeward, a negative normal force of about 100 N occurs in the rear part of the body (Fig. 21 to Fig. 23).

Meanwhile, regarding the pitching moment coefficient (CM), its sensitivity to changes in roll angle is low, as in the case of the axial force coefficient. The center of the pitching moment is the base of the "Resemblant TLV" and the distance to the umbilical plate from the base is short; hence, a large change in moment by the umbilical plate does not exist. Therefore, the change in pitching moment by the normal force difference owing to the change in pressure around the umbilical plate is small.

However, the non-dimensional center of pressure (XCP/D), which is the value obtained by dividing the pitching moment coefficient by the normal force coefficient, is greatly influenced by the changes in roll angle with a given Mach number owing to the change in normal force coefficient. The difference of the non-dimensional center of pressure was larger in the transonic region than that in the supersonic region in Fig. 16.

Fig. 24 to Fig. 27 show the aerodynamic coefficient according to the change in roll angle change and predicted by deviations of 15° in roll angle. The overall change pattern is similar to that in Fig. 13 to Fig. 16, where the change in roll angle is shown by decrements of

15°. In the case of 0° roll angle, which is the nominal flight attitude condition, the change in the center of pressure is the largest, and it is the smallest at a roll angle of 75°.

If the center of pressure moves forward to the payload fairing in accordance with the change in roll angle, it may cause problems in longitudinal controllability. The control ratio (CR), which is the controllability design requirement used in the launch vehicle design, is expressed as the ratio of control torque (CT) by thrust to aerodynamic torque (AT) (Fig. 28 and Eq. (5)). The control ratio is set at the initial design status of the launch vehicle, and the NASA Marshall Space Flight Center (MSFC) empirically designs the CT to be 1.5 times, or more, the AT [40]. Given that the TLV is controlled using the thrust vector control, if the nozzle deflection angle for the thrust vector control (TVC) is set to 6°, the thrust of the "Resemblant TLV" is set to 75 tonf, the center of gravity is set to the center of the cylinder body and the gimbal point is set to 0.5 m from the base of the "Resemblant TLV", the CR is obtained as in Fig. 29. It can be seen that, under many conditions, the CR is less than 1.5 when applying the design requirements of the NASA MSFC to the CR obtained here. In many cases, even with a Mach number of 1.5, the CR is less than 1.5 near the maximum dynamic pressure condition, which is considered an important variable in the launch vehicle control design. In this case, there is no margin in the control moment capable of canceling the moment owing to the aerodynamic force, which may cause problems in the launch vehicle control. In extreme cases, the launch vehicle could not fly with a designed trajectory. To obtain a CR higher than 1.5 for all the Mach number and roll angle conditions, with the configuration and flow conditions used in this work, the nozzle deflection angle should increase to at least 17° or the thrust should raise to more than

200 tonf. In this case, the size and/or weight of the TVC related equipment or engine will increase, and the entire design should be renewed. Therefore, to take advantage of the existing large protuberances on the launch vehicle, such as the umbilical plate, to minimize the TLV development costs, considerable attention is needed. If the umbilical plate is on the aft body of a launch vehicle such as the TLV, the height of the umbilical plate should be reduced to decrease the effect of aerodynamic characteristics near the umbilical plate on the launch vehicle controllability.

$$CR = \frac{Contol\,Torque\,(CT)}{Aerodynamic\,Torque\,(AT)} = \frac{Thrust \times \sin(\delta) \times L_{Gimbal}}{NormalForce \times L_{CP}} \qquad (5)$$

$$NormalForce = CN \times DynamicPressure \times ReferenceArea$$

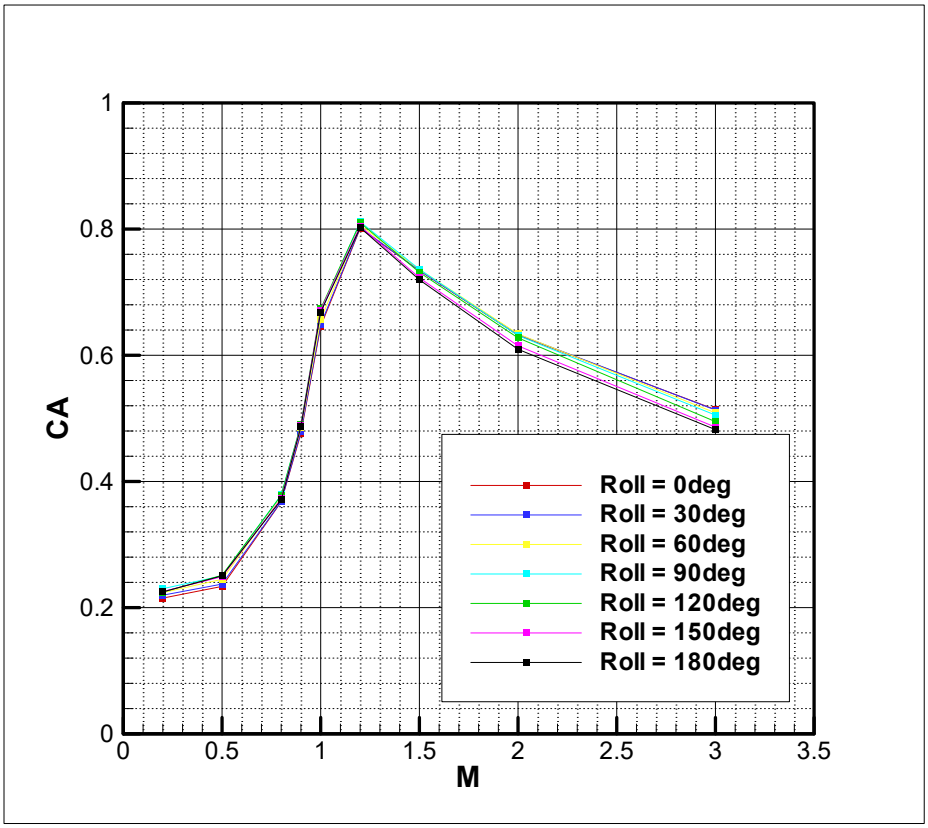

Fig. 13. Axial force coefficient of "Resemblant TLV" ($0.2 \leq M_\infty \leq 3.0$, $\alpha=5°$, $\triangle\phi=30°$)

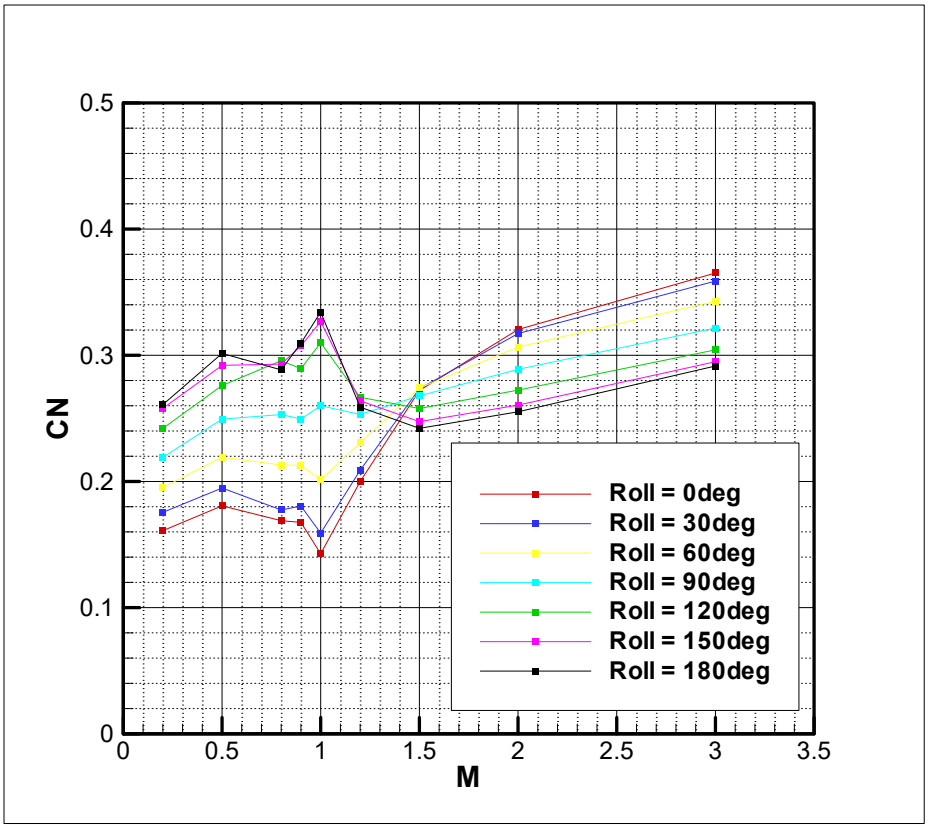

Fig. 14. Normal force coefficient of "Resemblant TLV" ($0.2 \leq M_{\infty} \leq 3.0$, $\alpha=5°$, $\triangle\phi=30°$)

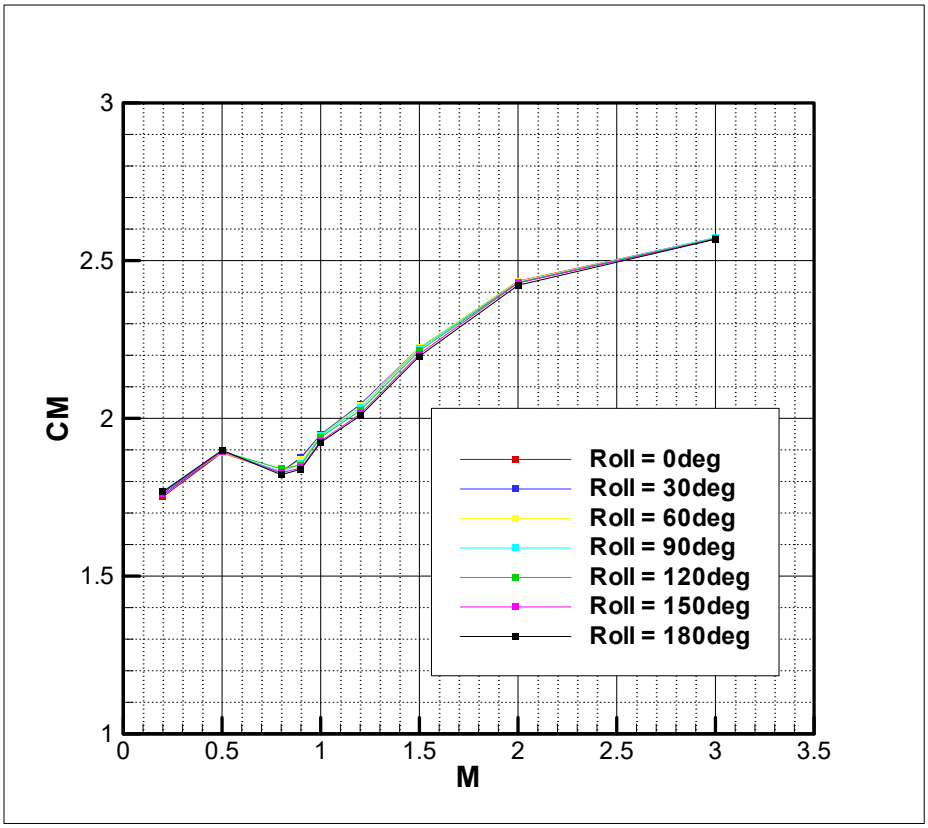

Fig. 15. Pitching moment coefficient of "Resemblant TLV"
($0.2 \leq M_{\infty} \leq 3.0$, $\alpha=5°$, $\triangle\phi=30°$)

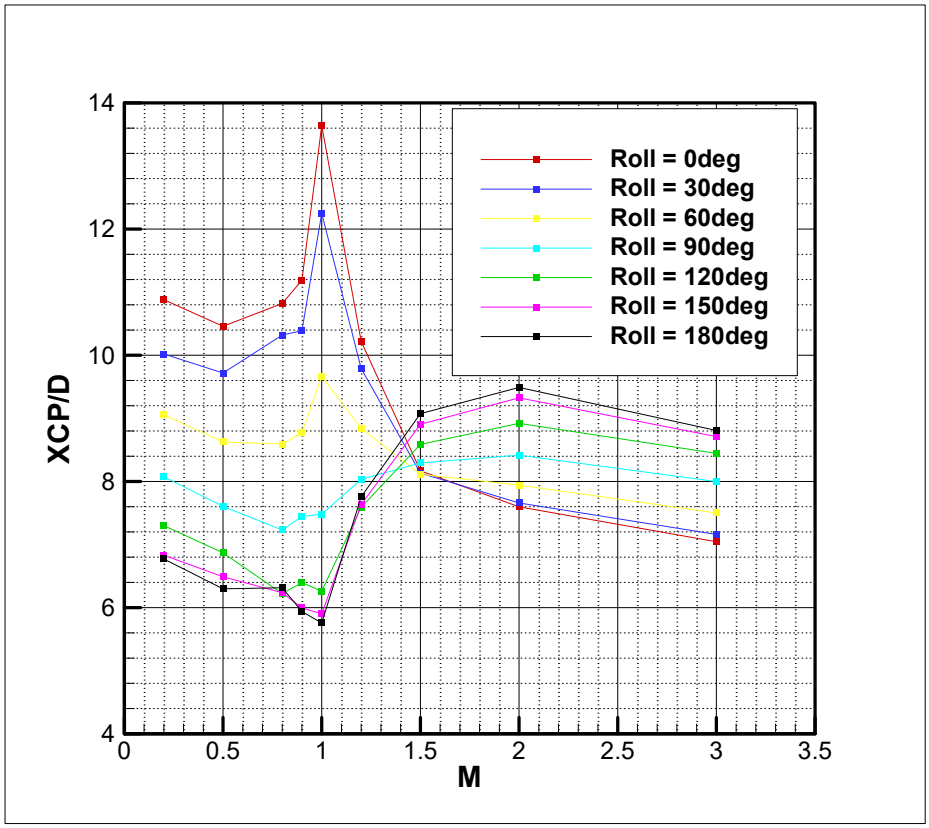

Fig. 16. Center of pressure of "Resemblant TLV" ($0.2 \leq M_{\infty} \leq 3.0$, $\alpha=5°$, $\triangle\phi=30°$)

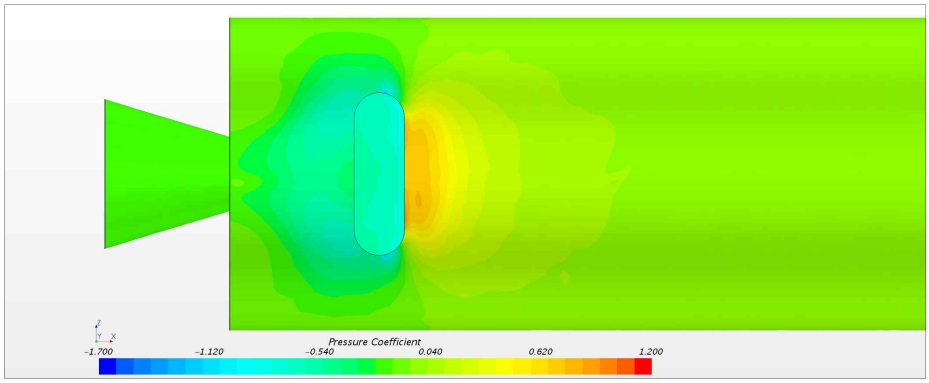

Windward

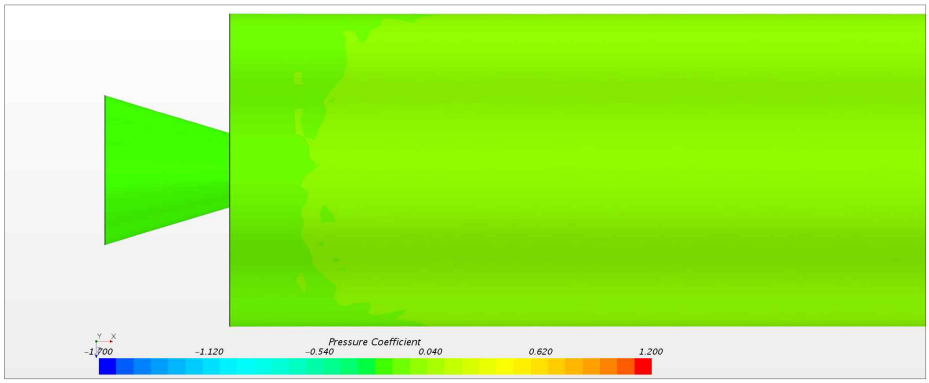

Leeward

Fig. 17. Comparison of surface pressure for "Resemblant TLV" (M_{∞}=0.8, α=5°, ϕ=0°)

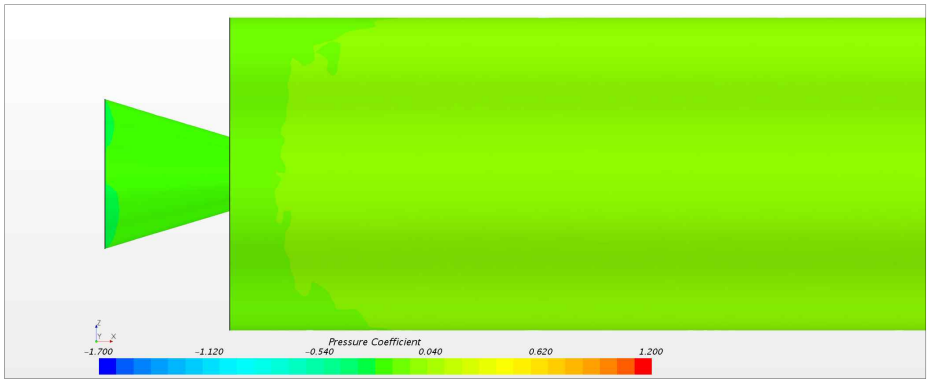

Windward

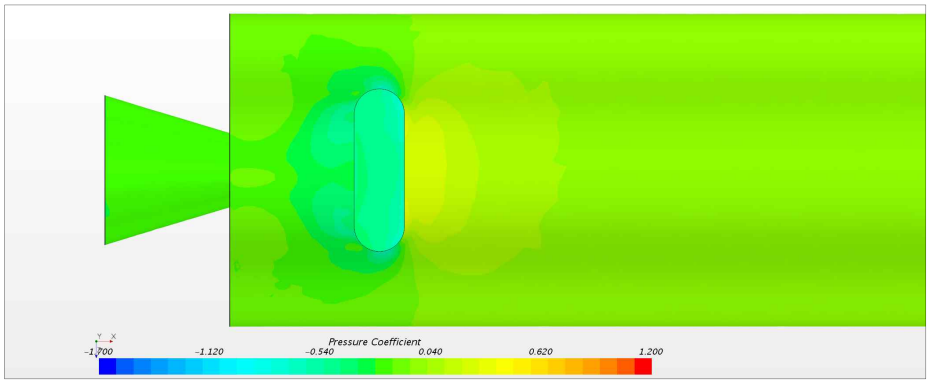

Leeward

Fig. 18. Comparison of surface pressure for "Resemblant TLV" (M_∞=0.8, α=5°, ϕ=180°)

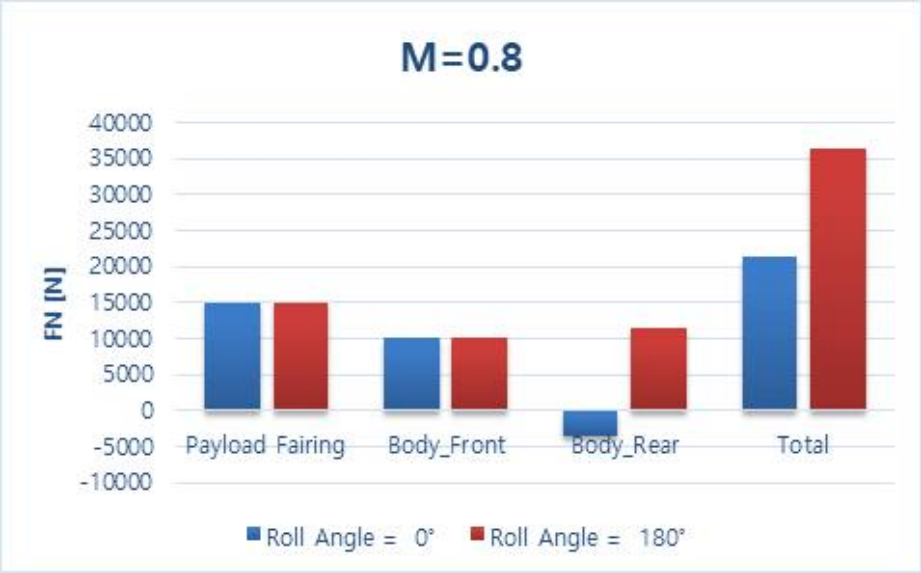

Fig. 19. Comparison of component normal force for "Resemblant TLV" (M_∞=0.8, α=5°)

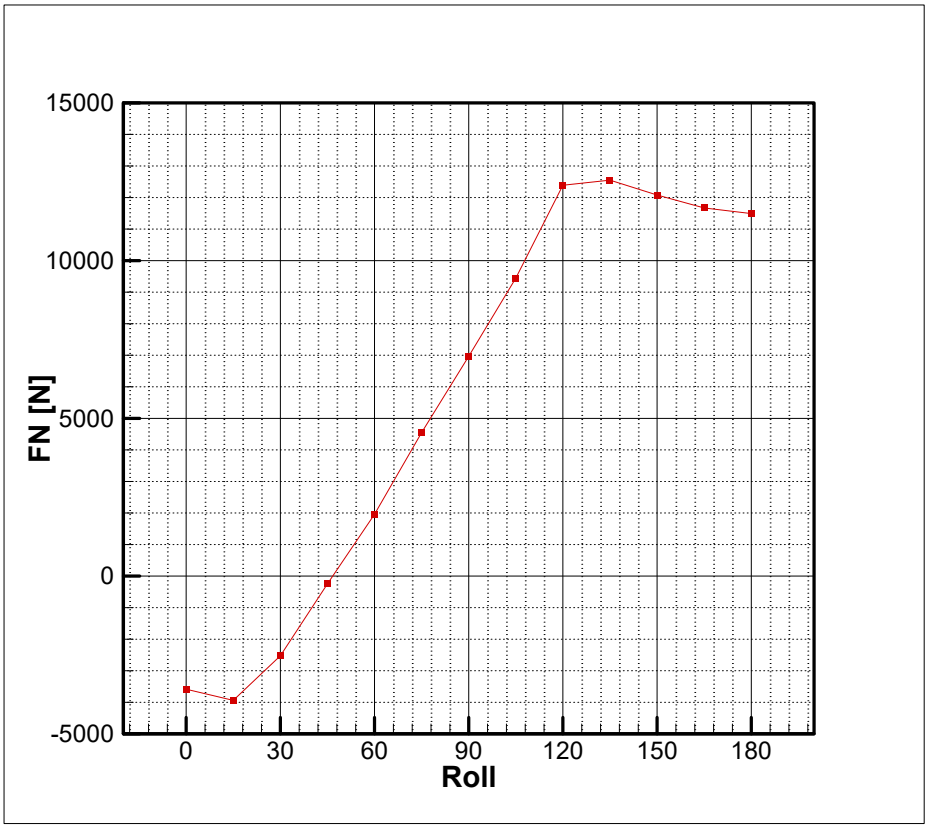

Fig. 20. Variation of normal force for body rear of "Resemblant TLV" (M_∞=0.8, α=5°, ϕ=0°)

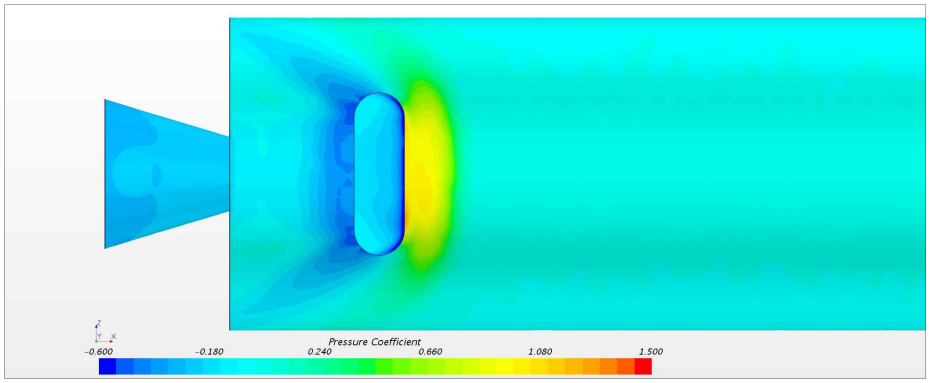

Windward

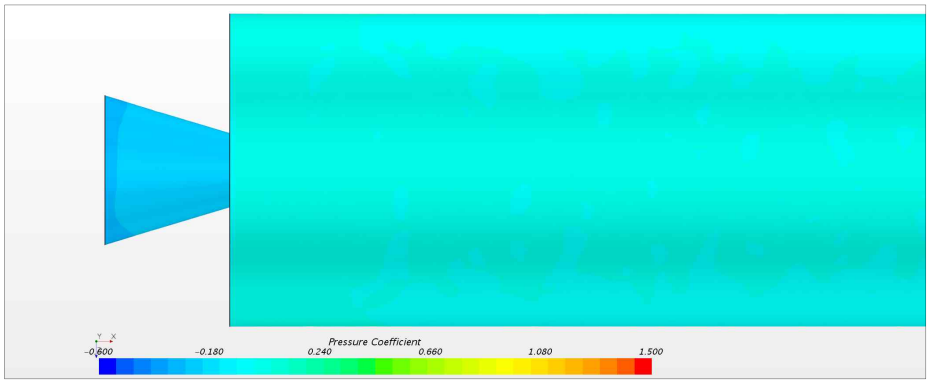

Leeward

Fig. 21. Comparison of surface pressure for "Resemblant TLV" (M_∞=1.5, α=5°, ϕ=0°)

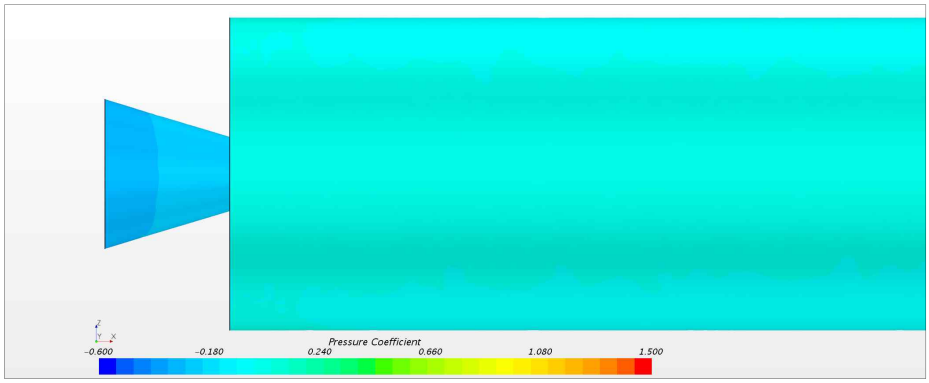

Windward

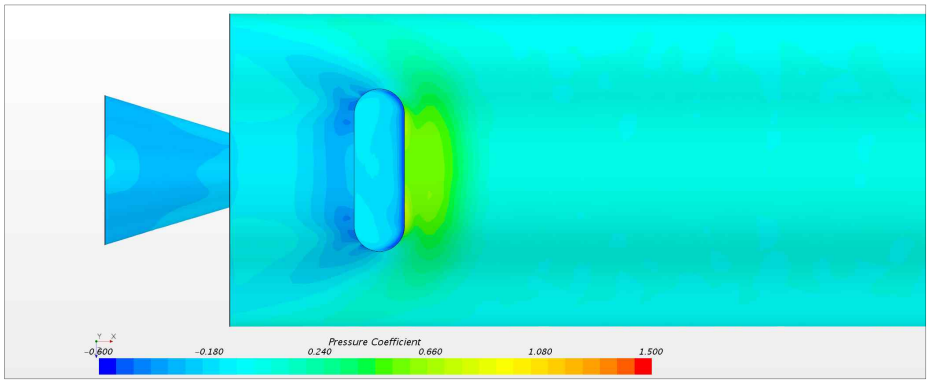

Leeward

Fig. 22. Comparison of surface pressure for "Resemblant TLV" (M_∞=1.5, α=5°, ϕ=180°)

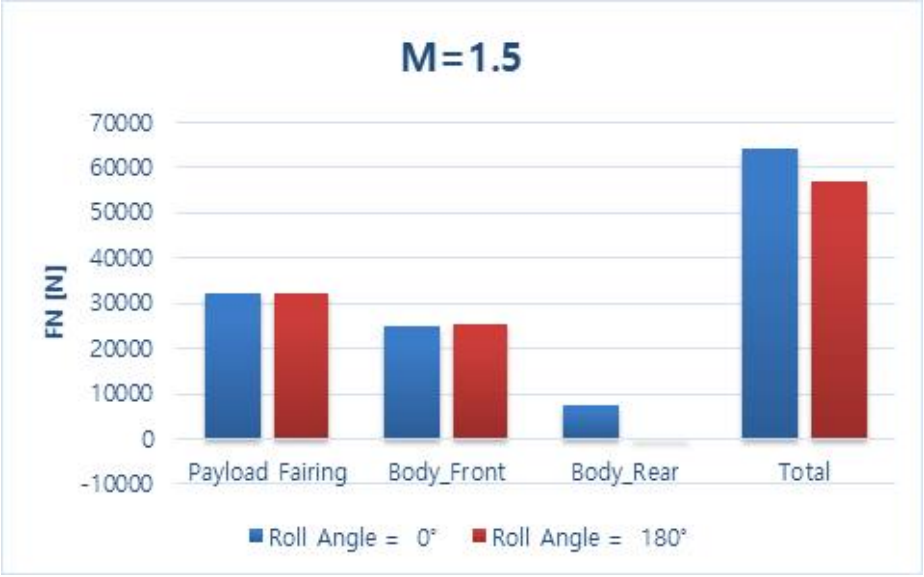

Fig. 23. Comparison of component normal force for "Resemblant TLV" (M_∞=1.5, α=5°)

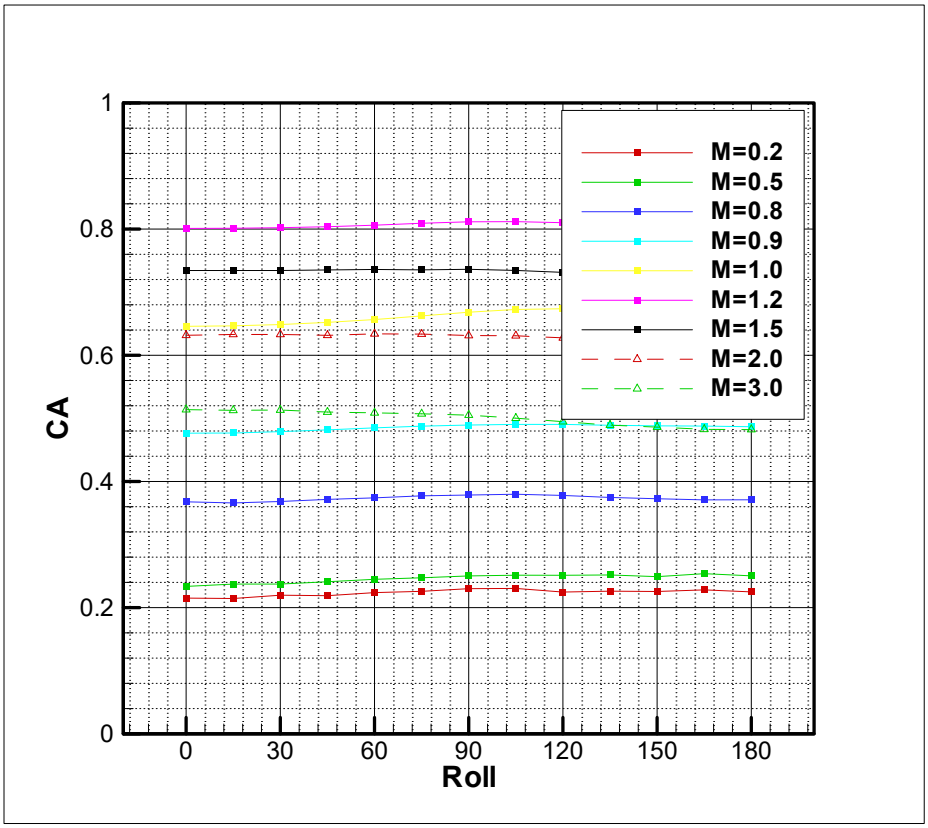

Fig. 24. Axial force coefficient of "Resemblant TLV" ($0.2 \leq M_\infty \leq 3.0$, $\alpha=5°$, $\triangle\phi=15°$)

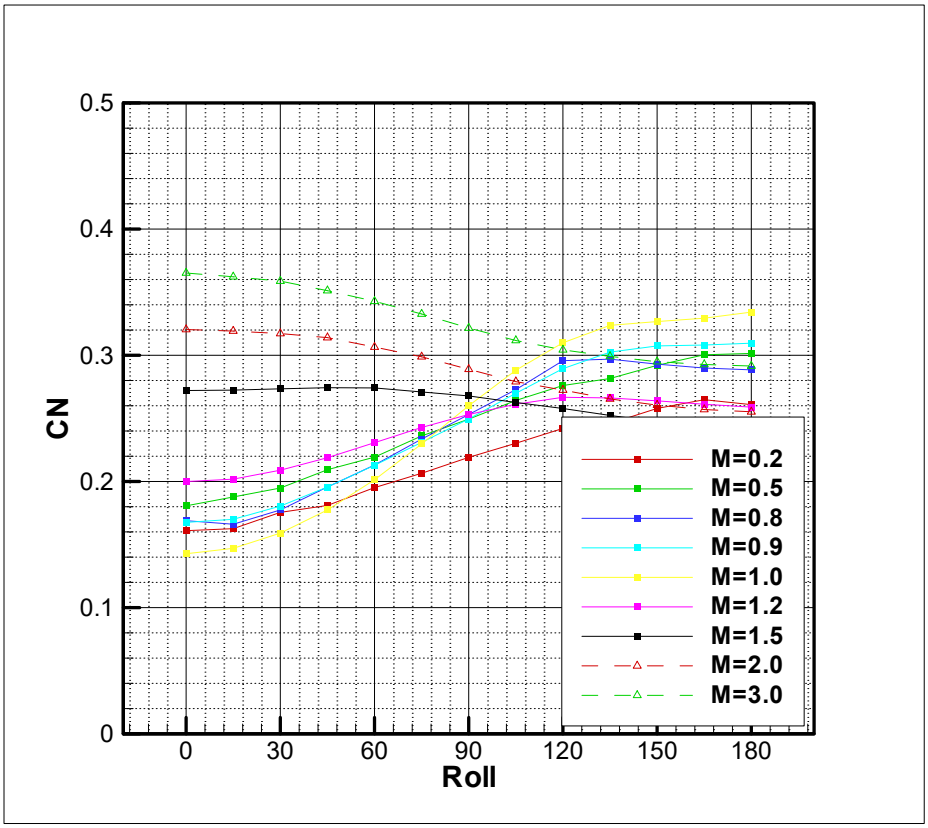

Fig. 25. Normal force coefficient of "Resemblant TLV" ($0.2 \leq M_{\infty} \leq 3.0$, $\alpha=5°$, $\triangle\phi=15°$)

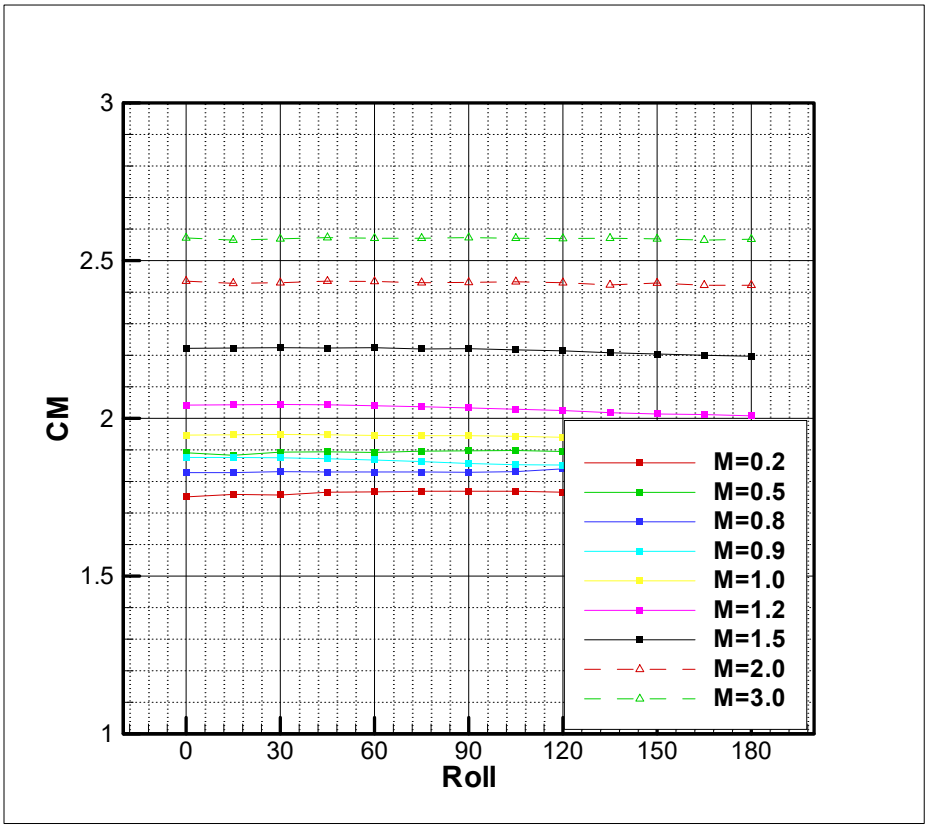

Fig. 26. Pitching moment coefficient of "Resemblant TLV" ($0.2 \leq M_\infty \leq 3.0$, $\alpha=5°$, $\triangle\phi=15°$)

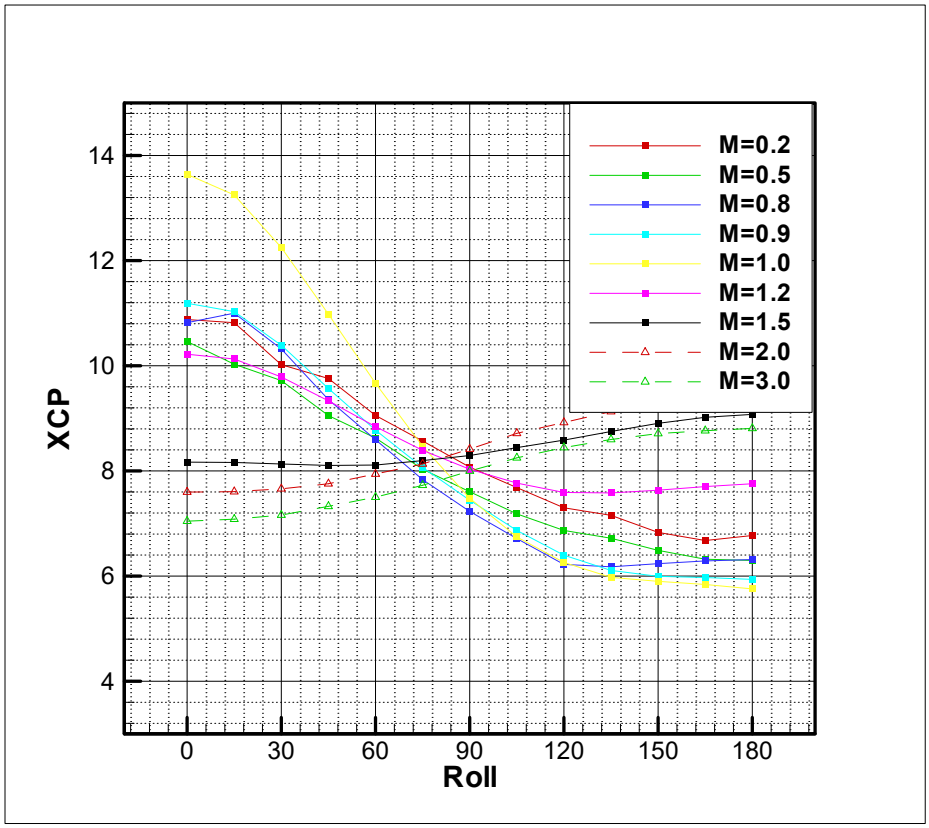

Fig. 27. Center of pressure of "Resemblant TLV" ($0.2 \leq M_{\infty} \leq 3.0$, $\alpha=5°$, $\triangle\phi=15°$)

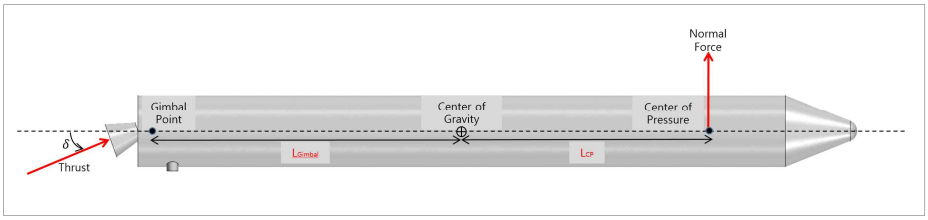

Fig. 28. Schematics to calculate control ratio (CR)

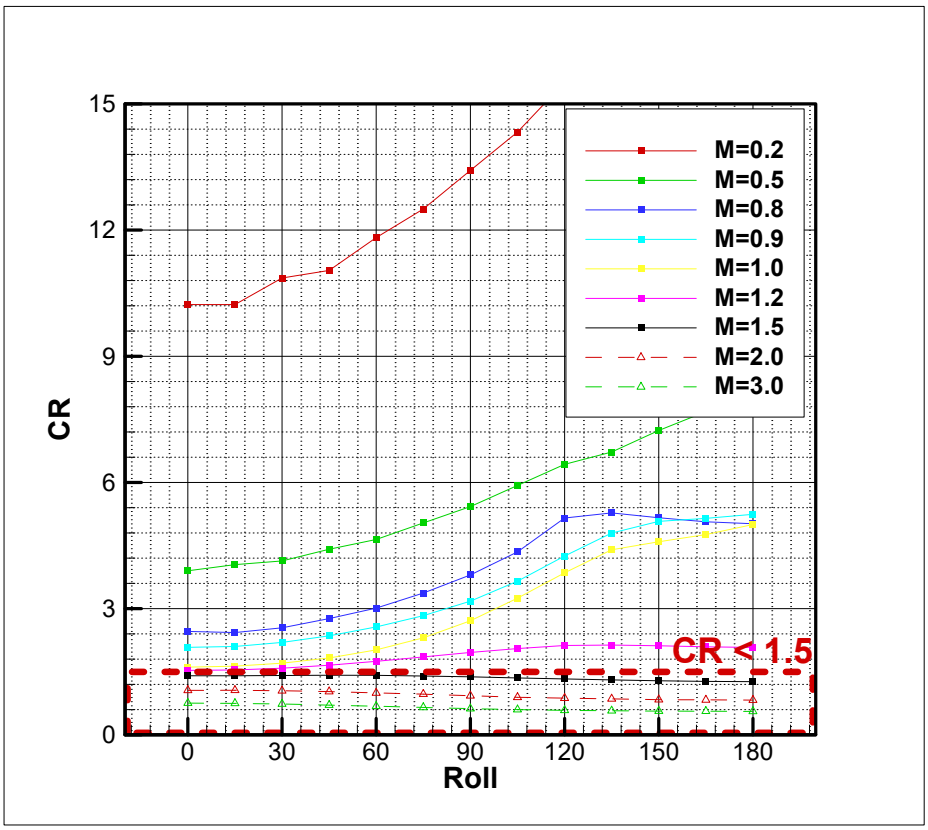

Fig. 29. Variation of control ratio of "Resemblat TLV" ($0.2 \leq M_{\infty} \leq 3.0$, $\alpha=5°$, $\triangle\phi=15°$)

4.1.2 Aerodynamic characteristics for TLV flight trajectory

At the beginning of this study, The TLV was under development, so the flight trajectory of this launch vehicle was not disclosed due to the confidentiality issue. After the flight test in November 2018, The flight trajectory of the TLV was released, and the aerodynamic analysis of the "Resemblant TLV" is conducted again using this actual flight trajectory of the TLV [41-45].

The inflow condition by changing only Mach number for the same Reynolds number and temperature is different from that by the actual flight trajectory of the TLV. In particular, since the dynamic pressure is different, the difference for the normal force used to obtain the CR is large. The aerodynamic coefficients using this actual flight trajectory are as shown in Fig. 30 to Fig. 33, and the overall tendency in the aerodynamic coefficients is similar to that of the previous analysis. In addition, the phenomenon that causes a change in the aerodynamic coefficients according to the change of the roll angle is similar to that of the previous study (Fig. 34 to Fig. 40). The CR in the previous study is very large in the subsonic region and decreases as the Mach number increases. And it shows a value less than 1.5 of the CR in the transonic region and a lower value of the CR in the supersonic region in the previous study.

However, when the analysis using the actual flight trajectory is performed, the pattern of change from subsonic to low transonic range is similar, but in the supersonic region, the CR values are over 1.5 (Fig. 41). When the actual flight trajectory is applied, the dynamic pressure is low in the supersonic region, so it is possible to sufficiently control with the 75 tonf engine. The CR value reflecting this is also increased, so there is no problem in the flight controllability in the

supersonic region using the 75 tonf engine. Meanwhile to achieve the CR of 1.5 or higher in this case for all Mach number range, the nozzle rotation angle must be 7° or higher, or the thrust must be increased to 87 tonf or higher.

In addition, comparing the normal forces of each section, even if the flight trajectory is changed, the normal force having a negative value occurs around the umbilical plate, thereby reducing the normal force. For this reason, it was confirmed once again that the CR decreased in some cases.

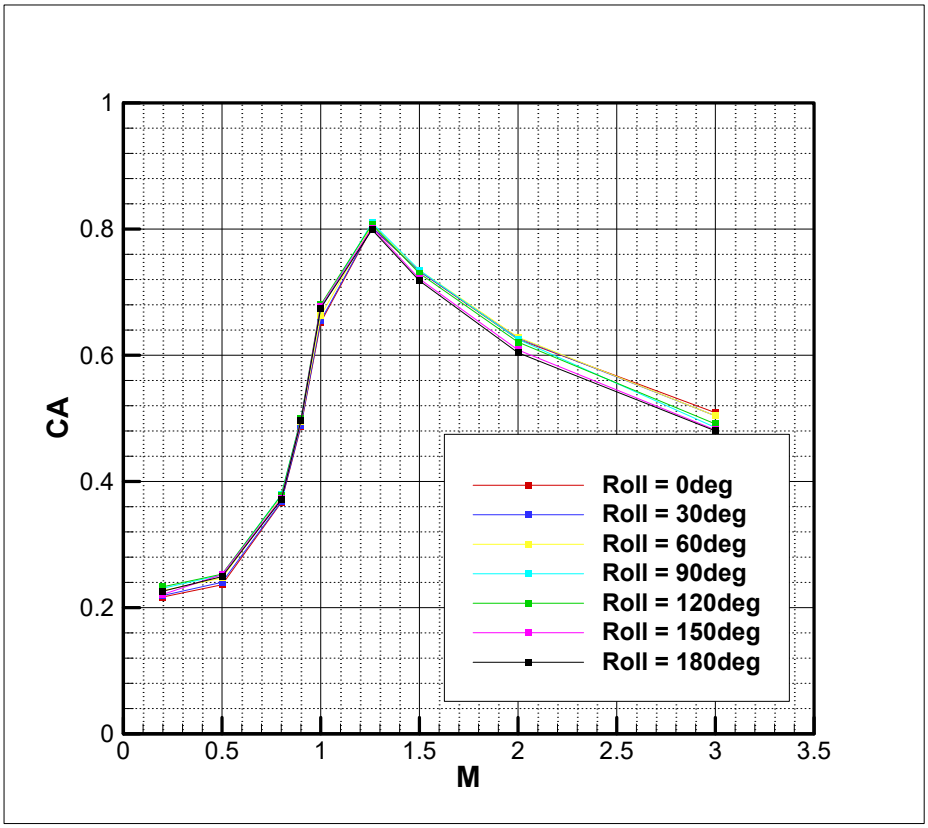

Fig. 30. Axial force coefficient for the actual flight trajectory ($0.2 \leq M_{\infty} \leq 3.0$, $\alpha=5°$, $\triangle\phi=30°$)

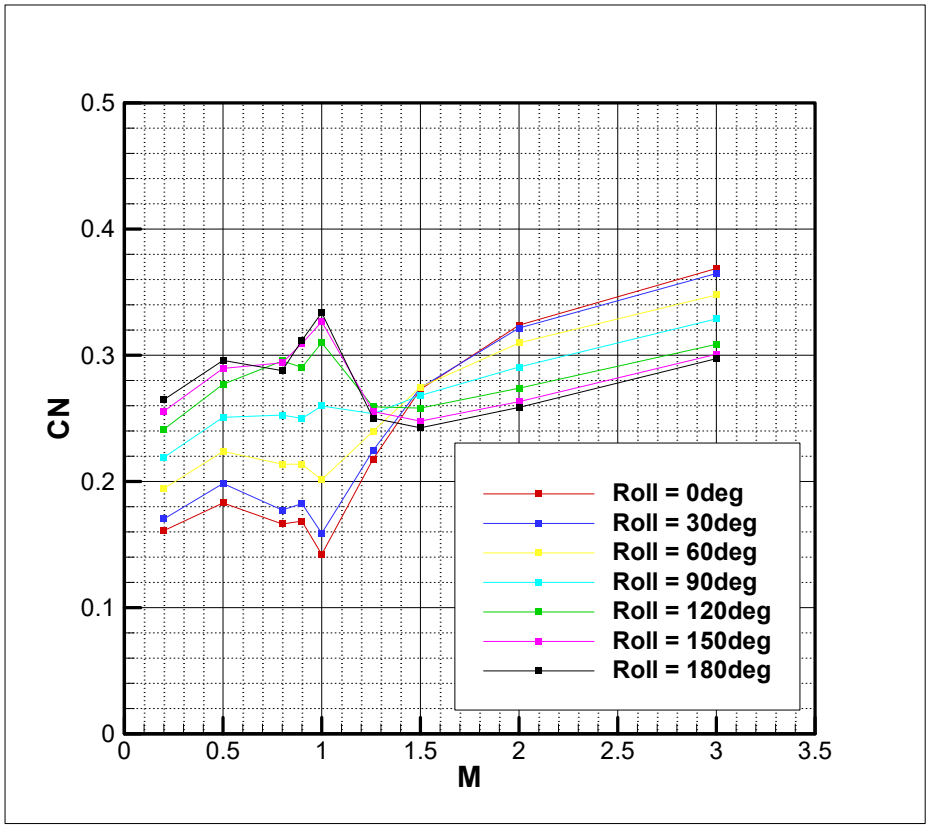

Fig. 31. Normal force coefficient for the actual flight trajectory ($0.2 \leq M_{\infty} \leq 3.0$, $\alpha=5°$, $\triangle\phi=30°$)

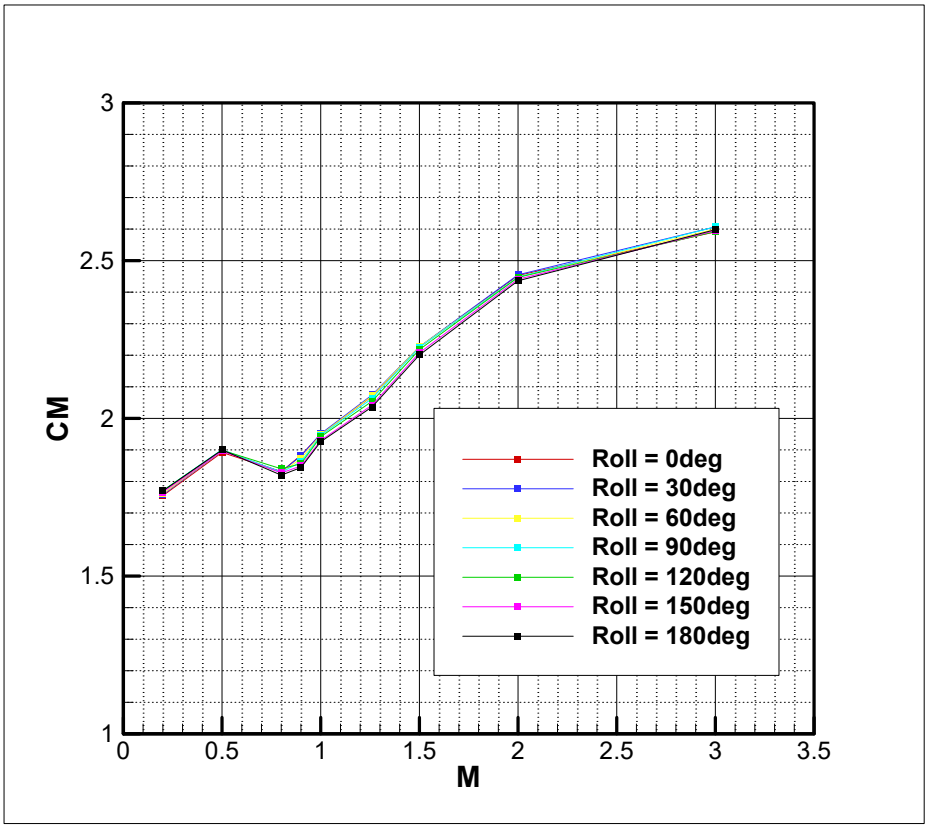

Fig. 32. Pitching moment coefficient for the actual flight trajectory ($0.2 \leq M_{\infty} \leq 3.0$, $\alpha=5°$, $\triangle\phi=30°$)

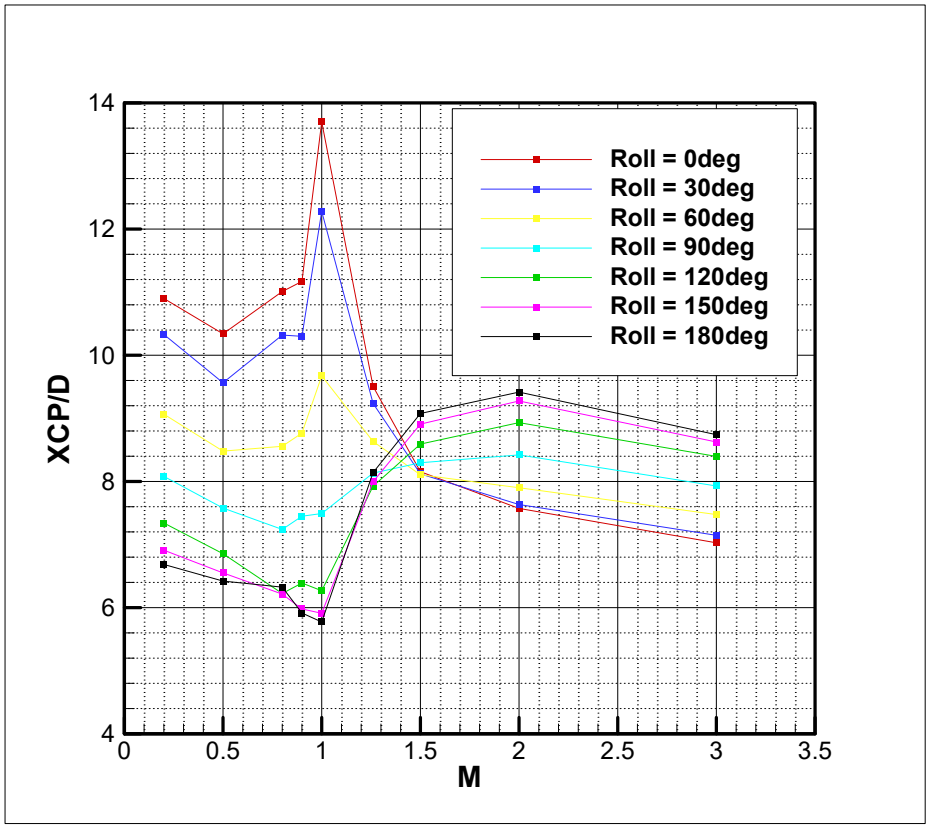

Fig. 33. Center of pressure for the actual flight trajectory ($0.2 \leq M_{\infty} \leq 3.0$, $\alpha=5°$, $\triangle\phi=30°$)

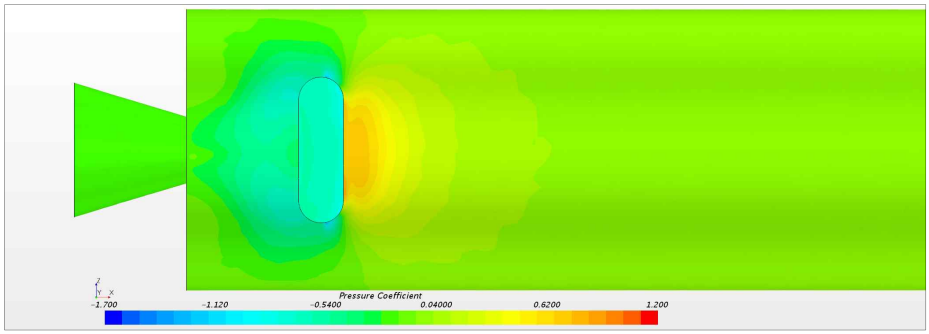

Windward

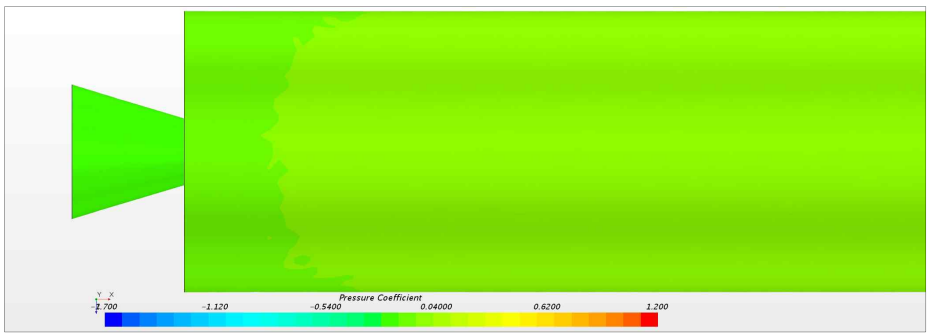

Leeward

Fig. 34. Comparison of surface pressure for the actual flight trajectory (M_{∞}=0.8, α=5°, ϕ=0°)

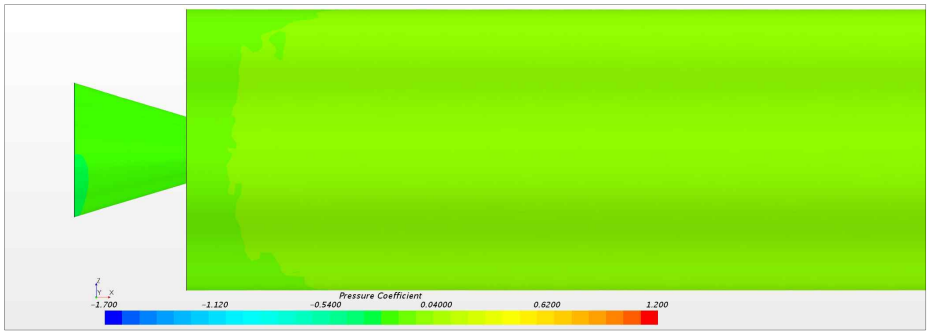

Windward

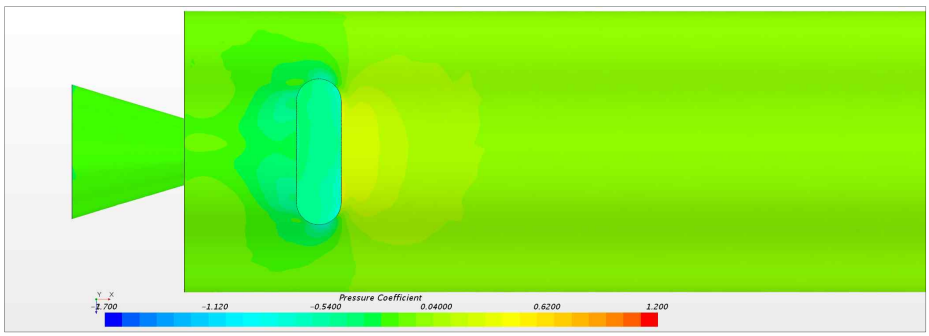

Leeward

Fig. 35. Comparison of surface pressure for the actual flight trajectory (M_∞=0.8, α=5°, ϕ=180°)

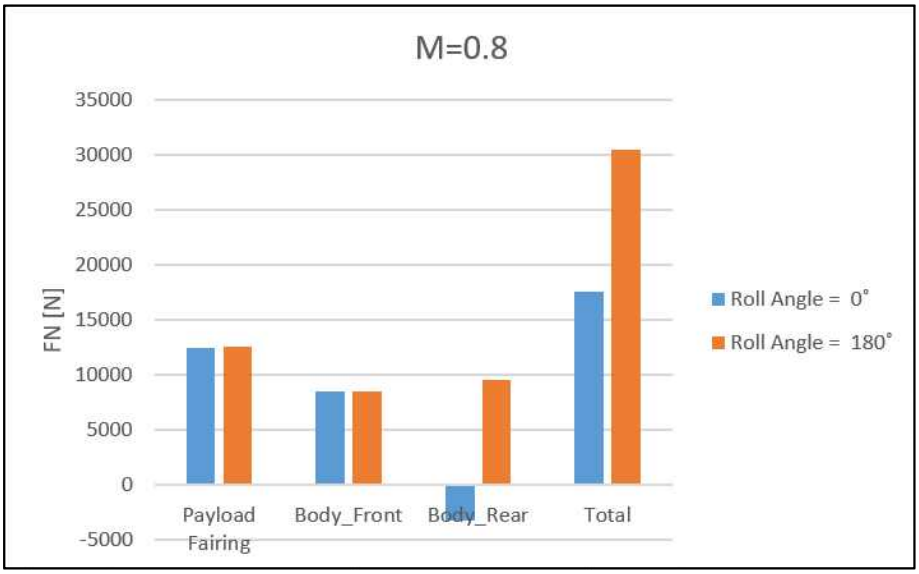

Fig. 36. Comparison of component normal force for the actual flight trajectory (M_∞=0.8, α=5°)

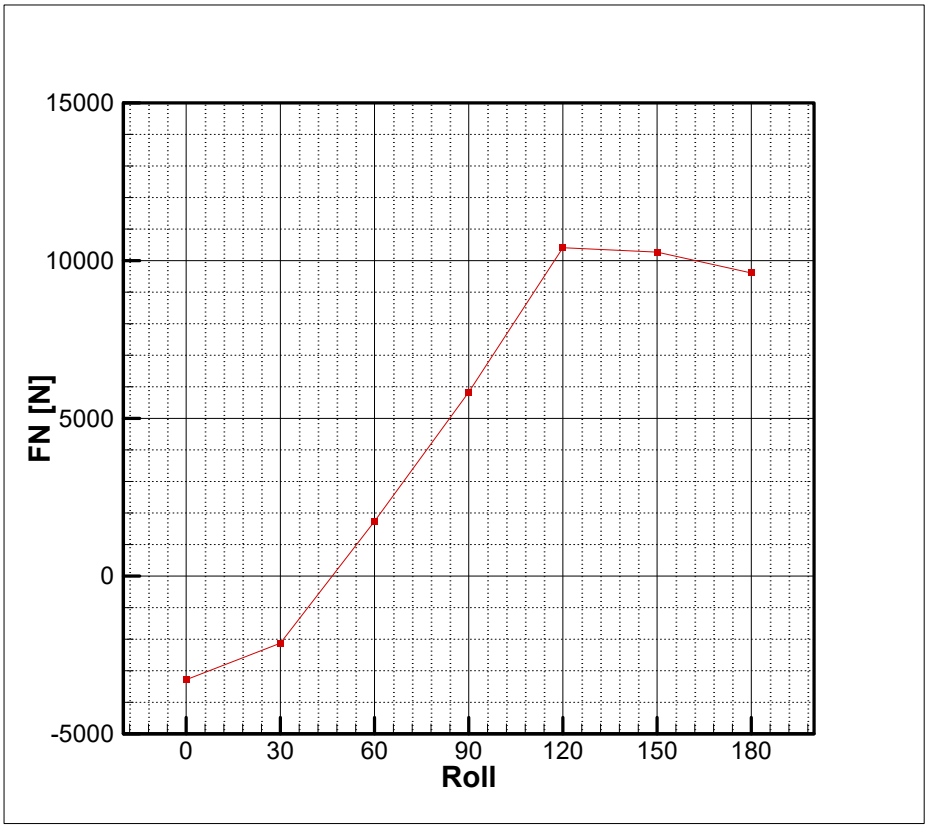

Fig. 37. Variation of normal force for body rear for the actual flight trajectory (M_∞=0.8, α=5°, ϕ=0°)

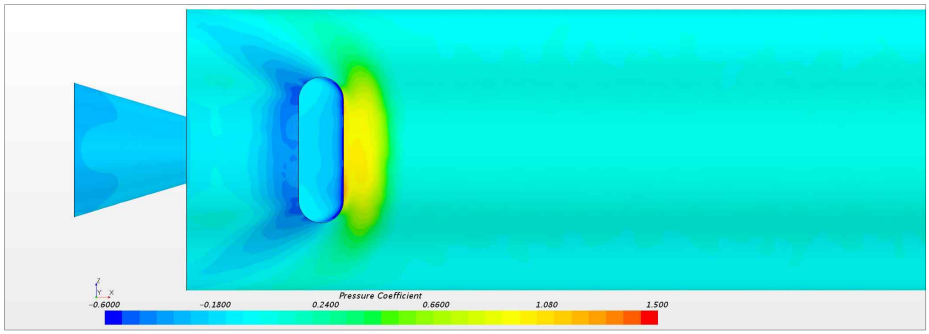

Windward

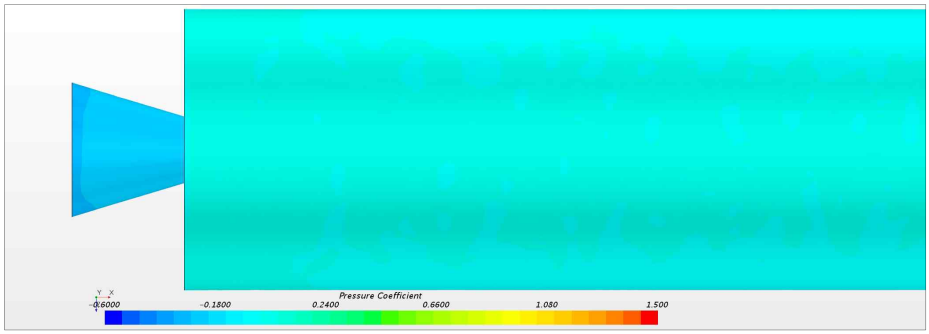

Leeward

Fig. 38. Comparison of surface pressure for the actual flight trajectory (M_∞=1.5, α=5°, ϕ=0°)

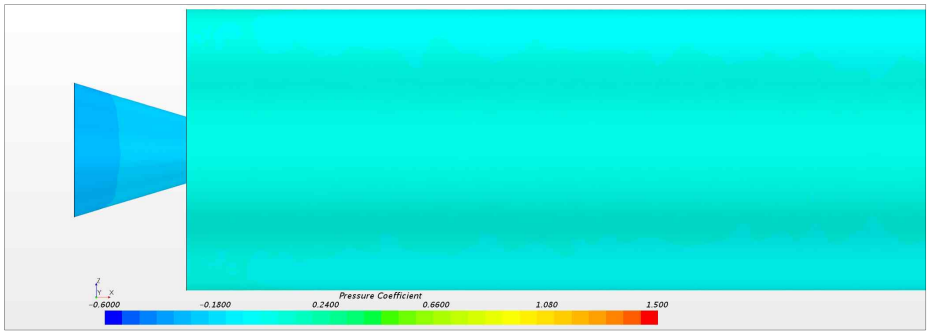

Windward

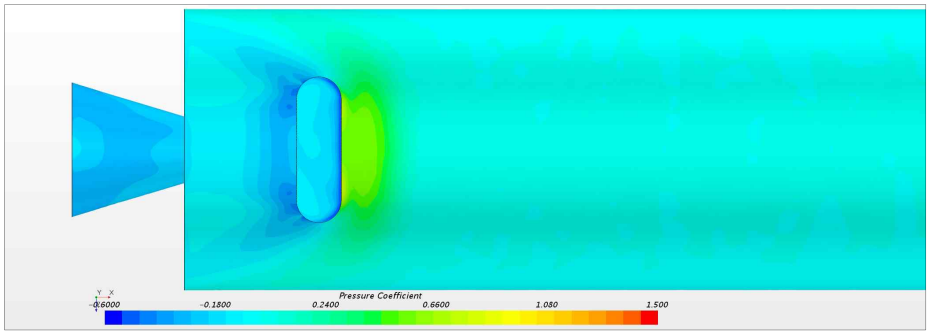

Leeward

Fig. 39. Comparison of surface pressure for the actual flight trajectory (M_∞=1.5, α=5°, ϕ=180°)

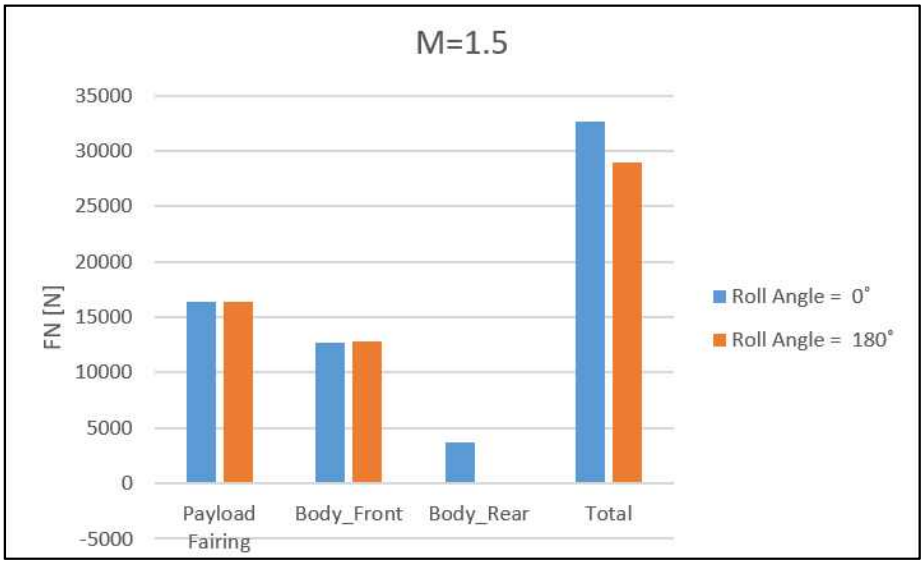

Fig. 40. Comparison of component normal force for the actual flight trajectory (M_∞=1.5, α=5°)

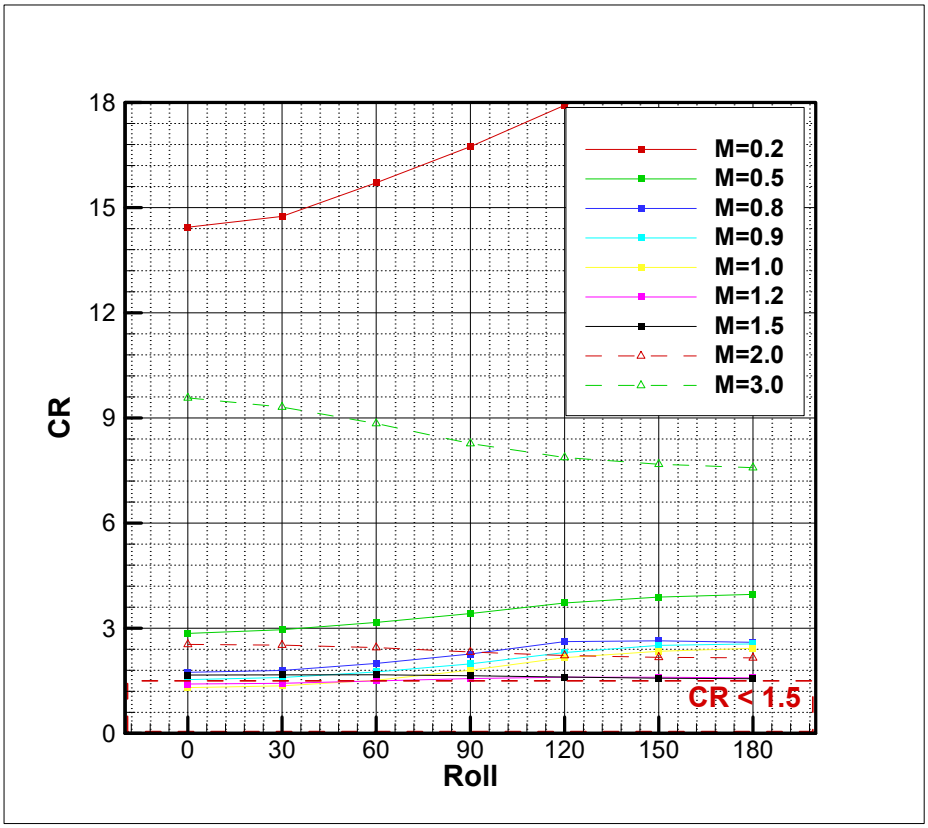

Fig. 41. Variation of control ratio of the actual flight trajectory ($0.2 \leq M_{\infty} \leq 3.0$, $\alpha=5°$, $\triangle\phi=30°$)

4.2. Effects of configurations of the umbilical plate regard to aerodynamic characteristics

4.2.1 Aerodynamic characteristics for LV without the umbilical plate

In order to investigate the effect of the shape of the umbilical plate on the CR, the prediction of the aerodynamic coefficients is first performed in the case where the umbilical plate is not present (Fig. 42 to Fig.45). In case of the absence of the umbilical plate, there is no change in the aerodynamic characteristics due to the change in the roll angle, so the analysis of the change in the roll angle is not conducted.

There is loss of the normal force in case of the umbilical plate for some cases but there is no loss of the normal force for the "Resemblant TLV" without the umbilical plate (Fig. 46 to Fig. 51). And the center of pressures moves to the nozzle in case of no umbilical plate than that in the case of the umbilical plate, The CRs for all Mach number range are 1.5 or more (Fig. 52).

The CR is reduced by about 14% due to the influence of the umbilical plate, compared with the minimum value of CR.

($CR_{\min_{Present}} = 1.502,\ CR_{\min_{UmbilicalPlate}} = 1.307$)

Meanwhile, when comparing the normal force of each section, the CR value is not reduced because the positive normal force is generated even around the Body_Rear section and the total normal force is not lowered.

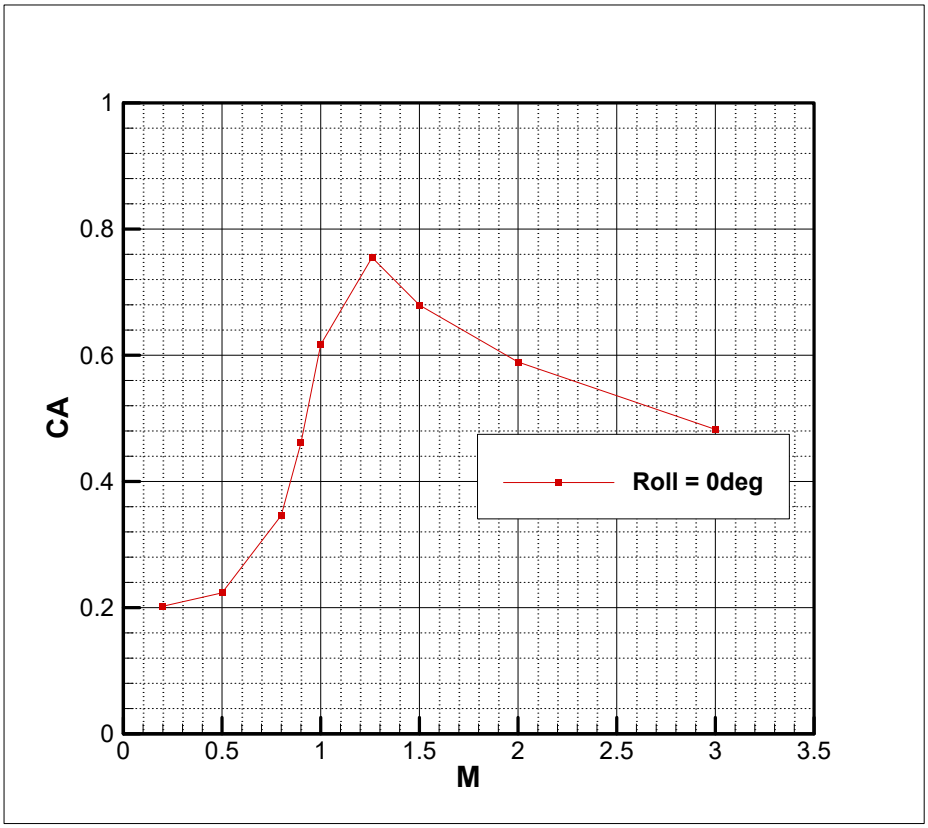

Fig. 42. Axial force coefficient for no umbilical plate ($0.2 \leq M_{\infty} \leq 3.0$, $\alpha=5°$)

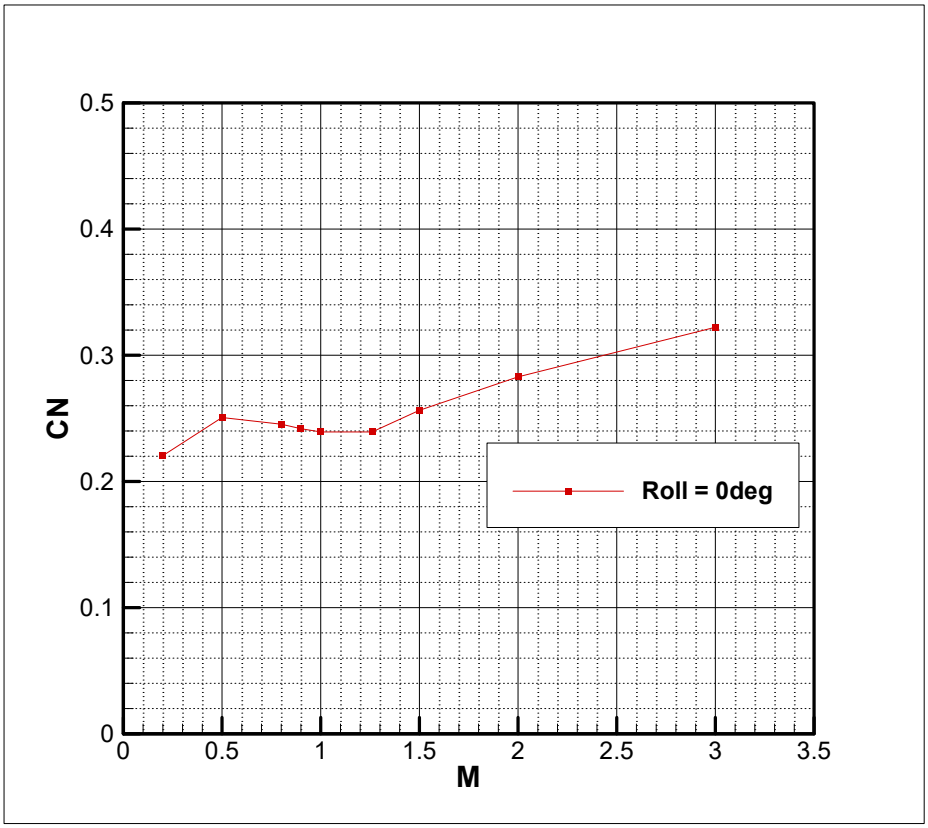

Fig. 43. Normal force coefficient for no umbilical plate ($0.2 \leq M_{\infty} \leq 3.0$, $\alpha=5°$)

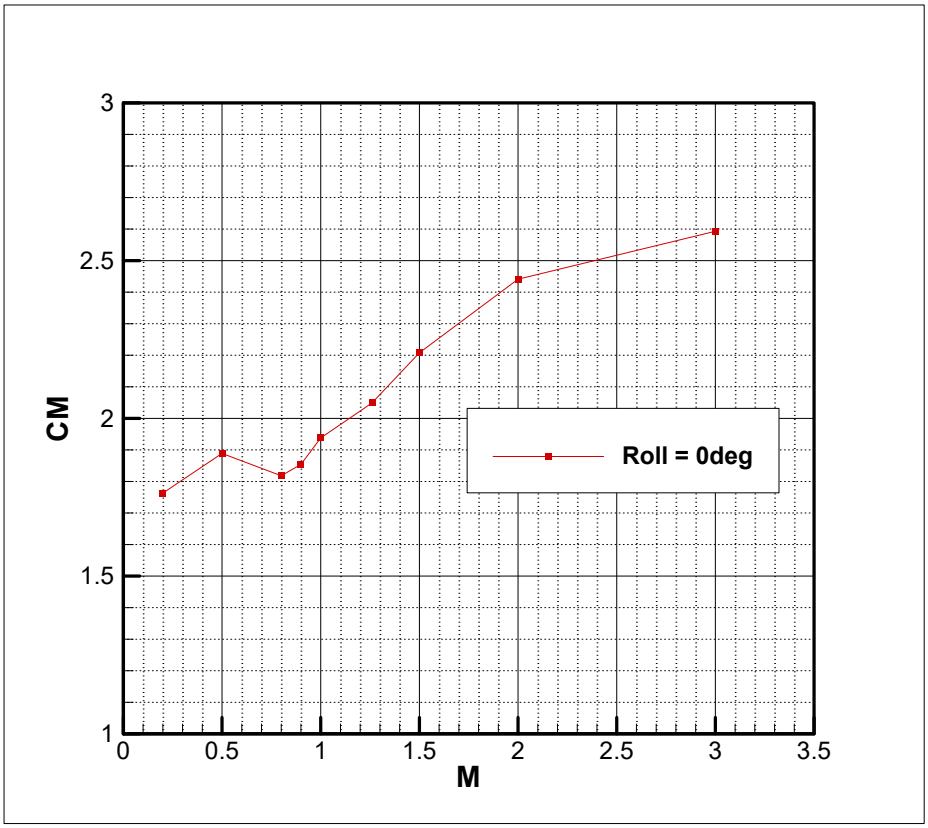

Fig. 44. Pitching moment coefficient for no umbilical plate ($0.2 \leq M_{\infty} \leq 3.0$, $\alpha=5°$)

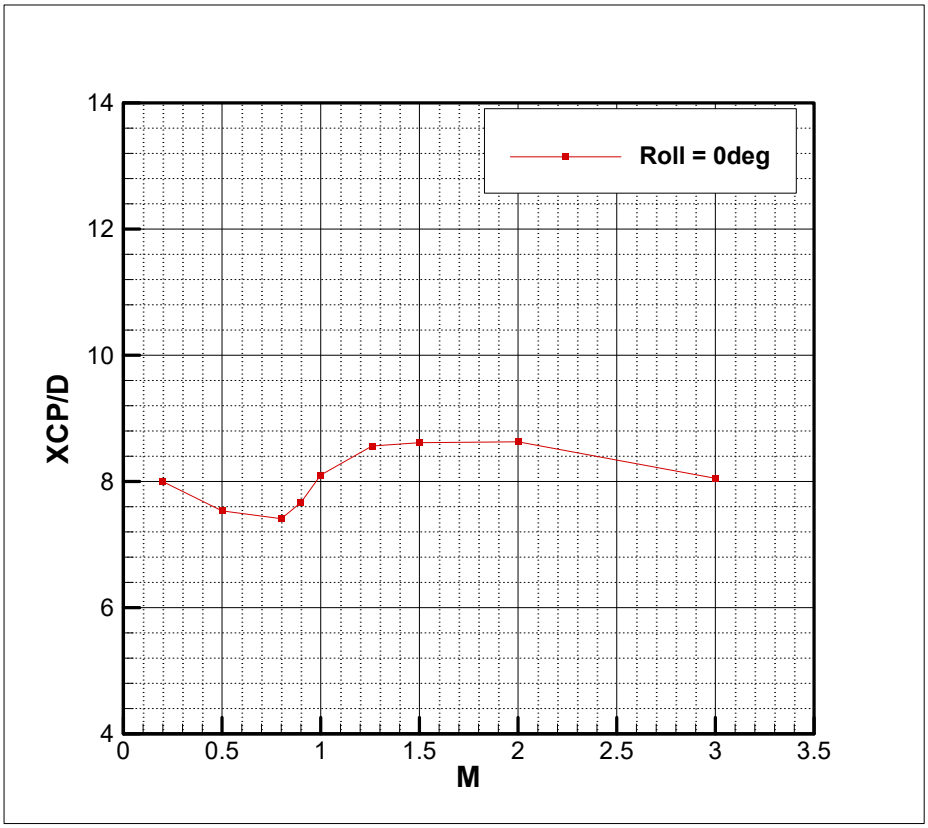

Fig. 45. Center of pressure for no umbilical plate ($0.2 \leq M_{\infty} \leq 3.0$, $\alpha=5°$)

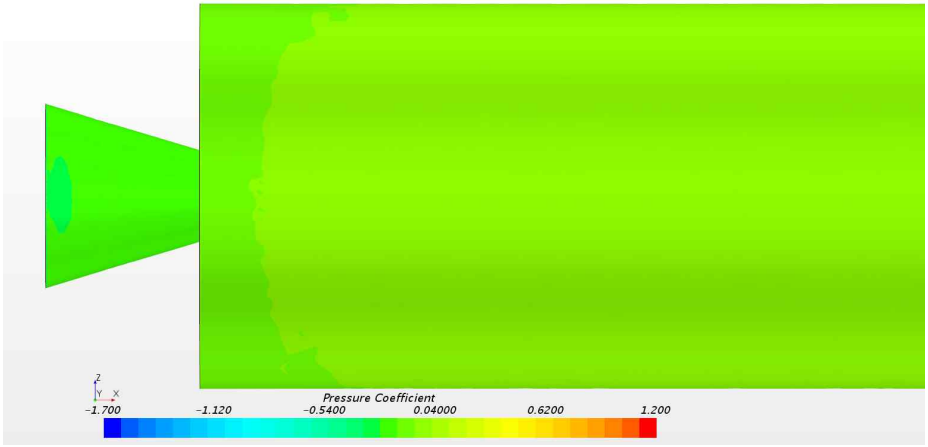

Windward

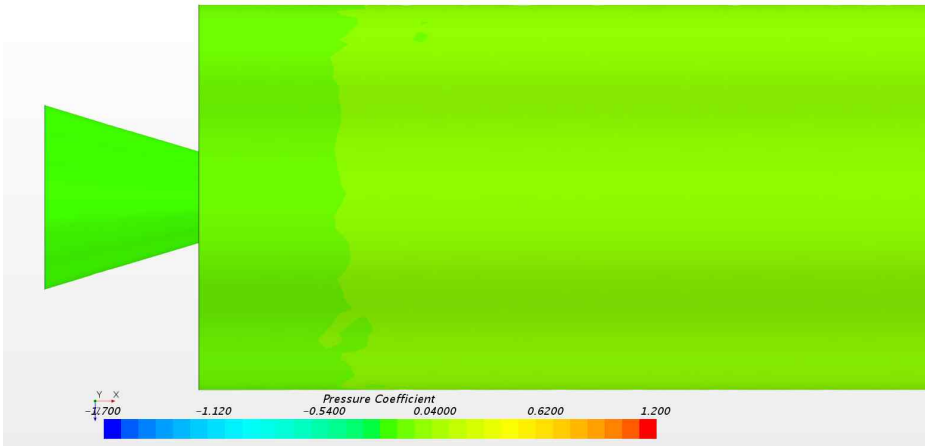

Leeward

Fig. 46. Comparison of surface pressure for no umbilical plate (M_∞=0.8, α=5°, Rear Part)

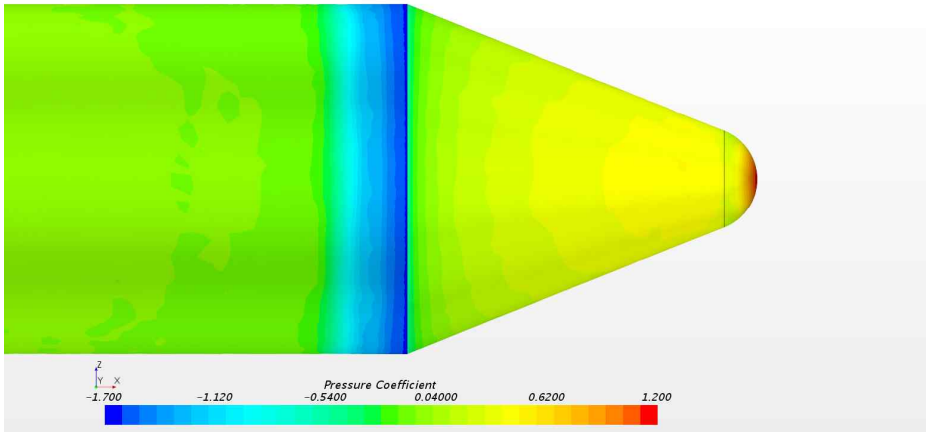

Windward

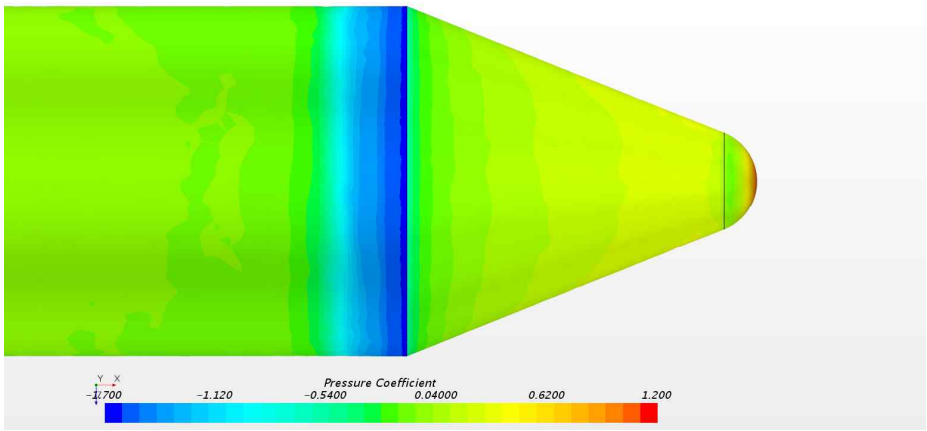

Leeward

Fig. 47. Comparison of surface pressure for no umbilical plate (M_∞=0.8, α=5°, Front Part)

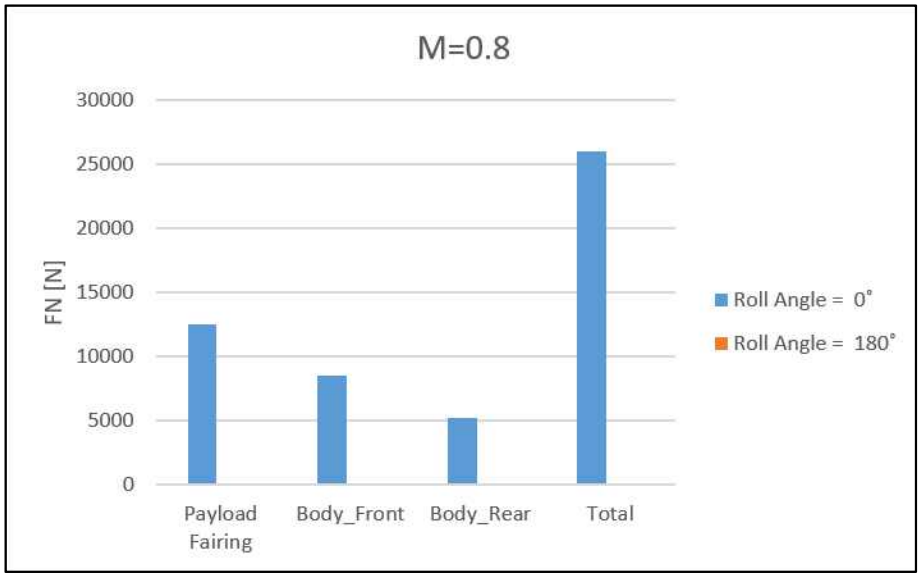

Fig. 48. Comparison of component normal force for no umbilical plate (M_∞=0.8, α=5°)

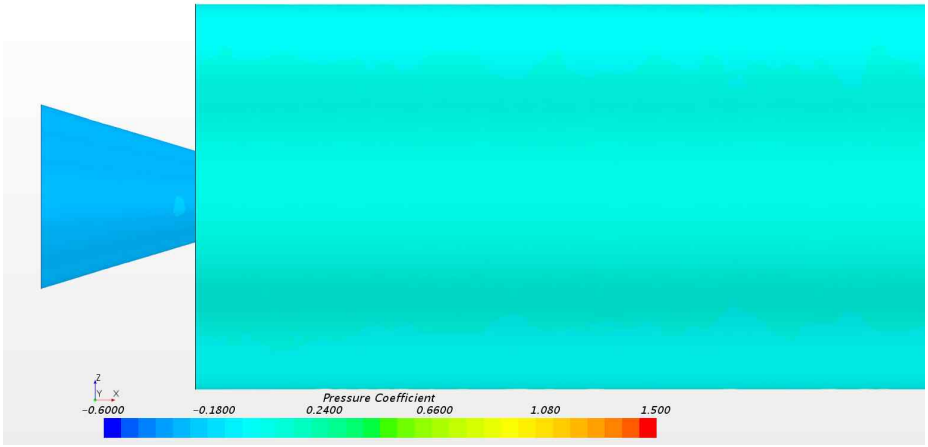

Windward

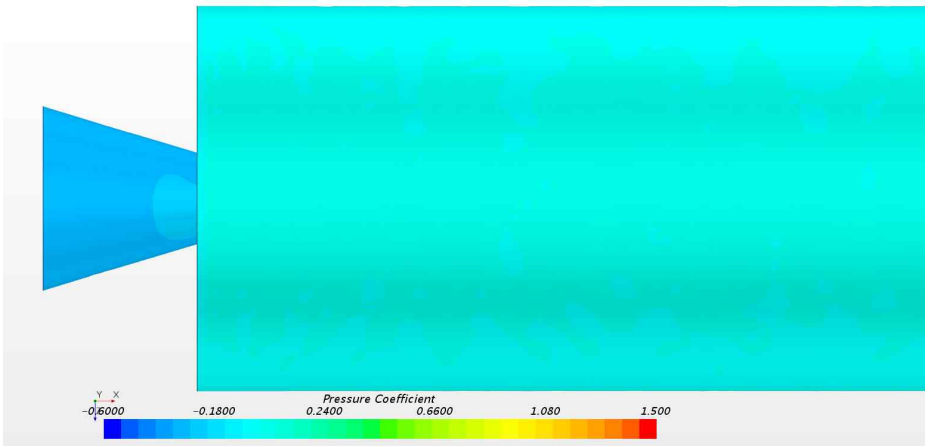

Leeward

Fig. 49. Comparison of surface pressure for no umbilical plate (M_∞=1.5, α=5°, Rear Part)

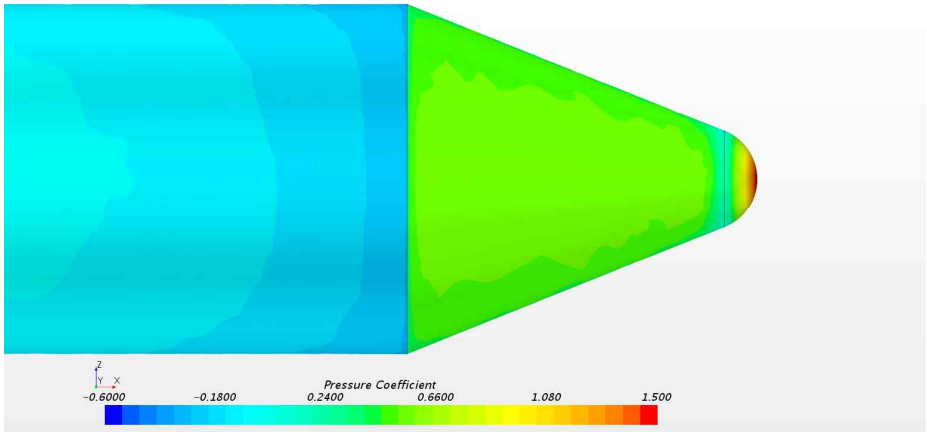

Windward

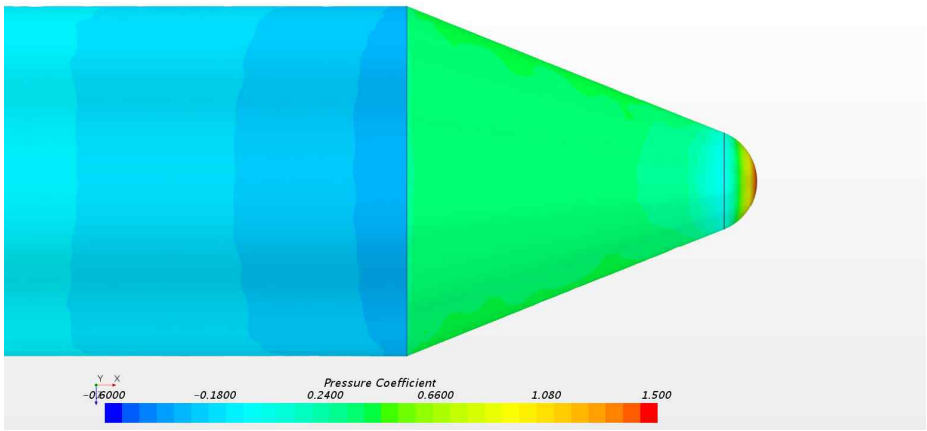

Leeward

Fig. 50. Comparison of surface pressure for no umbilical plate (M_∞=1.5, α=5°, Front Part)

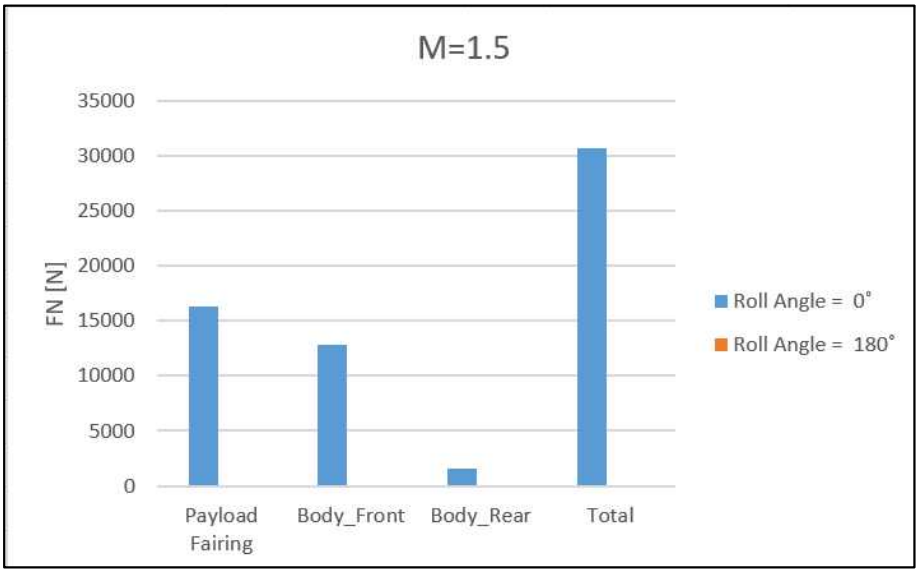

Fig. 51. Comparison of component normal force for no umbilical plate (M_∞=1.5, α=5°)

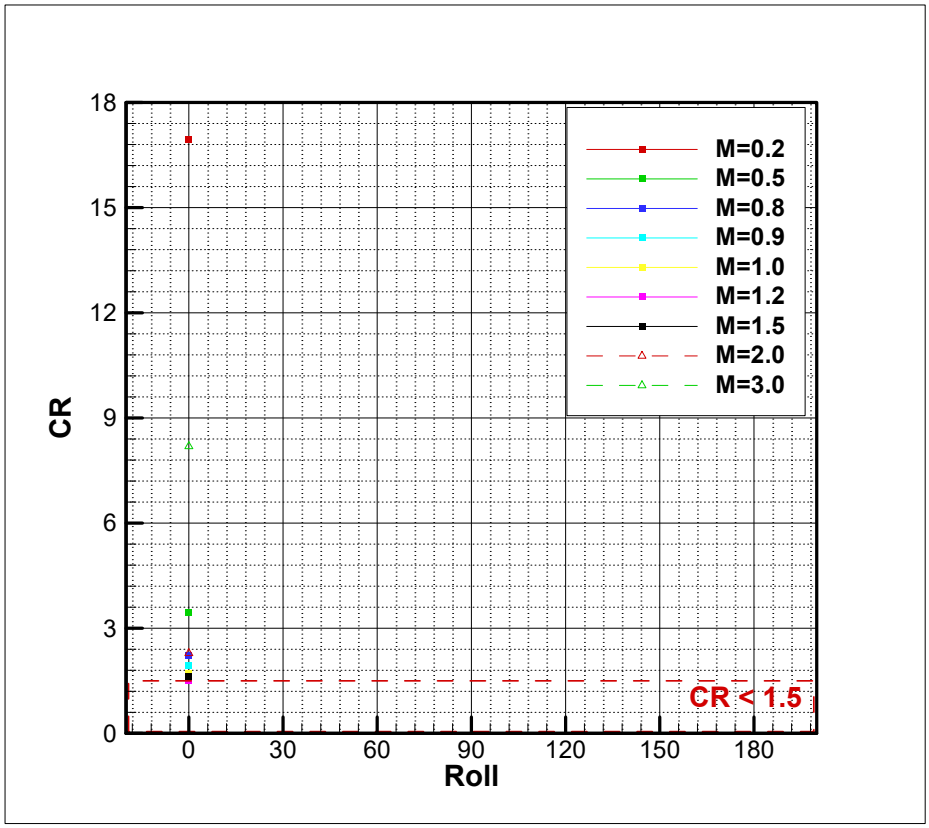

Fig. 52. Variation of control ratio of no umbilical plate ($0.2 \leq M_{\infty} \leq 3.0$, $\alpha=5°$)

4.2.2 Aerodynamic characteristics for LV with half umbilical plate

In this section, the aerodynamic analysis is conducted in case of the lower height of the umbilical plate in half to investigate the CR changes. Before the prediction of the CR, the normal force coefficients and the axial force coefficients on the section including the protuberance, Body_Rear are presented to analysis the effect of the configuration of the protuberance for the angle of attack of 0° and the roll angle of 0° in Fig. 53 and Fig. 54. And the effect of the protuberance for the angle of attack, 5° is also presented in Fig. 53. It is shown that the negative normal force is acted on the body in the transonic region although the angle of attack is 0°. However the magnitude of the negative normal force is reduced for half umbilical plate. And the minimum normal force appears when half cylindrical umbilical plates of which the CR is predicted in the next part are applied. The local axial force coefficients are reduced when the height of the external structure is lowered and the protuberance is separated to the smaller structures.

Fig. 55 through 65 represent the changes in the aerodynamic coefficients and the aerodynamic characteristics in some cases. The controllability increases when the present CR is compared to that of the original umbilical plate, but the CRs are under 1.5 in some conditions (Fig. 66). In these conditions, the TVC angle should be 6.4 ° or more, or the thrust should be increased to about 80 tonf to make the CR 1.5 or more.

Compared to the minimum CR when there is no umbilical plate and the minimum value of the present CRs when umbilical plate height is halved, 6.9% of CR is reduced due to the influence of the umbilical

plate. However, it can be seen that the controllability increases by about 7% if CR of the original umbilical plate is compared.

$$(CR_{\min_{Present}} = 1.415,\ CR_{\min_{Umbilical\ Plate}} = 1.307,\ CR_{\min_{No\ Umbilical\ Plate}} = 1.520)$$

In addition, although the normal force around the umbilical plate is negative when the height of the umbilical plate is lowered, the absolute value of the negative normal force decreases, so the overall normal force does not decrease significantly.

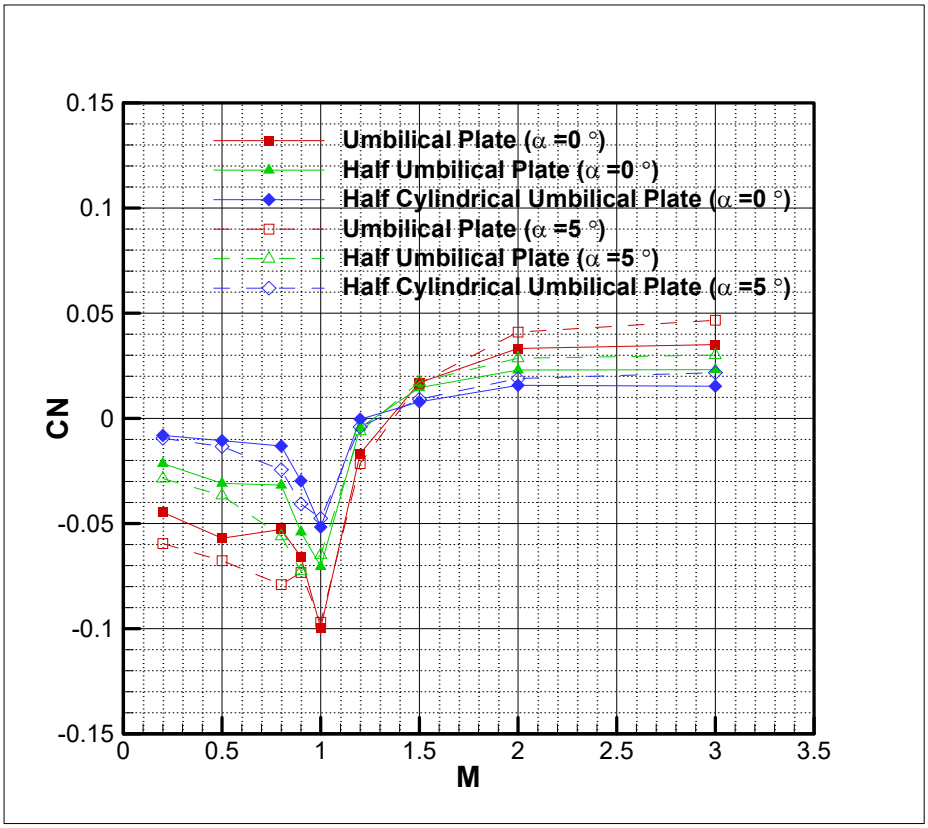

Fig. 53. Normal force coefficient for α=0°, 5° and ϕ=0° ($0.2 \leq M_{\infty} \leq 3.0$)

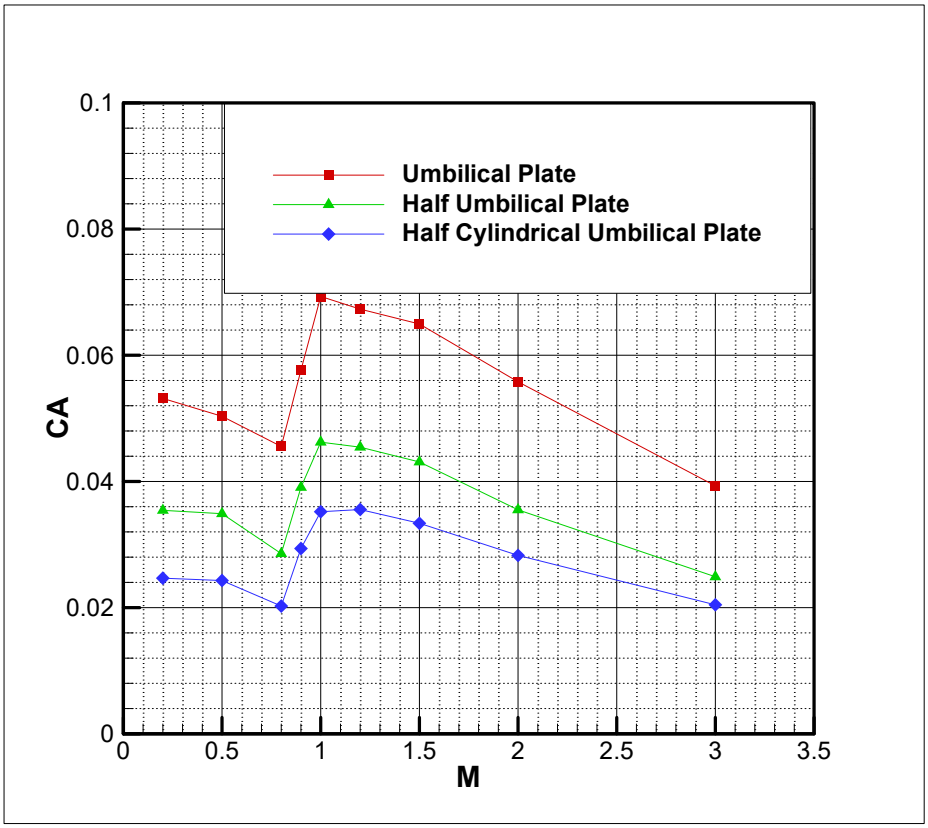

Fig. 54. Axial force coefficient for $\alpha=0°$ and $\phi=0°$ $(0.2 \leq M_{\infty} \leq 3.0)$

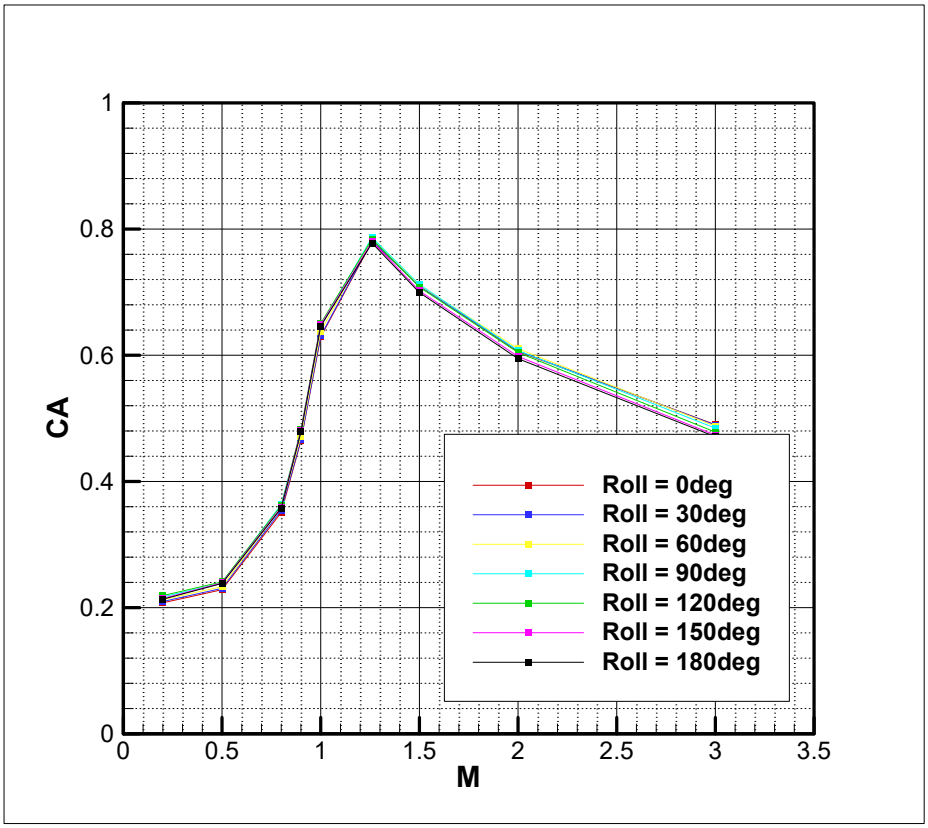

Fig. 55. Axial force coefficient for half umbilical plate ($0.2 \leq M_{\infty} \leq 3.0$, $\alpha=5°$, $\triangle\phi=30°$)

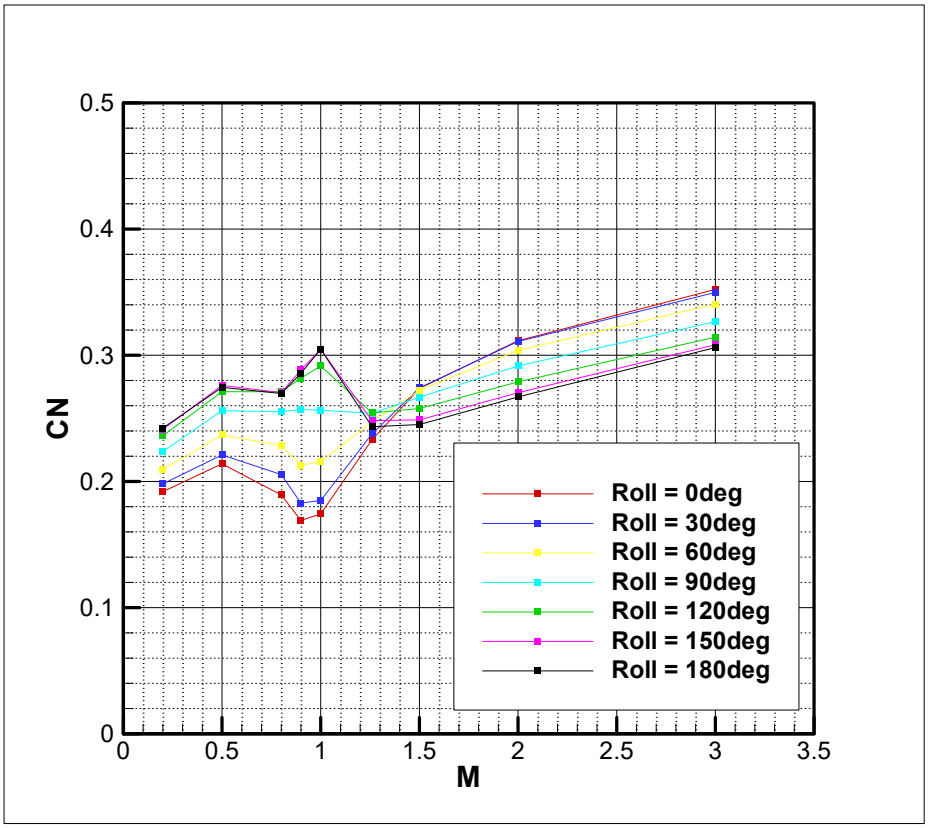

Fig. 56. Normal force coefficient for half umbilical plate ($0.2 \leq M_{\infty} \leq 3.0$, $\alpha=5°$, $\triangle\phi=30°$)

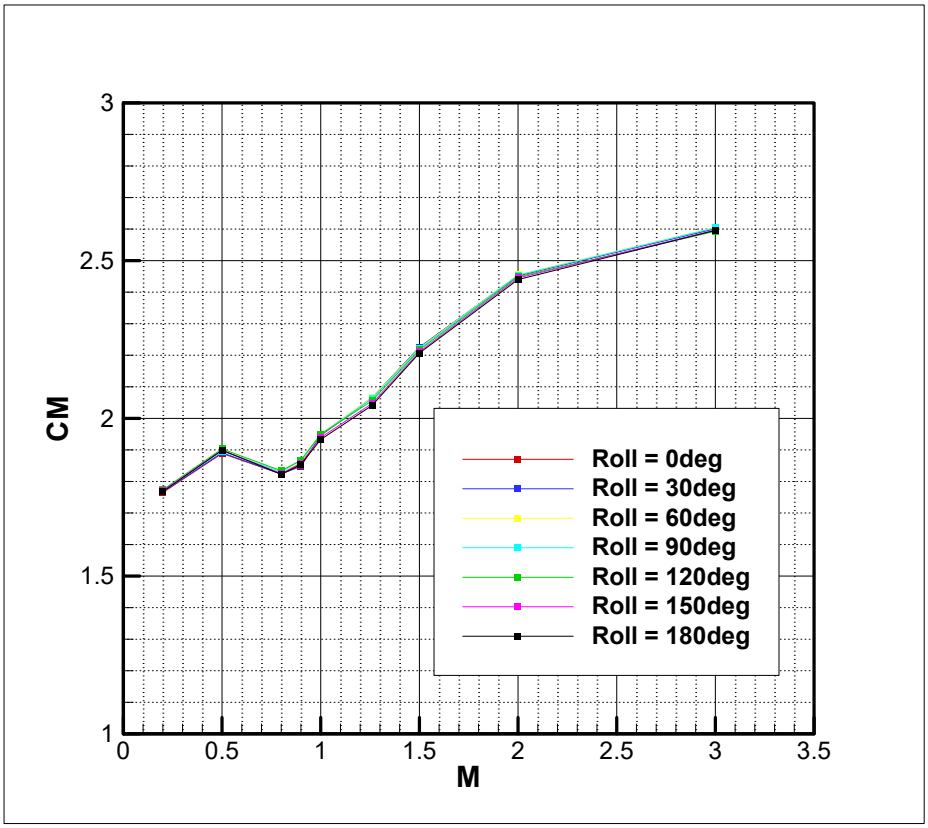

Fig. 57. Pitching moment coefficient for half umbilical plate ($0.2 \leq M_{\infty} \leq 3.0$, $\alpha=5°$, $\triangle\phi=30°$)

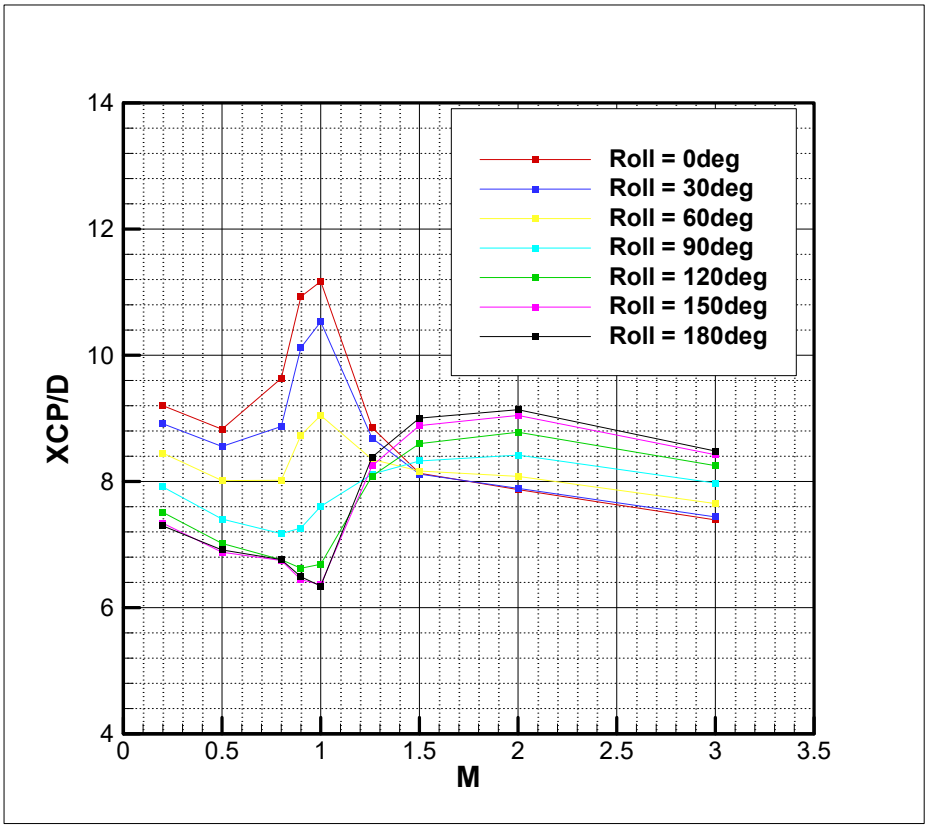

Fig. 58. Center of pressure for half umbilical plate ($0.2 \leq M_{\infty} \leq 3.0$, $\alpha=5°$, $\triangle\phi=30°$)

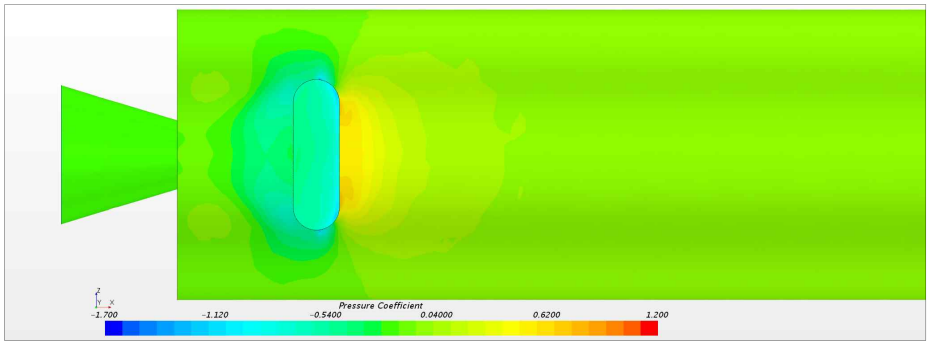

Windward

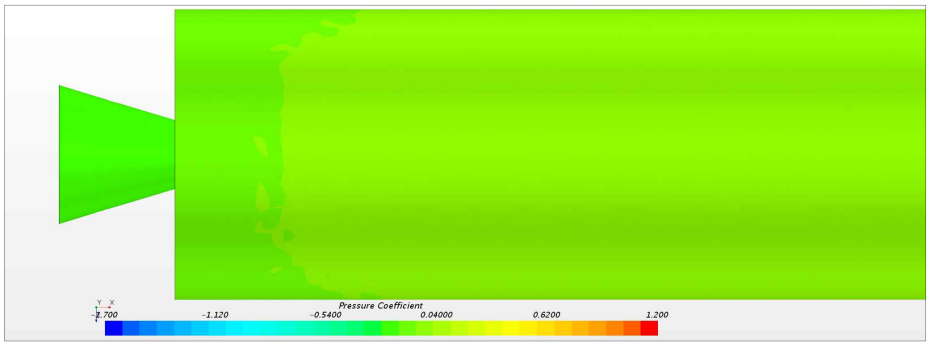

Leeward

Fig. 59. Comparison of surface pressure for half umbilical plate (M_∞=0.8, α=5°, ϕ=0°)

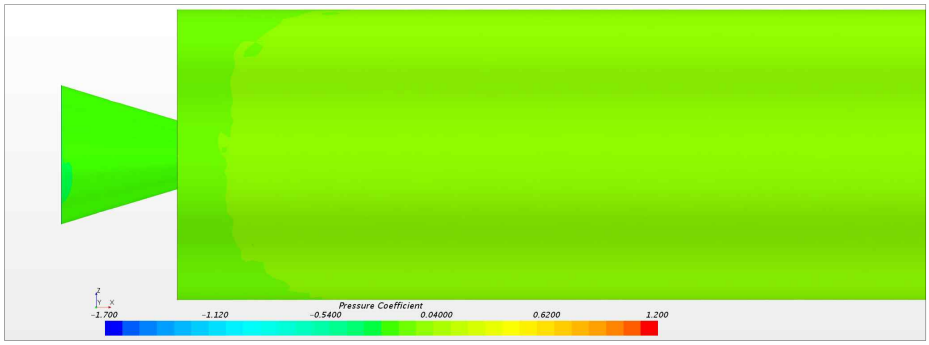

Windward

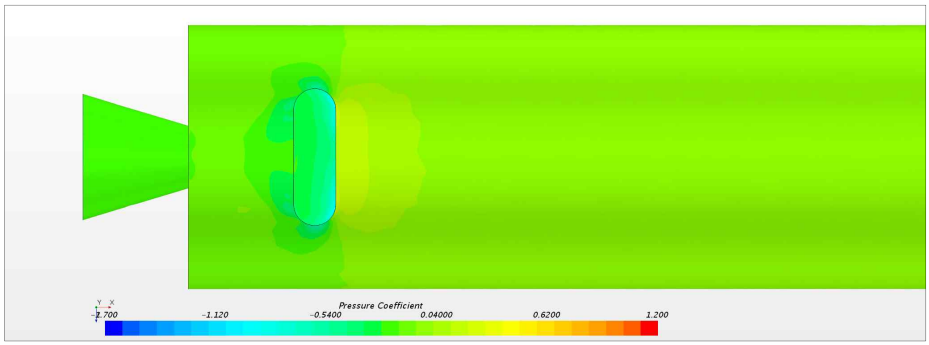

Leeward

Fig. 60. Comparison of surface pressure for half umbilical plate (M_∞=0.8, α=5°, ϕ=180°)

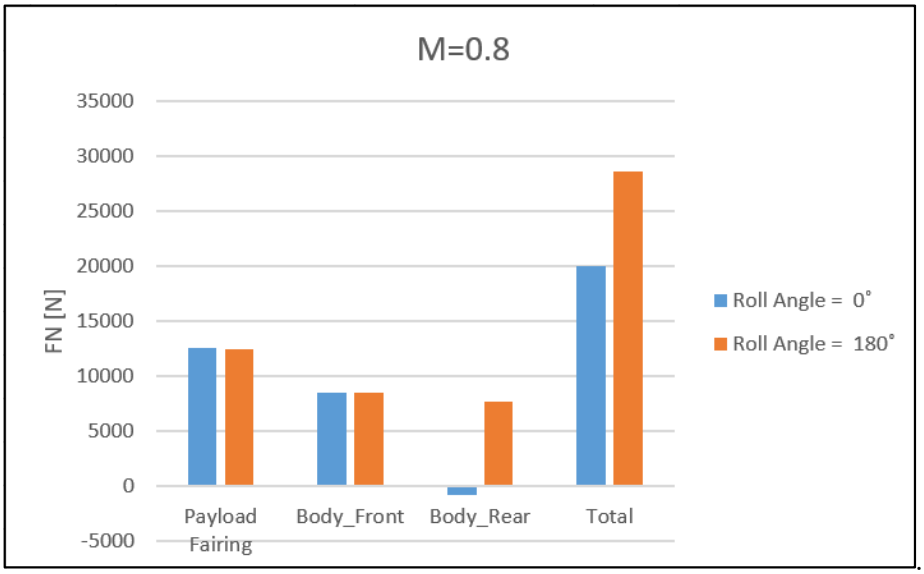

Fig. 61. Comparison of component normal force for half umbilical plate (M_∞=0.8, α=5°)

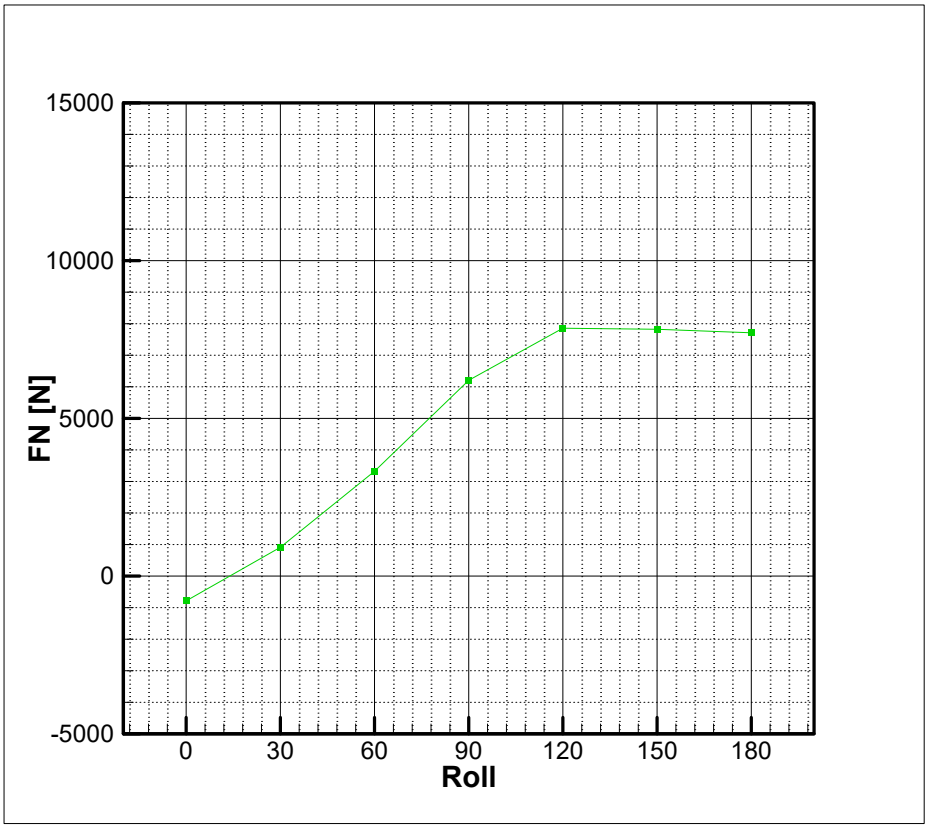

Fig. 62. Variation of normal force for body rear for half umbilical plate (M_∞=0.8, α=5°, ϕ=0°)

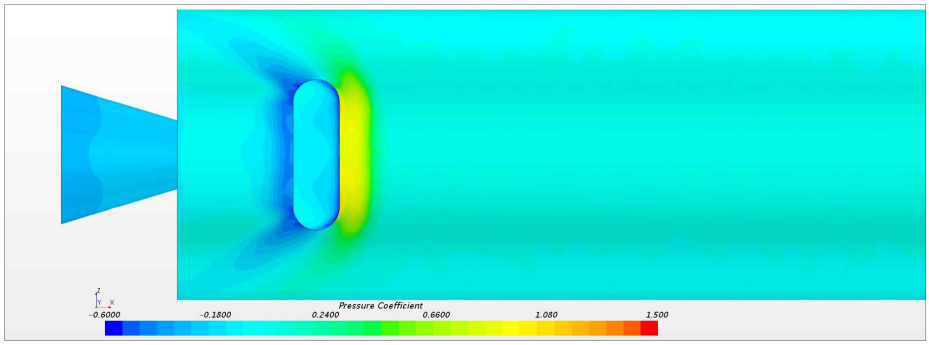

Windward

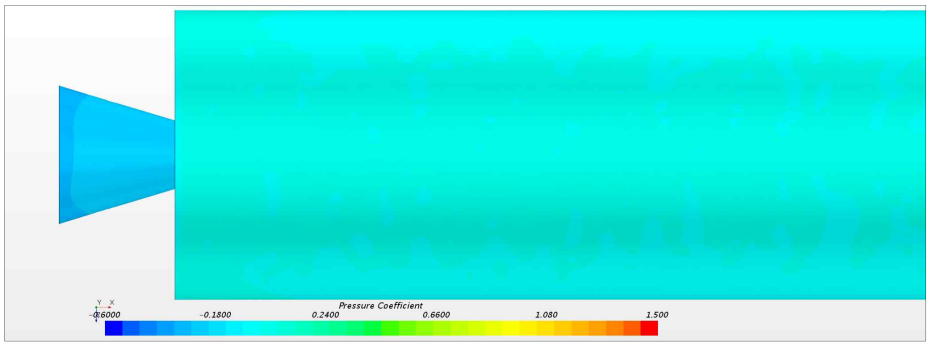

Leeward

Fig. 63. Comparison of surface pressure for half umbilical plate (M_∞=1.5, α=5°, ϕ=0°)

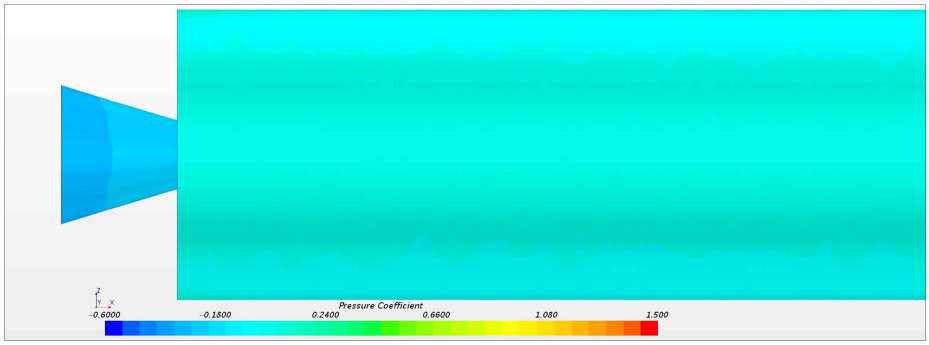

Windward

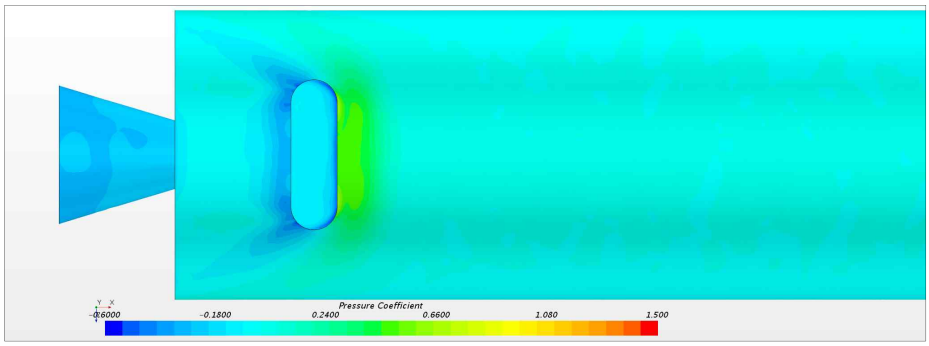

Leeward

Fig. 64. Comparison of surface pressure for half umbilical plate (M_∞=1.5, α=5°, ϕ=180°)

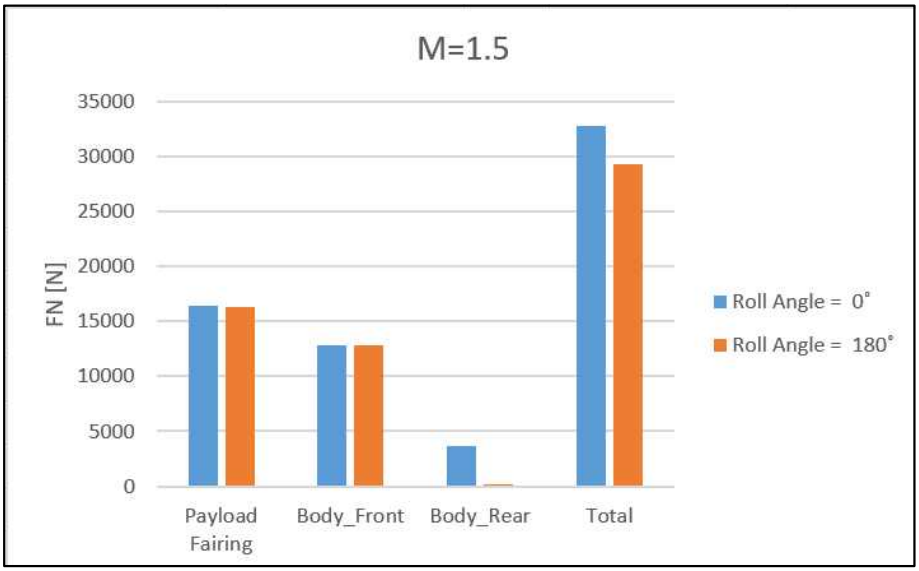

Fig. 65. Comparison of component normal force for half umbilical plate (M_∞=1.5, α=5°)

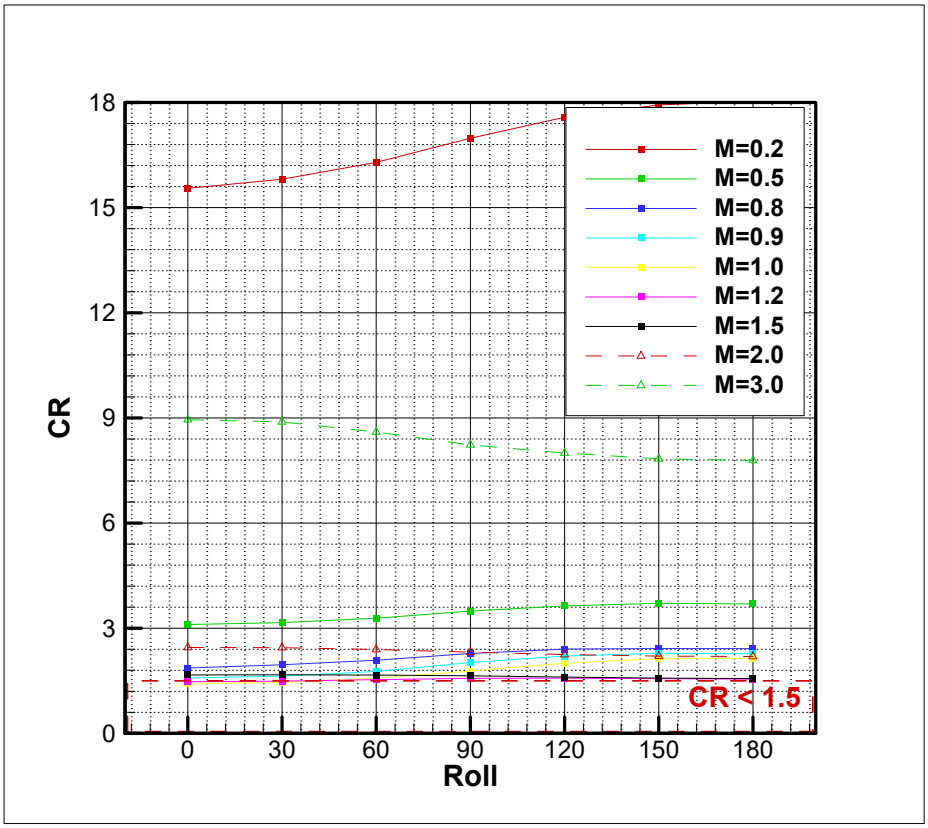

Fig. 66. Variation of control ratio of half umbilical plate ($0.2 \leq M_{\infty} \leq 3.0$, $\alpha=5°$, $\triangle\phi=30°$)

4.2.3 Aerodynamic characteristics for LV with half cylindrical umbilical plate

For the actual flight trajectory, two smaller circular umbilical plates instead of an elliptical umbilical plate are applied to compare the results in this part (Fig. 67 to Fig. 70). In these two small cylindrical umbilical plates, there is additional flow between the two umbilical plates, resulting in the loss of the less normal force. Through this, the controllability increases (Fig. 71 to Fig. 77). However, there are some conditions in which the CR value is 1.5 or less, TVC angle should be 6.1° or more, or the thrust should be increased to about 76 tonf to get more than 1.5 of CR (Fig. 78).

Compared to the minimum value of CR when there is no umbilical plate and the minimum value of the present CRs when two cylindrical umbilical plates are considered, 2.5% of CR is reduced due to the influence of half cylindrical umbilical plate. However, it can be seen that the controllability increases by about 11.5% if CR of the original umbilical plate is compared and by about 4.4% if CR of the half umbilical plate is compared.

($CR_{\min_{Present}} = 1.482$, $CR_{\min_{UmbilicalPlate}} = 1.307$, $CR_{\min_{NoUmbilicalPlate}} = 1.520$, $CR_{\min_{HalfUmbilicalPlate}} = 1.415$)

In addition, although the normal force around the umbilical plate is positive, the normal force is reduced compared to the case where there is no umbilical plate, and the total normal force is reduced. However, the normal force around the umbilical plate is higher than that of the elliptical umbilical plate, and the overall normal force increases when the circular umbilical plate is applied.

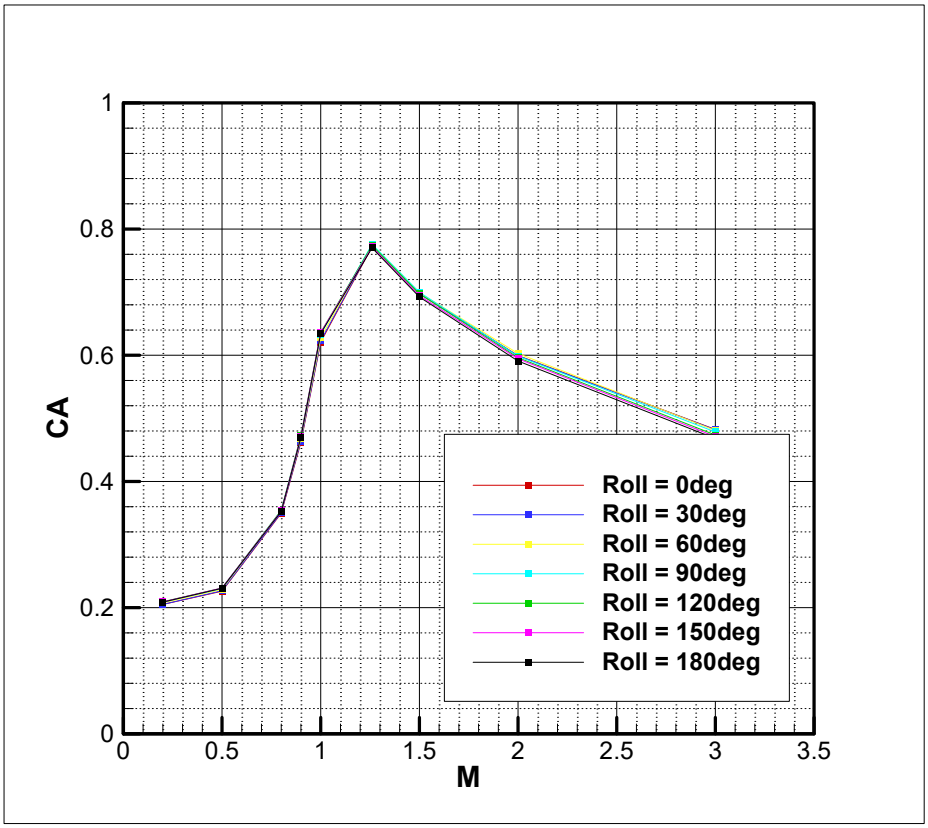

Fig. 67. Axial force coefficient for half cylindrical umbilical plate ($0.2 \leq M_{\infty} \leq 3.0$, $\alpha=5°$, $\triangle\phi=30°$)

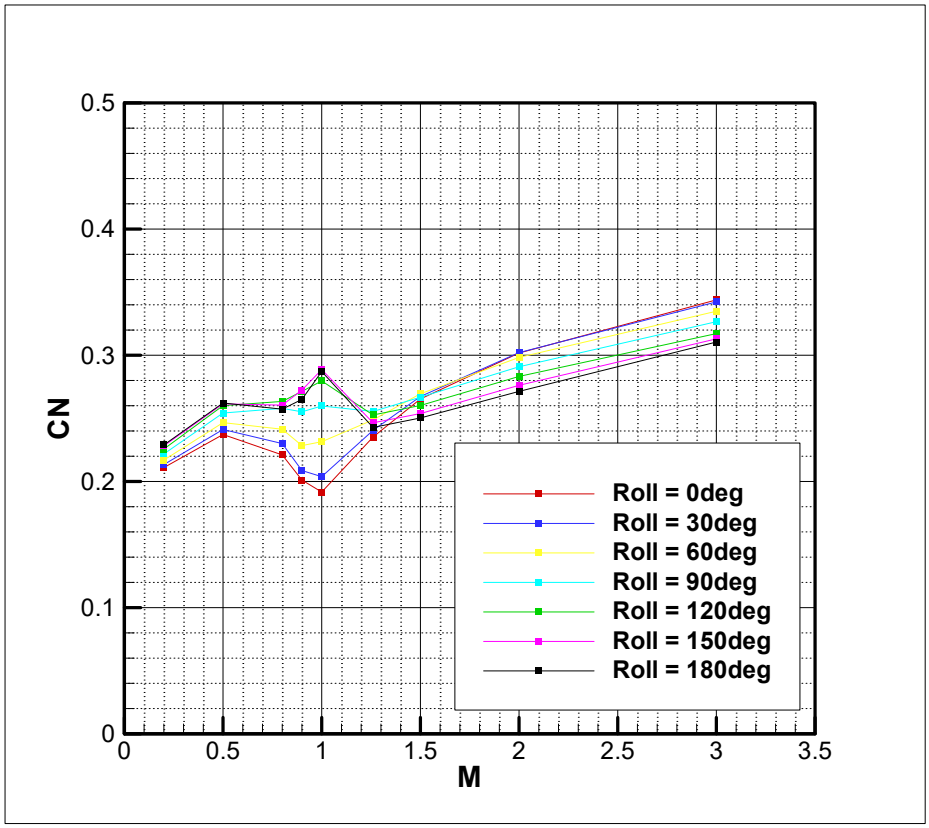

Fig. 68. Normal force coefficient for half cylindrical umbilical plate ($0.2 \leq M_{\infty} \leq 3.0$, $\alpha=5°$, $\triangle\phi=30°$)

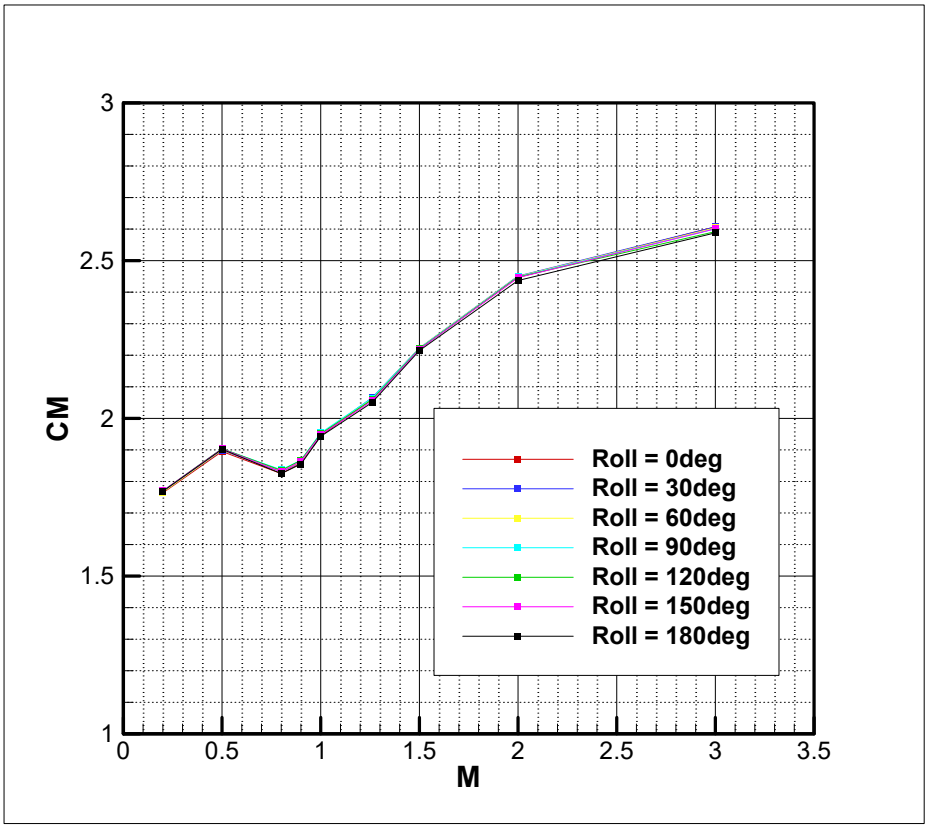

Fig. 69. Pitching moment coefficient for half cylindrical umbilical plate ($0.2 \leq M_{\infty} \leq 3.0$, $\alpha=5°$, $\triangle\phi=30°$)

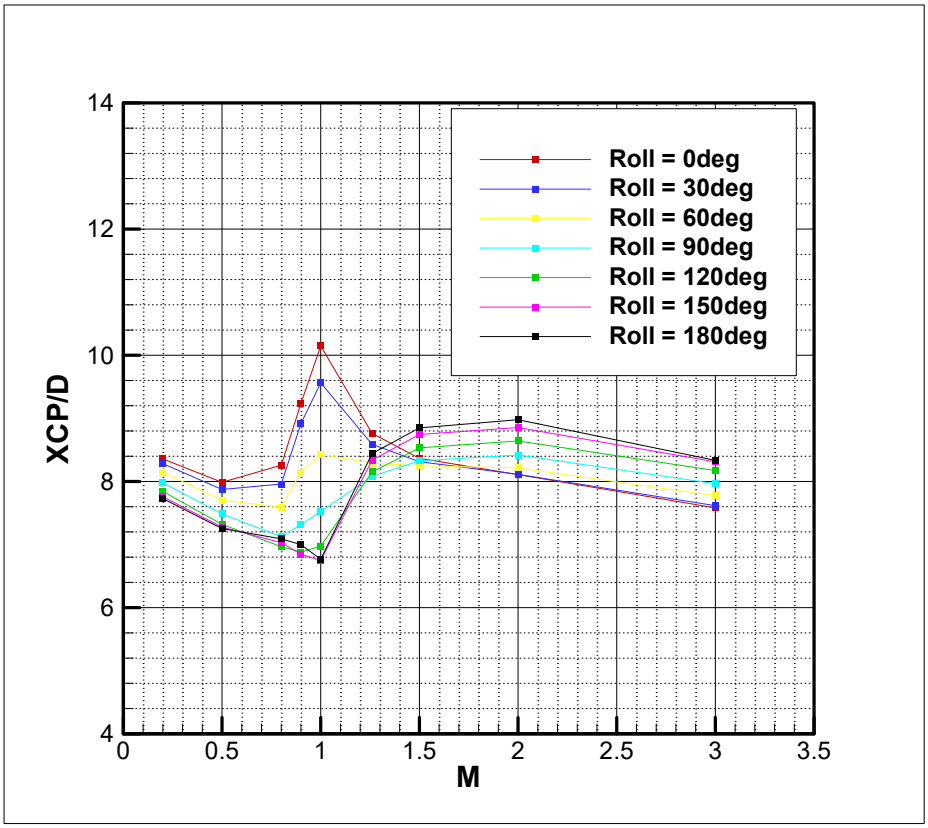

Fig. 70. Center of pressure for half cylindrical umbilical plate ($0.2 \leq M_\infty \leq 3.0$, $\alpha=5°$, $\triangle\phi=30°$)

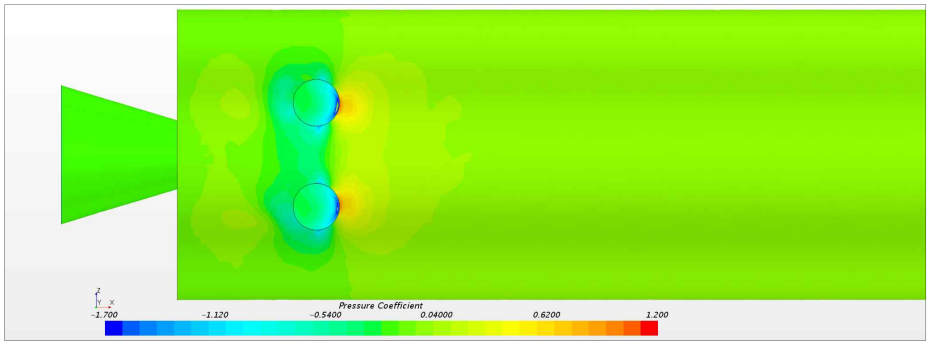

Windward

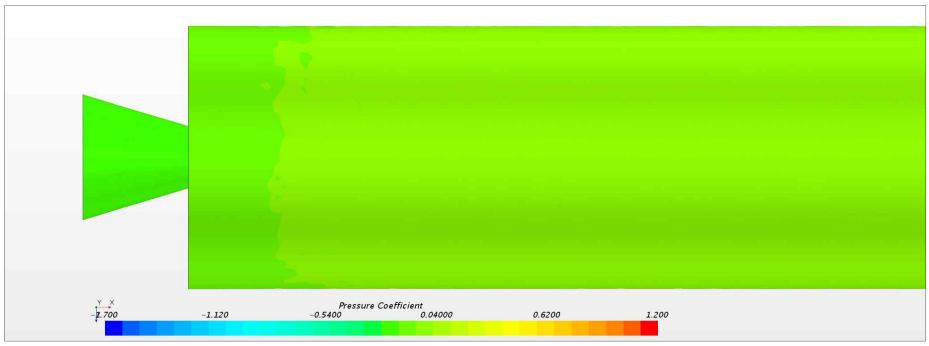

Leeward

Fig. 71. Comparison of surface pressure for half cylindrical umbilical plate (M_∞=0.8, α=5°, ϕ=0°)

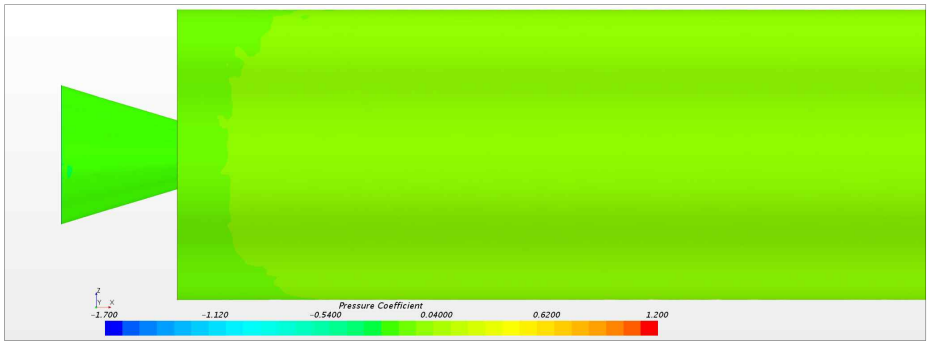

Windward

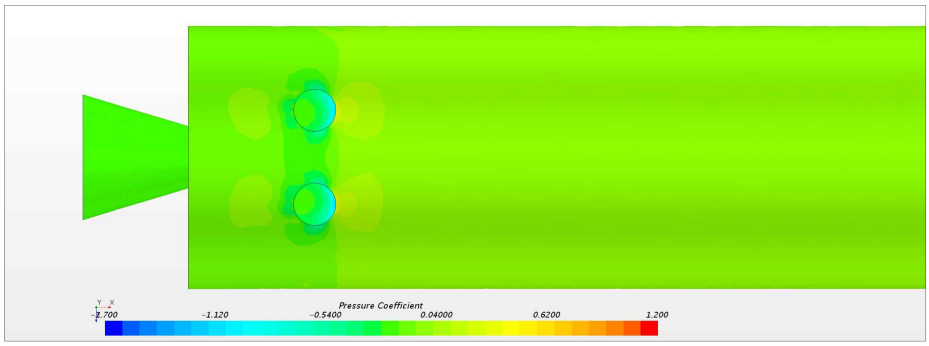

Leeward

Fig. 72. Comparison of surface pressure for half cylindrical umbilical plate (M_∞=0.8, α=5°, ϕ=180°)

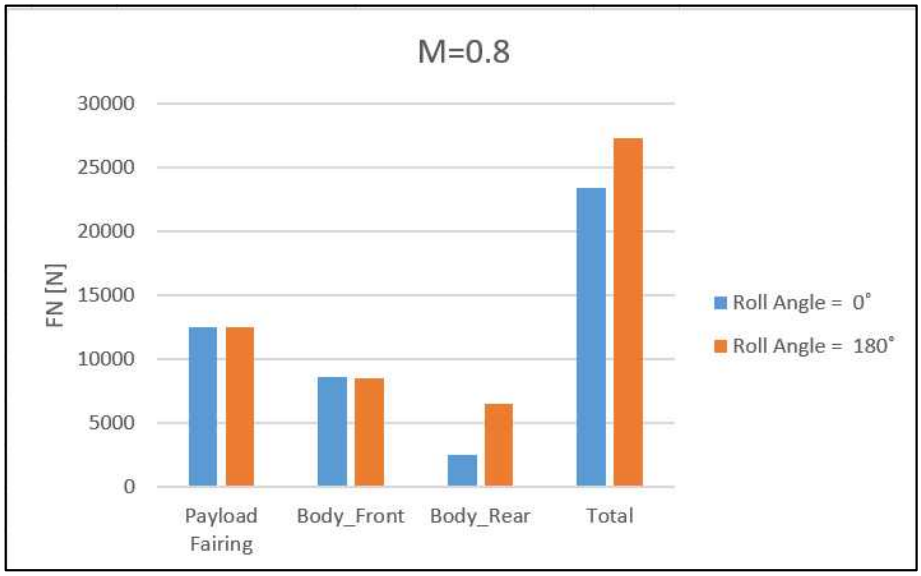

Fig. 73. Comparison of component normal force for half cylindrical umbilical plate (M_∞=0.8, α=5°)

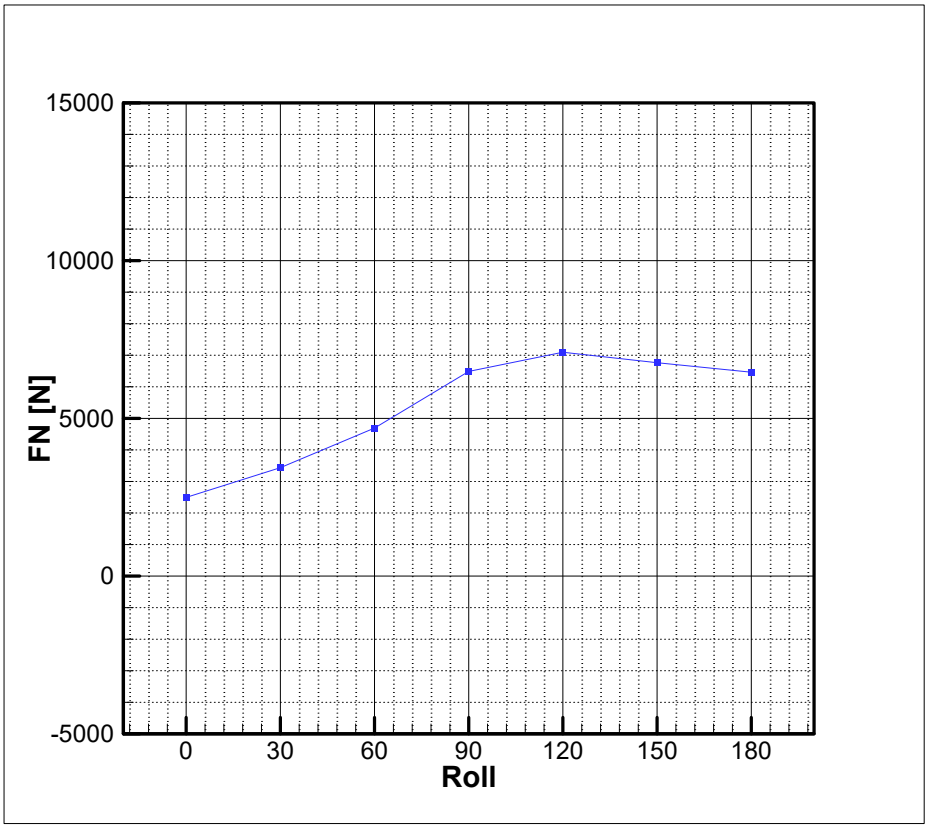

Fig. 74. Variation of normal force for body rear for half cylindrical umbilical plate (M_∞=0.8, α=5°, ϕ=0°)

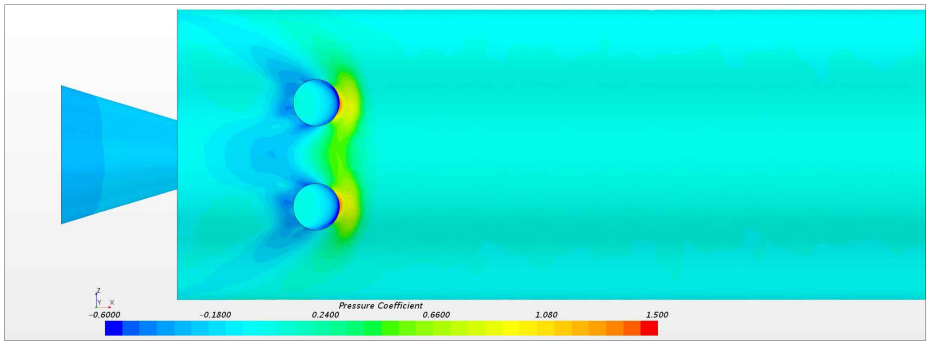

Windward

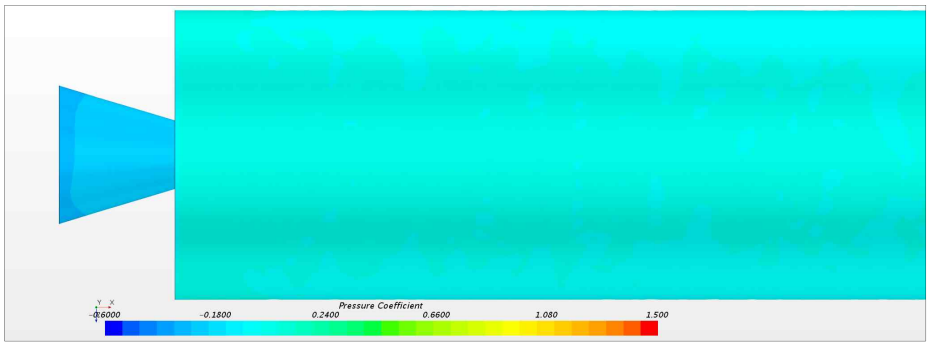

Leeward

Fig. 75. Comparison of surface pressure for half cylindrical umbilical plate (M_∞=1.5, α=5°, ϕ=0°)

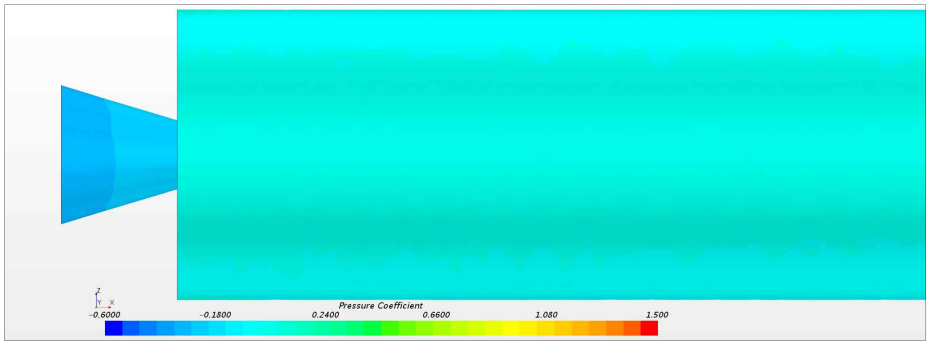

Windward

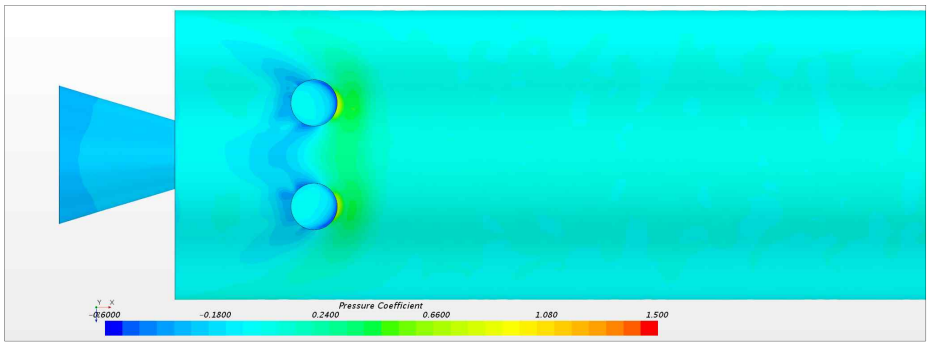

Leeward

Fig. 76. Comparison of surface pressure for half cylindrical umbilical plate (M_∞=1.5, α=5°, ϕ=180°)

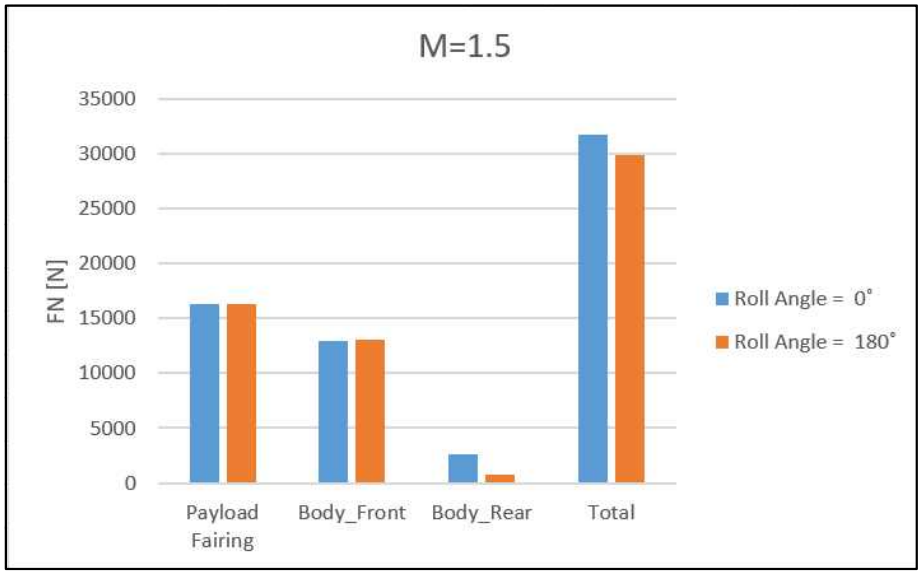

Fig. 77. Comparison of component normal force for half cylindrical umbilical plate (M_{∞}=1.5, α=5°)

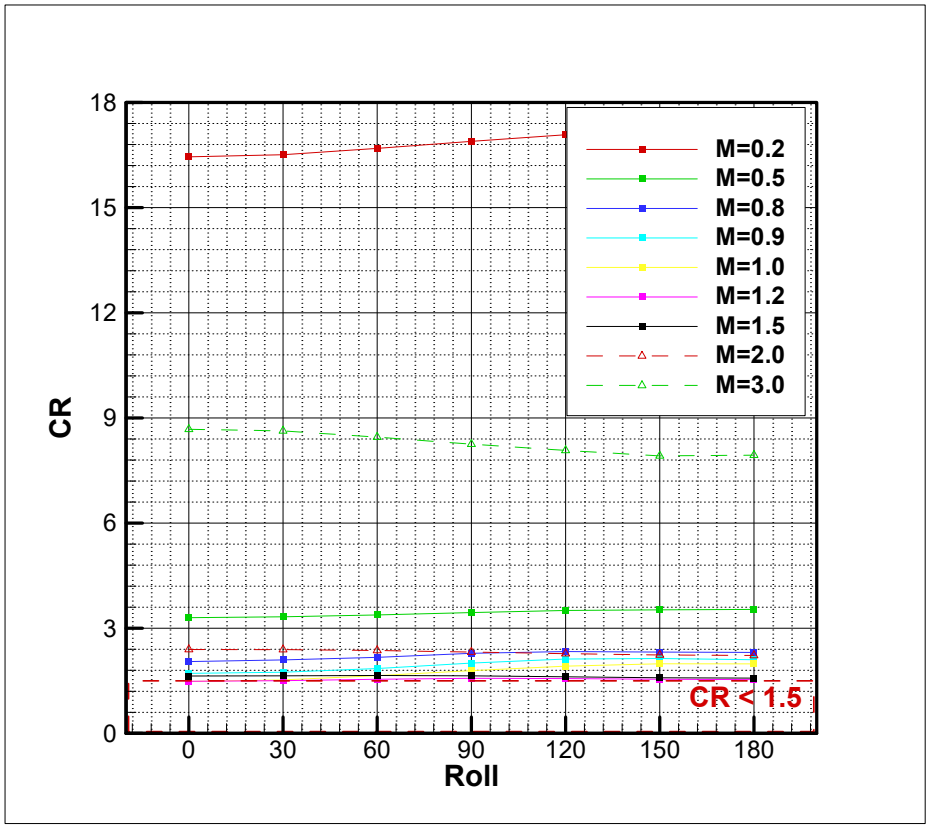

Fig. 78. Variation of control ratio of half cylindrical umbilical plate ($0.2 \leq M_{\infty} \leq 3.0$, $\alpha=5°$, $\triangle\phi=30°$)

4.3. Effects of location of the umbilical plate regard to aerodynamic characteristics

In this part, the aerodynamic characteristics is predicted when the umbilical plate moves forward to Payload Fairing. Fig. 79 through Fig. 82 show the changes of the aerodynamic coefficients according to Mach number and roll angle change. The change in the axial coefficient is small whether the position of the umbilical plate is forward or backward. However, the normal force coefficient and the pitching moment coefficient show that there are many differences.

Even if the umbilical plate is positioned forward, the normal force loss at a specific roll angle occurs (Fig. 83 to Fig. 89). There are some conditions in which the CR value is 1.5 or less, TVC angle should be 6.2° or more, or the thrust should be increased to about 78 tonf to get more than 1.5 of CR (Fig. 90).

Compared to the minimum value of CR when there is no umbilical plate and the minimum value of the present CRs when the umbilical plate moves forward, 3.9% of the CR is reduced due to the influence of the umbilical plate. However, it can be seen that the controllability increases by about 10.1% if the CR of the original umbilical plate is compared.

$$(CR_{\min_{Present}} = 1.460,\ CR_{\min_{Umbilical\,Plate}} = 1.307,\ CR_{\min_{No\,Umbilical\,Plate}} = 1.520)$$

The CR in this case is similar to CR in case of the half and cylindrical umbilical plate. However, it should be confirmed that the controllability always increase when the protuberance moves forward. the further research on the effect of the aerodynamic characteristics when the external structure settles on the changed location will be conducted by analyzing the flow field around the protuberance in detail.

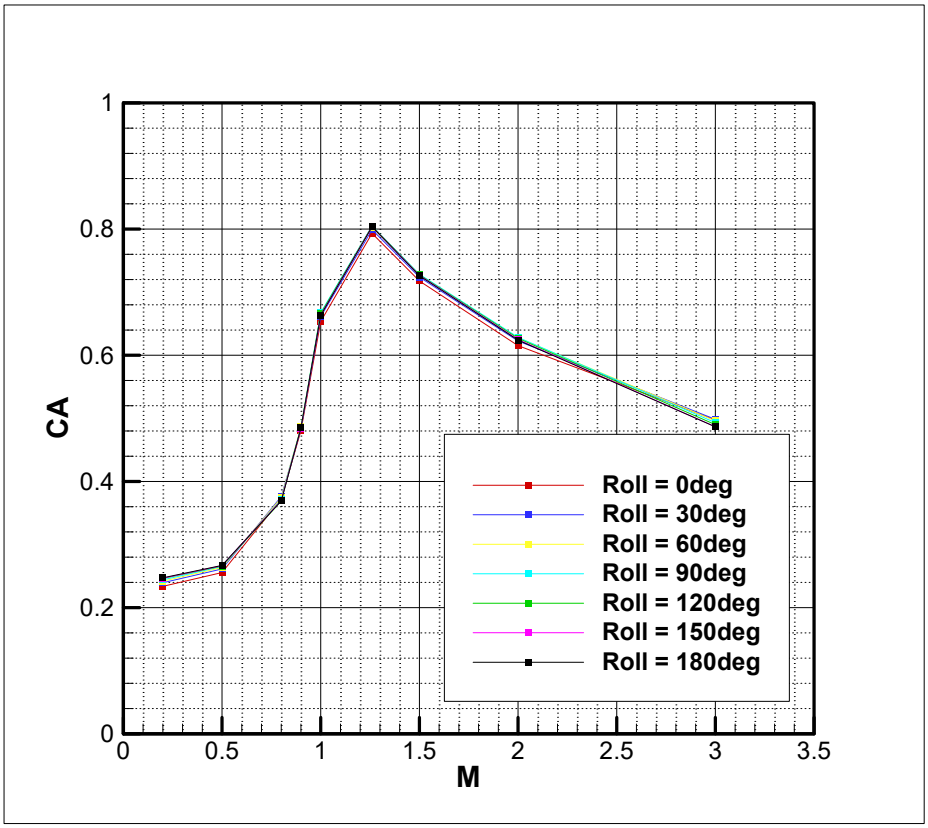

Fig. 79. Axial force coefficient for front umbilical plate ($0.2 \leq M_{\infty} \leq 3.0$, $\alpha=5°$, $\triangle\phi=30°$)

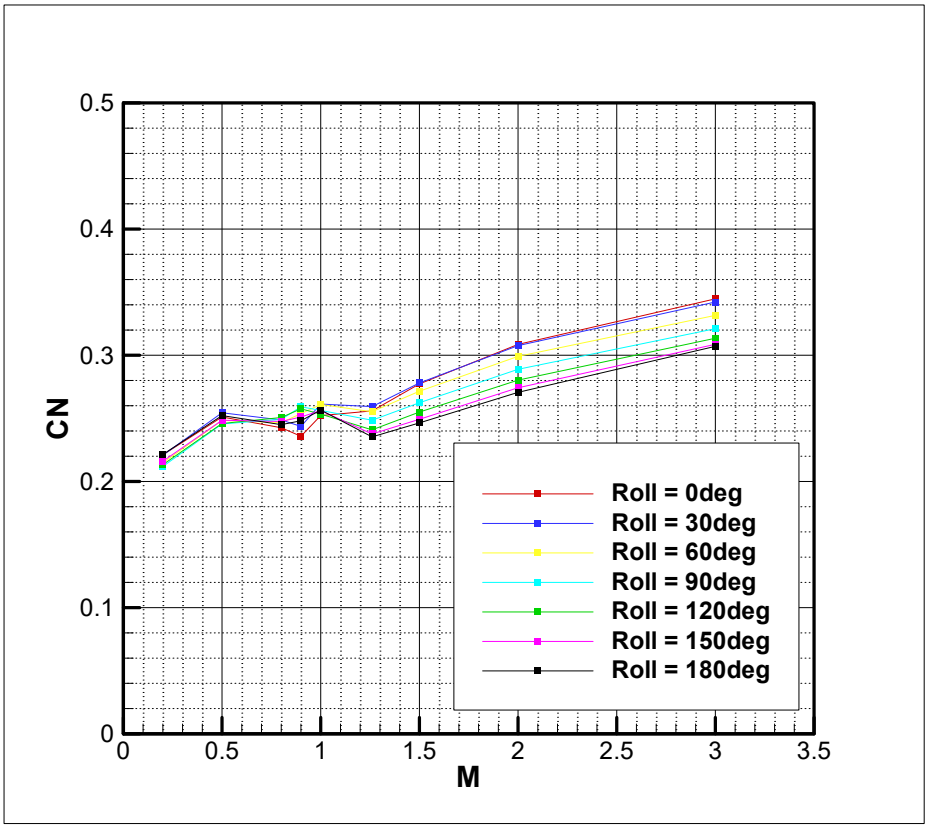

Fig. 80. Normal force coefficient for front umbilical plate ($0.2 \leq M_{\infty} \leq 3.0$, $\alpha=5°$, $\triangle\phi=30°$)

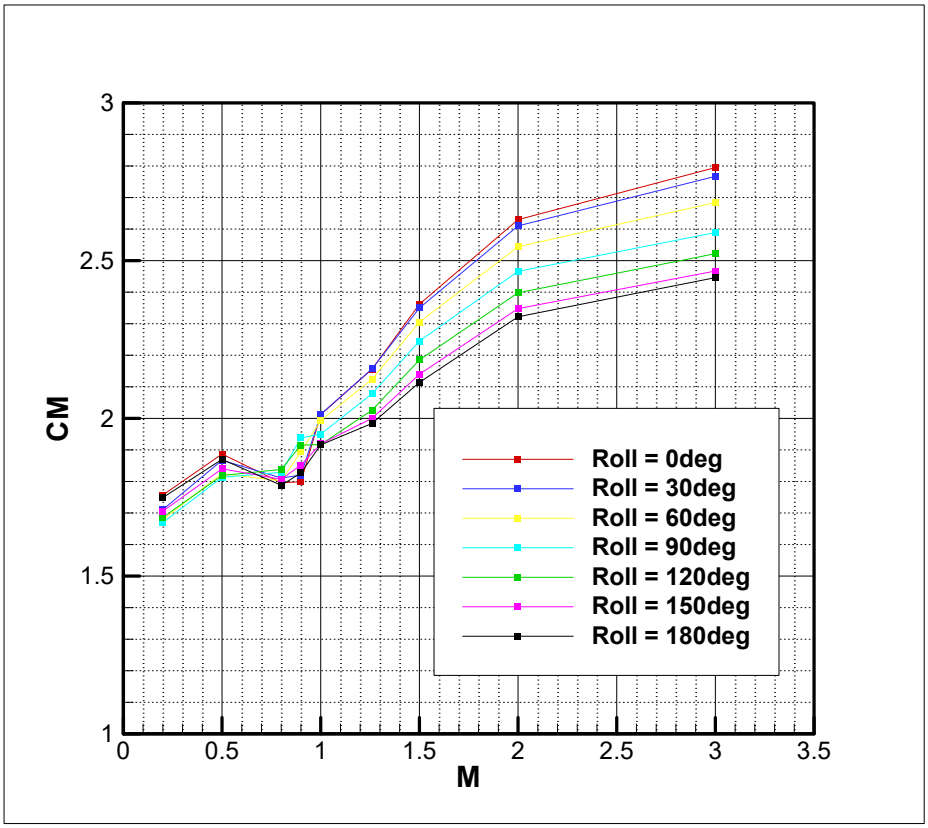

Fig. 81. Pitching moment coefficient for front umbilical plate ($0.2 \leq M_{\infty} \leq 3.0$, $\alpha=5°$, $\triangle\phi=30°$)

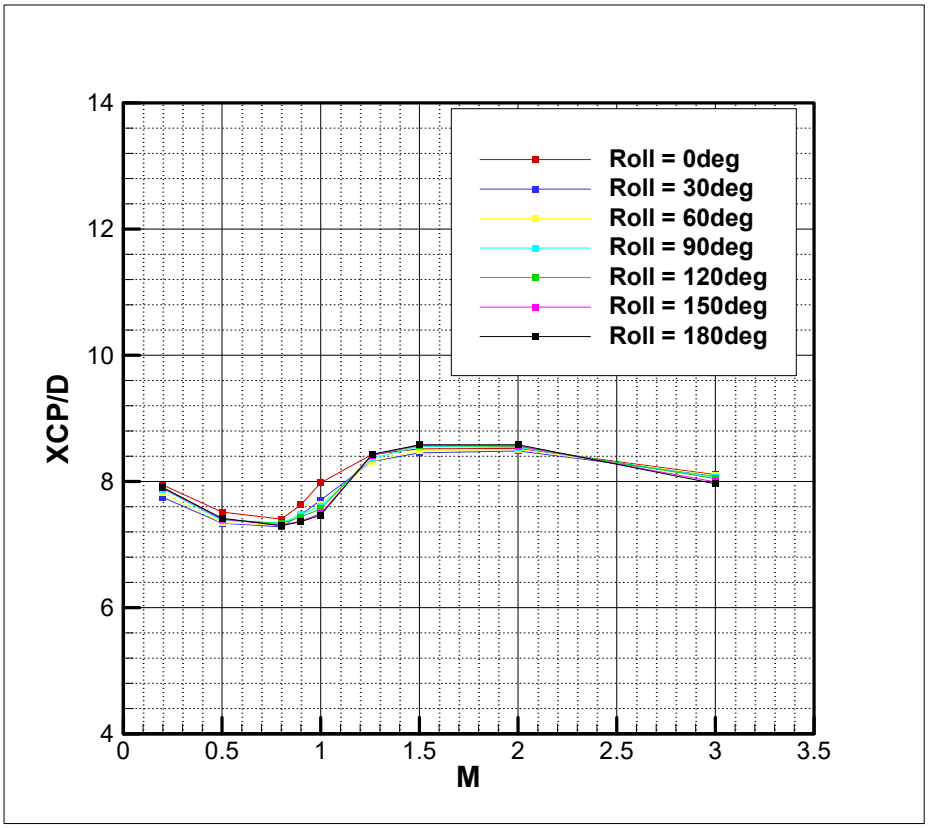

Fig. 82. Center of pressure for front umbilical plate ($0.2 \leq M_{\infty} \leq 3.0$, $\alpha=5°$, $\triangle\phi=30°$)

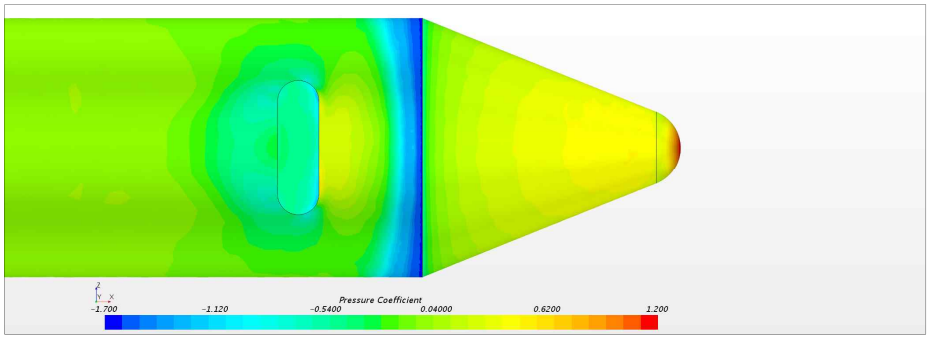

Windward

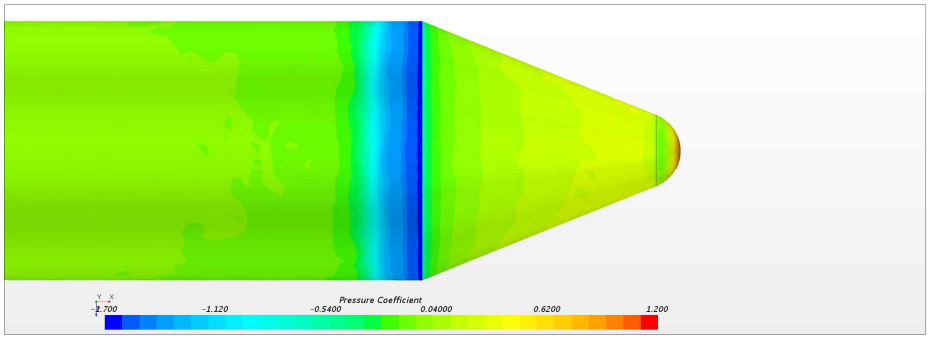

Leeward

Fig. 83. Comparison of surface pressure for front umbilical plate (M_{∞}=0.8, α=5°, ϕ=0°)

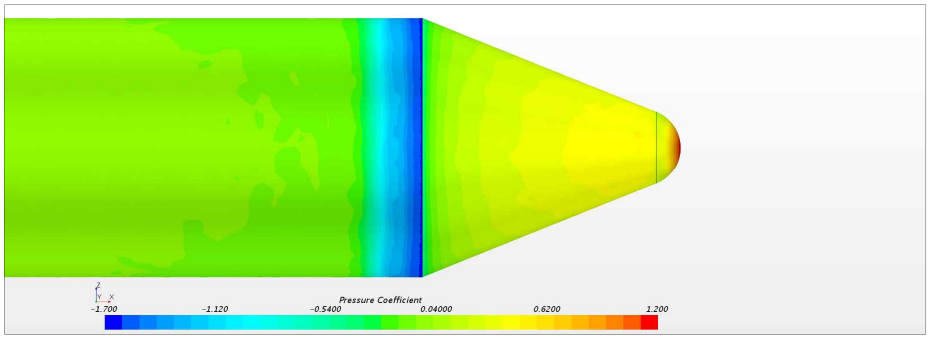

Windward

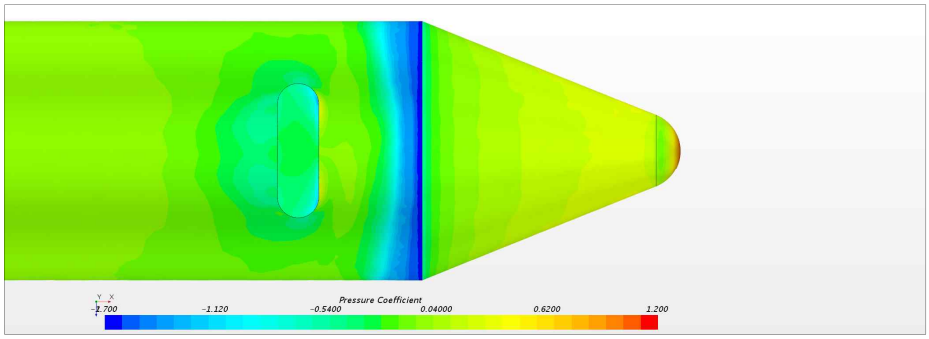

Leeward

Fig. 84. Comparison of surface pressure for front umbilical plate (M_{∞}=0.8, α=5°, ϕ=180°)

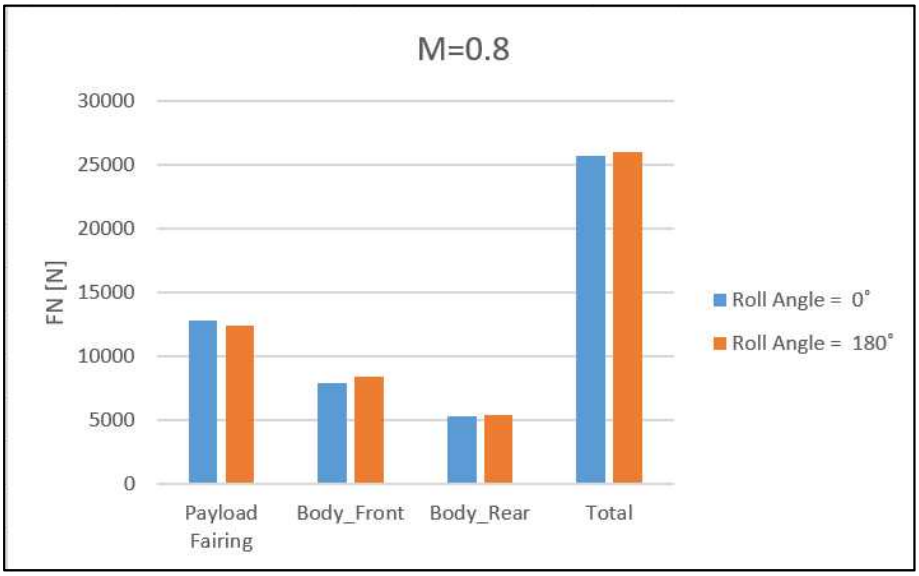

Fig. 85. Comparison of component normal force for front umbilical plate (M_∞=0.8, α=5°)

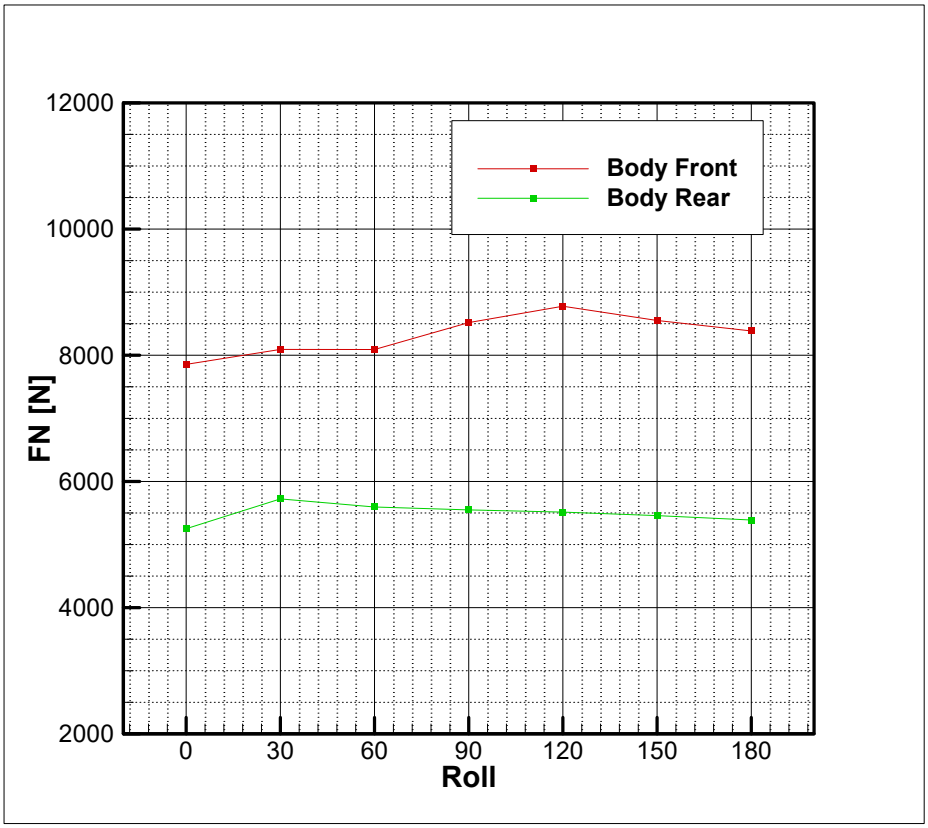

Fig. 86. Variation of normal force for body for front umbilical plate (M_∞=0.8, α=5°, ϕ=0°)

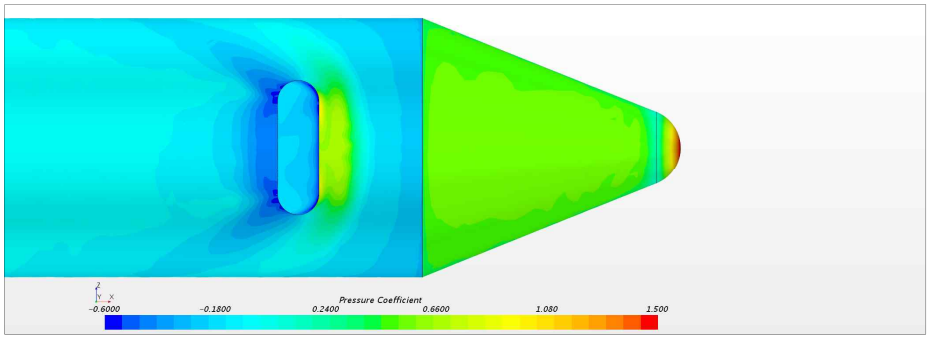

Windward

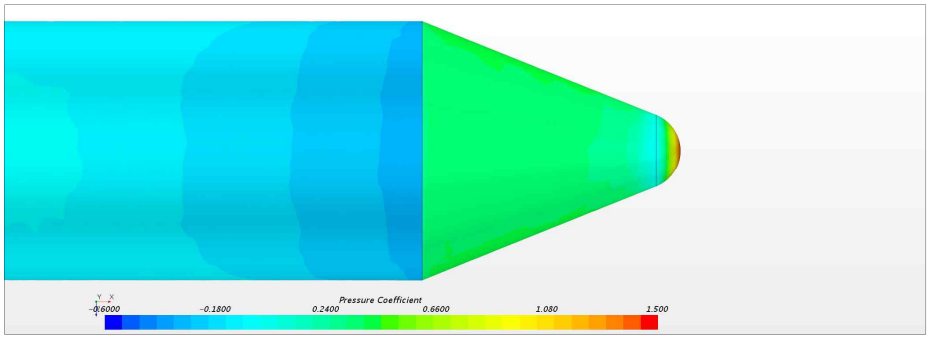

Leeward

Fig. 87. Comparison of surface pressure for front umbilical plate (M_∞=1.5, α=5°, ϕ=0°)

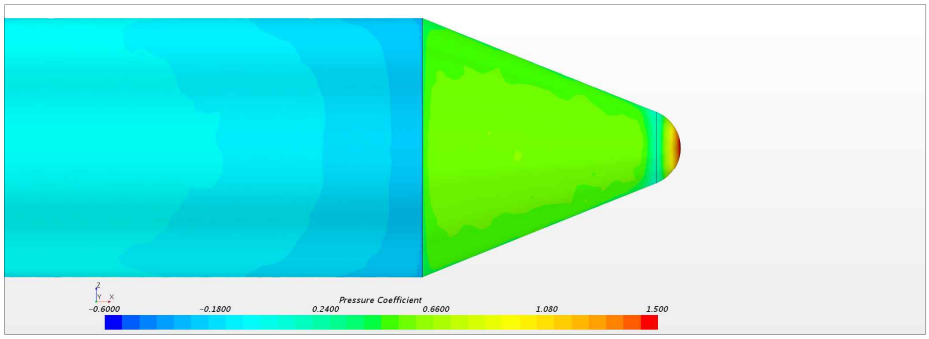

Windward

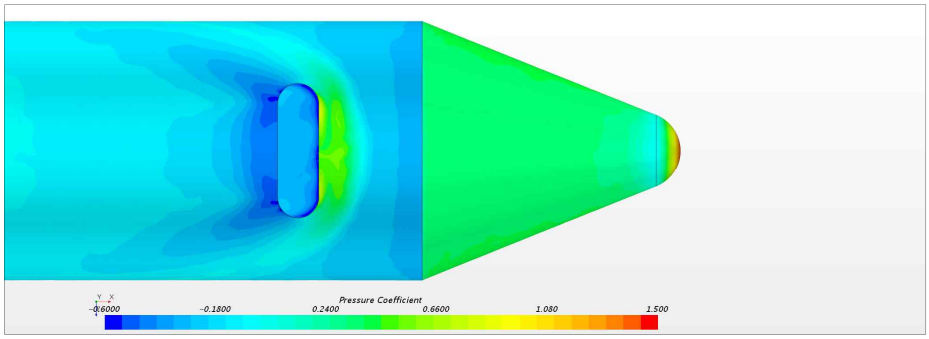

Leeward

Fig. 88. Comparison of surface pressure for front umbilical plate (M_∞=1.5, α=5°, ϕ=180°)

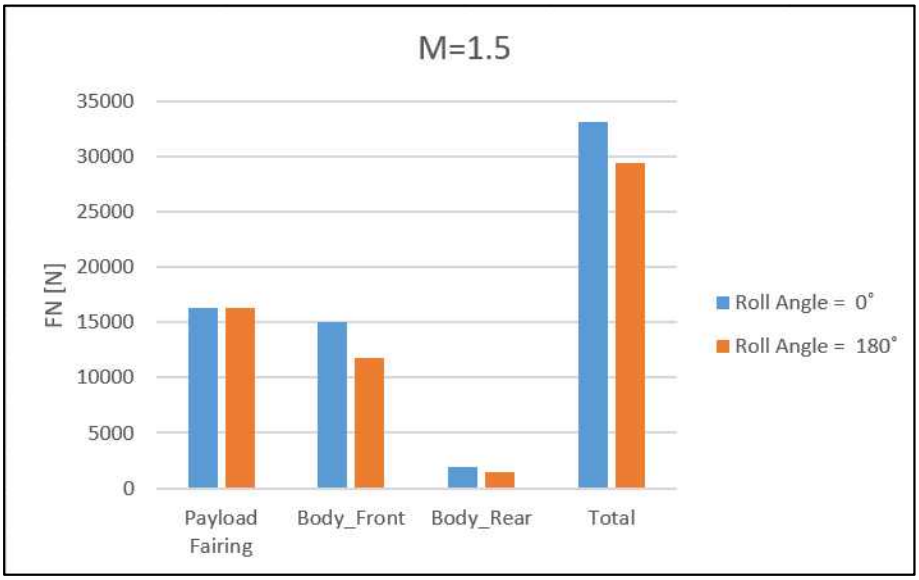

Fig. 89. Comparison of component normal force for front umbilical plate (M_∞=1.5, α=5°)

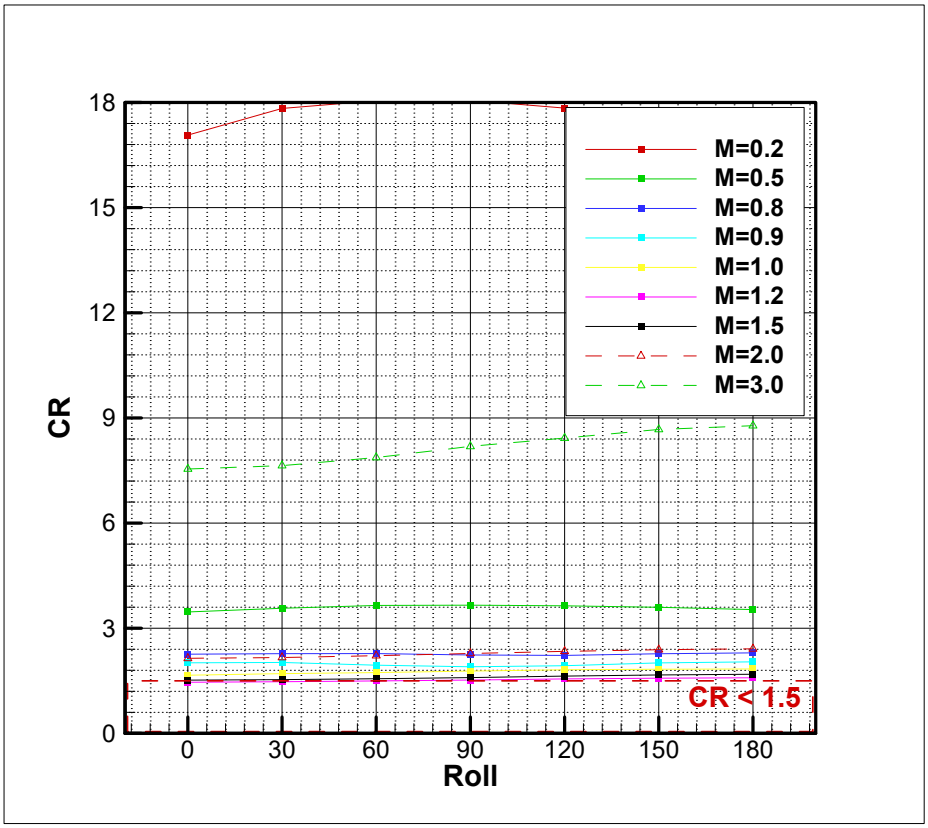

Fig. 90. Variation of control ratio of front umbilical plate ($0.2 \leq M_{\infty} \leq 3.0$, $\alpha=5°$, $\triangle\phi=30°$)

5. Conclusions

The KARI has developed the TLV to confirm the performance of a 75 tonf engine in the KSLV-II. In this paper, the solutions of the problem related to the longitudinal control of the launch vehicle by the flow around the umbilical plate during the development process of the TLV, which intends to use the second and third stages of the KSLV-II with slight changes in configuration has been summarized. Owing to the influence of the flow around the umbilical plate, the normal force changed with the change in roll angle, and the center of pressure shifted accordingly. The controllability of the “Resemblant TLV” was verified by obtaining the Control Ratio(CR, the ratio of control torque to aerodynamic torque), which is the control requirement of the launch vehicle. Furthermore, when the CR design specification of the NASA MSFC was applied, the “Resemblant TLV” CR showed a value of less than 1.5 under some conditions.

After the TLV flight test was successful on November 28, 2018, the flight trajectory was released and applied to the aerodynamic analysis of the Resemblant TLV. The overall characteristics are similar to those of the previous analysis, but the CR in the supersonic region increases. Meanwhile, the height of the umbilical plate is lowered and the aerodynamic characteristics are predicted to confirm that the controllability increases compared to the original umbilical plate. In addition, the section shape of the umbilical plate is changed from one ellipse to two small circles to confirm that the CR increases. Finally, the position of the umbilical plate moves forward to Payload Fairing, and it is confirmed that the CR value increases as much as CR of the half and circular umbilical plate. However, the further research will be conducted for this change of the protuberance location.

There are various possible approaches to increase the CR of the “Resemblant TLV”, such as increasing the deviation angle of the nozzle and increasing the thrust of the engine. However, the simplest way to improve the controllability by increasing the CR is to reduce the height of the protuberance such as the umbilical plate and minimize the influence of the flow around the protuberance. And the section of this plate is smaller circular shape rather than an elliptical shape to increase the controllability. These are also reflected in the initial design state of the launch vehicle.

When developing the low aspect ratio launch vehicle, e.g., the TLV, using some stages and parts of the mother launch vehicle, the KSLV-II, for the specific purpose such as the engine performance testing during the development of the mother launch vehicle, careful attention should be paid to the design of the protuberance such as the umbilical plate owing to control problems. This study confirmed that controllability can be a problem when the umbilical plate is mounted in the aft body of the low aspect ratio launch vehicle. It is expected that this paper could be used as a reference material in the design of low aspect ratio launch vehicles by providing an intuitive input for the design of the protuberance and control device of this type of launch vehicle.

In the privately led New Space Era, the design, the manufacturing and the operation of the launch vehicle include the reusability and the low cost, etc. [46-48]. Using an existing launch system such as the sub-parts and the launch complex is important in order to reduce the cost. In this era, the launch vehicle with the low aspect ratio depending on the specific mission objective such as the space tourism will be developed such as Blue Origin's launch vehicle New Shepherd (Fig. 91) for the visit to the space of the mankind. When developing this kind

of the launch vehicle, the design of this launch vehicle should include the guides in this study in order to secure the sufficient controllability of the launch vehicle. And this paper will help to reduce the number of trial and error in the design of the launch vehicle with the low aspect ratio in the New Space Era.

The further research for the configuration of the protuberance will be conducted to improve the aerodynamic characteristics of the external structure to obtain the proper controllability of the launch vehicle. This work will also be done in consideration of the overall system design including the aerodynamic design such as the change of the weight, the structural reinforcement, the leakage during the charge or discharge of the propellant and the configuration of the retraction device in case of the umbilical plate and so forth for the newly designed protuberance.

Fig. 91. Blue Origin New Shepard [47]

References

[1] Korea Space Launch Vehicle KSLV-II, http://kslvii.kari.re.kr.

[2] Oh, H., Lee, J., Um, H. and Huh, H., “Numerical study for flame deflector design of a space launch vehicle”, Advances in Space Research, Vol. 59, 2017, pp. 1833-1847.

[3] Sun, B., Park, Y., Roh, W. and Cho, G., “Attitude Controller Design and Test of Korea Space Launch Vehicle-I Upper Stage”, International Journal of Aeronautical and Space Science, Vol. 11, No. 4, 2010, pp. 303-312.

[4] Kim, Y., Lee, J. H. and Kim, K., “A Numerical Study on the Effect of the Umbilical Plate on Longitudinal Controllability of a Low Aspect Ratio Launch Vehicle”, International Journal of Aeronautical and Space Sciences, Vol. 20, No. 4, 2019, pp. 870-878.

[5] Bartels, R. E., Carlson, J., Park, M. and Mineck, R. E., “ FUN3D Grid Refinement and Adaptation Studies for the Ares Launch Vehicle”, 28th AIAA Applied Aerodynamics Conference, 2010.

[6] Applebaum, M., Eppard, M., Hall, L. and Blevins, J., “ Protuberance Aerodynamic Loads for Space Launch Vehicle Systems Using Computational Fluid Dynamics”, Journal of Spacecraft and Rocket, Vol. 49, No. 5, 2012, pp. 779-787.

[7] Claus W., “Aerodynamic Data of Space Vehicles”, Springer, 2014.

[8] Suresh, B. N., Silvan, K., “Integrated Design for Space Transportaion System”, Springer, 2015.

[9] Hammond, W. E., Design Methodologies for Space Transportaion Systems, AIAA, 2001.

[10] Sutton, G. P., “Rocket Propulsoin Element”, WILEY, 1992.

[11] Isakowitz, S. J., Hopkins, J. B. and Hopkins, J. P. Jr.,

"International Reference Guide to Space Launch System", AIAA, 2004.

[12] Anderson, J. D., 2001, "Fundamentals of aerodynamics", Third ed. McGRAW-HILL, New York.

[13] Blevins, J. A., Campbell, J. R. Jr, Bennett, D. W., Rausch, R. D., Gomez, R. J. and Kiris, C. C., "An overview of the Characterization of the Space Launch Vehicle Aerodynamic Environments", 52nd Aerospace Sciences Meeting, AIAA, 2014.

[14] Hammond, W., "Space Transportation: A Systems Approach to Analysis and Design", AIAA, 1999.

[15] Mendenhall, M. R., " Tactical Missle Aerodynamics: Prediction Methodology", AIAA, 1991.

[16] Kim, J., "Thermal Analysis of Thermal Protection System of Test Launch Vehicle", International Journal of Thermophysics, Vol. 38, No. 10, 2017, pp. 1-11.

[17] Kim, J., "Pre- and Postflight Thermal Analysis of Test Launche Vehicle Fuselage", Journal of Spacecraft and Rocket, Vol. 56, No. 6, 2019, pp. 1786-1794.

[18] Oh, T. H., Ko, J. Y., Kim, Y., Lee, J. H. and Ok, H., "Vent Valve for Test Launch Vehicle of Korea Space Launch Vehicle II", Journal of Spacecraft and Rocket, Vol. 55, No. 3, 2018, pp. 681-686.

[19] Ko, J. Y., Kim, Y., Lee, J. H. and Ok, H., "Venting Analysis of the Payload Fairing of Korea Space Launch Vehicle II", Journal of Spacecraft and Rocket, Vol. 56, No. 4, 2019, pp. 1039-1044.

[20] Kitamura, K., Nonaka, S., Kuzuu, K., Aono, J., Fujimoto, K. and Shima, E., "Numerical and Experimental Investigations of Epsilon Launch Vehicle Aerodynamics at Mach 1.5", Journal of Spacecraft and Rocket, Vol. 50, No. 4, 2013, pp. 896-916.

[21] Bell, M., Watterson, J. K. and Lisk, D., “A Numerical Study into a Local Protuberance Interaction with a Fin on a Supersonic Projectile”, AIAA Paper 2009-1092, 2009.

[22] White, J. T., “A Navier-Stokes CFD Analysis of the Flowfield about a Circular-Cylinder Protuberance Mounted Perpendicular to a Flat Plate in Supersonic Flow”, AIAA Paper 95-1789, 1995.

[23] Sahu, J. and Danberg, J. E., “A Combined Computational and Experimental Study of Supersonic Flow over as Protuberance”, 14th Atmospheric Flight Mechanics Conference, 1987.

[24] Manokaran, K., Vidya, G. and Goyal, V. K., “CFD Simulation of Flowfield over a Large Protuberance on a Flat Plate at High Supersonic Mach Number”, 41st Aerospace Sciences Meeting and Exhibit, 2003.

[25] Catalano, P., Marini, M., Nicoli, A., and Pizzicaroli, A., “CFD Contribution to the Aerodynamic Data Set of the Vega Launcher”, Journal of Spacecraft and Rocket, Vol. 44, No. 1, 2007, pp. 42-51.

[26] Hall, R. M., Holland, S. D. and Blevins, J. D., “Aerodynamic Characterization of a Modern Launch Vehicle”, AIAA Paper 2011-10, 2011.

[27] Kim, J. G., Lee, J. W. and Kim, K. H., “Investigation on the Characteristics of Plume-Induced Flow Separation and Wall Heat Transfer”, Journal of Spacecraft and Rocket, Vol. 49, No. 1, 2012, pp. 189-191.

[28] STAR-CCM+ Documentation, Siemens PLM Software, 2018.

[29] Anderson, J.D., Computational Fluid Dynamics: the basics with applications, McGraw-Hill, 1995.

[30] J. B., “Computational Fluid Dynamics: Principles and Applications”, ELSEVIER, 2001.

[31] Tannehill, J. C., Anderson, Dale A. and Pletcher, Richard H., “Comptutational Fluid Mechanics and Heat Transfer”, Tayler & Francis, 1997.

[32] Liou, M.-S, “A Sequel to AUSM: AUSM+”, Journal of Computational Physics, Vol. 129, 1996, pp. 364-382.

[33] Liou, M.-S, “Ten Years in the Making-AUSM-Family”, AIAA Paper 2001-2521, 2001.

[34] Menter, F. R., “Two-equation eddy-viscosity turbulence models for engineering applications”, AIAA Journal, Vol. 32, No. 8, 1994, pp. 1598-1605.

[35] Kim, Y., Lee, J. H. and Ok, H., “A Numerical Study on the Effects of External Flanges/Stringers and Protuberances on the Aerodynamic Characteristics of a Launch Vehicle”, 27th International Conference on Parallel Computational Fluid Dynamics, 2015.

[36] Nicoli, A., Imperatore, B., Fauci, R. and Pizzicaroli, A., “Wind Tunnel Test Campaign of the VEGA Launcher”, AIAA Paper 2006-257, 2006.

[37] Kelly, T. C., Ross, T. P., “Effects of Configuration Geometry on the Transonic Aerodynamic Characteristics of a Simulatted Launch Vehicle”, NASA TN X-976, 1964.

[38] Samuels, R. D. and Blackwell, J. A., Jr., “Effects of Configuration Geometry on the Supersonic Aerodynamic Characteristics of a Simulated Launch Vehicle”, NASA TN D-3755.

[39] Kim, Y., Ok, H. and Kim, I., “A Study on the Influence of the Base Region Modeling on the Aerodynamic Characteristics of a Launch Vehicle Using CFD”, Journal of the Korean Society for Aeronautical and Space Science, Vol. 33, No. 9, 2005, pp. 27-33.

[40] Barret, C., “Design of Launch Vehicle Flight Control Augmentors

and Resulting Flight Stability and Control", NASA Technical Paper 3704, 1997.

[41] Lee, S., Cho, S. and Sun, B., "Flight Test Trajectory Data of Test Launch Vehicle", KSAS 2019 Spring Conference, 2019.

[42] Song, E., Cho, S. and Sun, B., "Trajectory and Impact Point Dispersion Analysis for Test Launch Vehicle", KSAS 2019 Spring Conference, 2019.

[43] Cho, S. and Sun, B., "Overall Performance Analysis of Test Launch Vehicle", KSAS 2019 Spring Conference, 2019.

[44] Park, Y. K., Sun, B., "Attitude Control Design and Flight Results of Test Launch Vehicle", KSAS 2019 Spring Conference, 2019.

[45] Jo, S., Park, Y. K., Sun, B., "TVC Nozzle Alignment and Gimbaling Characteristics of Test Launch Vehicle", KSAS 2019 Spring Conference, 2019.

[46] Klevanski, J., Ecker, T., Riehmer, J., Reimann, B., Dumont, E. and Chavagnac, C., "Aerodynamic Studies in Preparation for CALLISTO-Reusable VTVL Launcher First Stage Demonstrator", 69th International Astronautical Congress(IAC), 2018.

[47] Blue Origin New Shepard, http://www.blueorigin.com/

[48] SPACEX Falcon 9, http://www.spacex.com/

[49] Blake, W. B., "MISSILE DATCOM USER'S MANUAL-1997 FORTRAN 90 REVISION", Air Force Research Laboratory, 1998.

Appendix. The aerodynamic prediction using the empirical approach

In this part, the empirical approach using MISSILE DATCOM[9, 49] is applied. And the results using this method are compared to the numerically predicted data. Fig. A.1 to Fig. A.4 show the comparison of the CFD results and the empirical results. A good agreement for a number of Mach numbers between the CFD results and the empirical results is presented. However, there is remarkable difference for some Mach numbers. Especially, the illogical aspect appears in Mach number of 1.2 which is near Mach number where the dynamic pressure is maximum. Fig. A.5 shows the axial force coefficients for the various protuberances. these results represent the effect of the different external structures. But the CR can not be obtained unfortunately since the normal force coefficients and the pitching moment coefficients considering the protuberances are not presented in this empirical method.

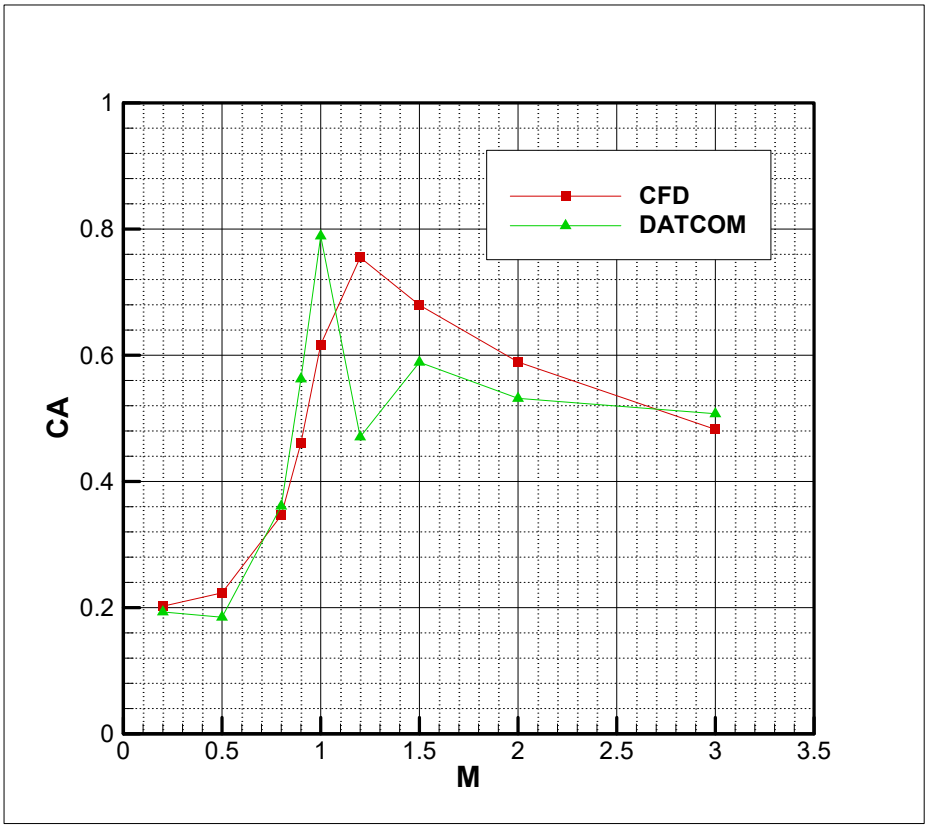

Fig. A.1. Axial force coefficient using the empirical approach ($0.2 \leq M_{\infty} \leq 3.0$, $\alpha=5°$)

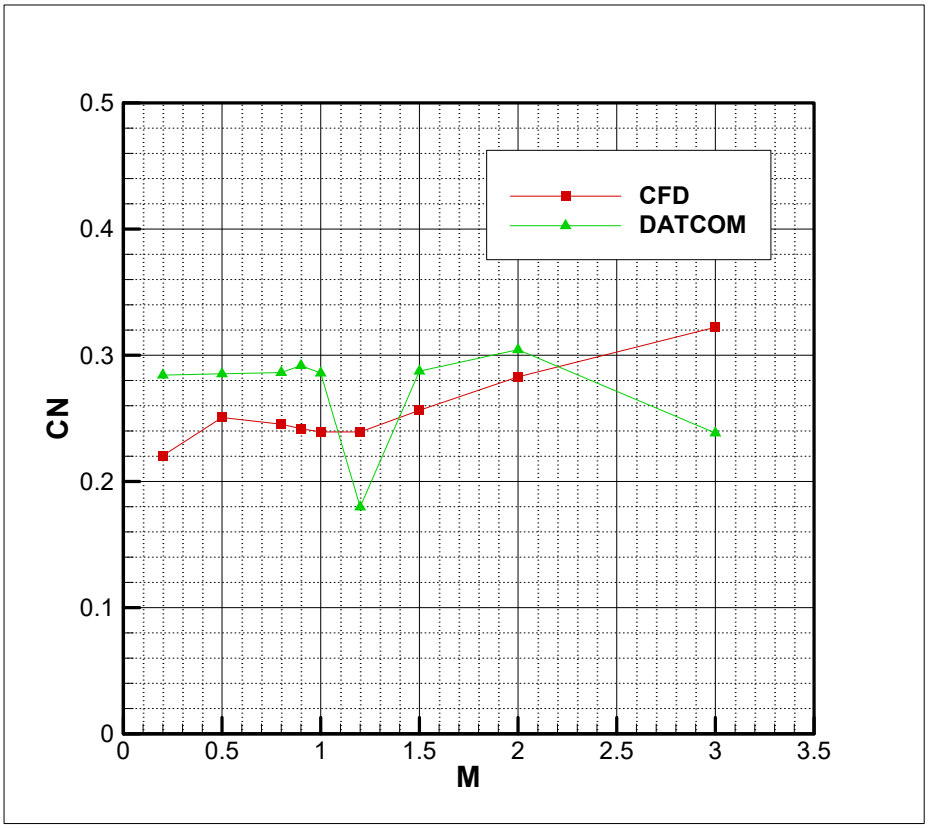

Fig. A.2. Normal force coefficient using the empirical approach ($0.2 \leq M_{\infty} \leq 3.0$, $\alpha=5°$)

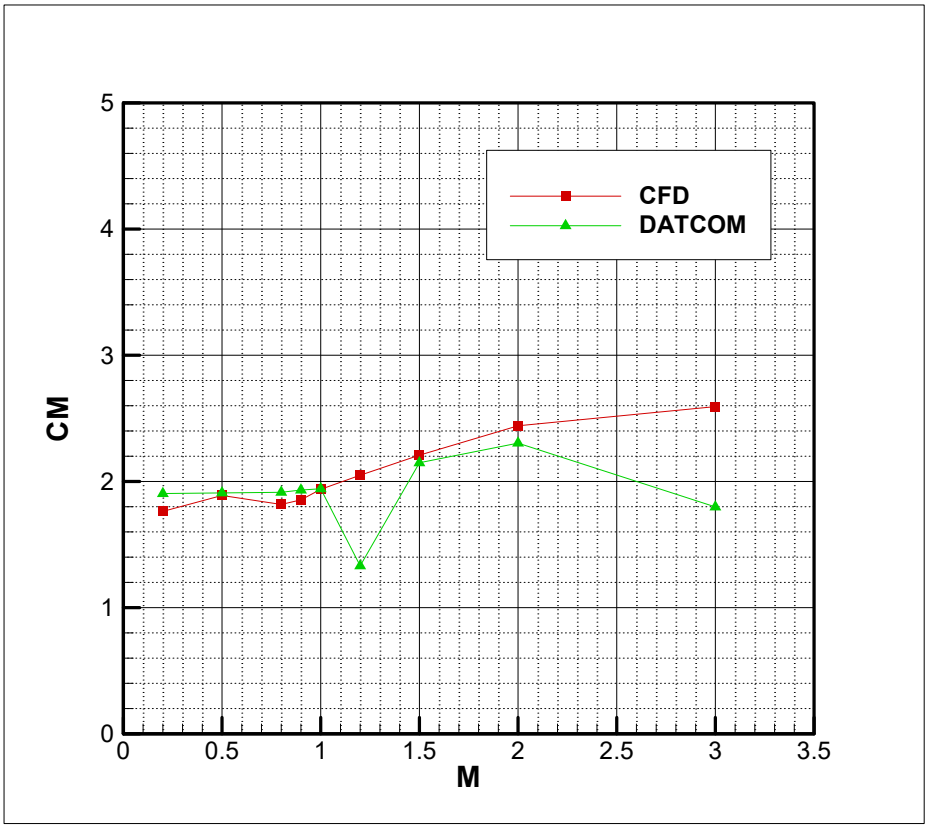

Fig. A.3. Pitching moment coefficient using the empirical approach ($0.2 \leq M_{\infty} \leq 3.0$, $\alpha=5°$)

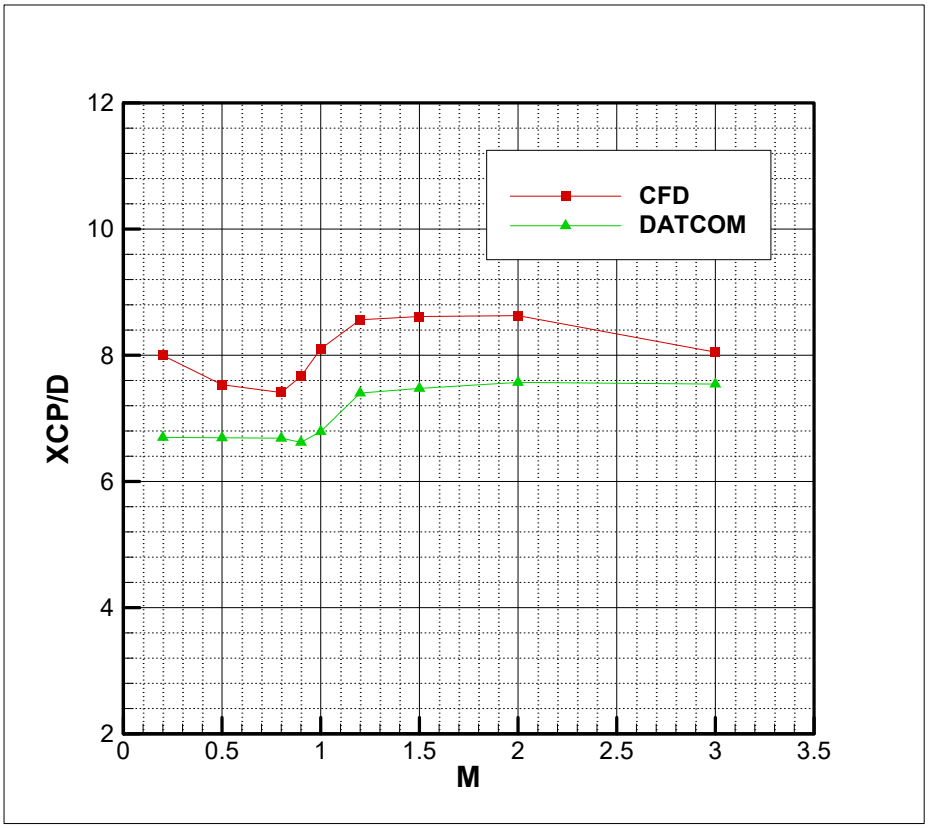

Fig. A.4. Center of pressure using the empirical approach ($0.2 \leq M_{\infty} \leq 3.0$, $\alpha=5°$)

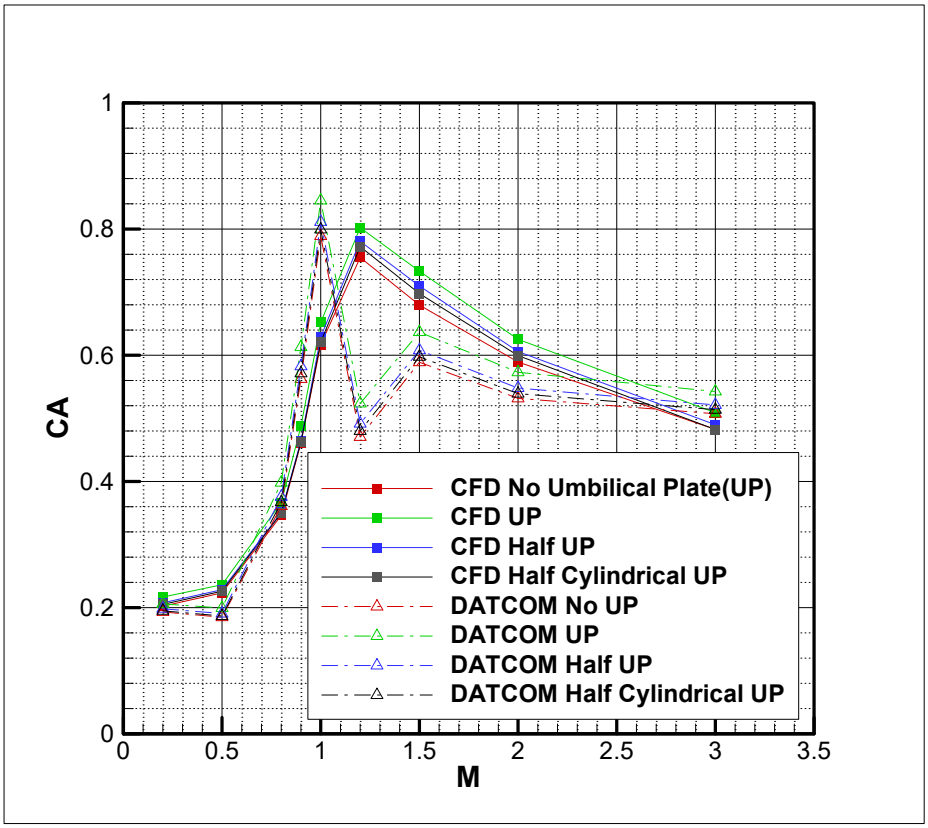

Fig. A.5. Axial force coefficient using the empirical approach and considering the protuberance ($0.2 \leq M_{\infty} \leq 3.0$, $\alpha=5°$)

국문초록

외부 구조물을 장착한 저 세장비 발사체의 공력 특성 연구

김영훈
기계항공공학부 기계항공공학전공
서울대학교

한국항공우주연구원에서는 한국형발사체를 개발 중에 있으며, 한국형발사체의 75톤 액체로켓엔진의 성능 시험을 위해 시험발사체를 개발하여 2018년 11월 28일 비행시험을 성공하였다.

본 연구에서는 전산유동해석기법을 적용하여 엄빌리칼 플레이트와 같은 외부 구조물을 장착한 시험발사체 유사 형상에 대해 공력 특성을 예측하고, 돌출물 주변 유동 현상을 분석하여 발사체 종안정성에 미치는 영향을 확인하였다. 외부 구조물 주변 유동 현상은 수직력의 변화를 야기하여 최종적으로 발사체 종안정성에 영향을 미칠 수 있다. 이를 확인하기 위해 돌출물의 높이, 단면 형상 및 장착 위치를 변화시켜 가며, 그 영향을 분석하였다. 대형 구조물을 장착한 저 세장비 발사체의 종안정성을 확보하려면, 엔진 추력을 높이거나 엔진 노즐의 회전각을 증가시키는 방법 등이 있지만, 가장 간단한 방법은 구조물의 높이를 최대한 낮추는 것이다. 또한 구조물의 단면 형상은 단일 타원 보다는 복수의 작은 원형으로 구성하는 것이 바람직하다.

한국형발사체 시험발사체와 같이 세장비가 작으며 기존 발사체 설계 자료와 부품 및 발사 설비를 이용하여 단시간에 저비용으로 개발할 경우, 본 연구가 저 세장비 발사체의 종안정성 확보에 도움이 될 것이다. 특히 민간 주도의 새로운 우주 개발 시대에 저 세장

비 발사체 설계에 본 연구결과를 활용하면 발사체 설계 과정에서 시행착오를 줄일 수 있을 것이다.

주요어 : 한국형발사체, 시험발사체, 공력 특성, 종안정성, 저 세장비, 돌출물, 전산유체역학

학 번 : 2013 - 30946